17th International Symposium on Ice
Saint Petersburg, Russia, 21 - 25 June 2004
International Association of Hydraulic Engineering and Research

FREEZING OF WATER IN AN OPEN CHANNEL FLOW UNDER SUPERCOOLED AMBIENT CONDITIONS: PRELIMINARY RESULTS

Anatolij R. Karev[1], Masoud Farzaneh[1], Laszlo Kollar[1] and Sandy Vaslon[1]

ABSTRACT
The thermal structure of an experimentally modeled ice accretion with a water film in an icing wind tunnel is investigated here at both inner and outer interfaces using non-destructive remote sensing techniques and traditional thermometry. The water film developing into rivulets was produced by spraying of an aerosol flow from a single water-dispersing nozzle cloud onto the iced bottom of a thermally insulated channel. The water film was then driven by a concurrent air flow at negative temperatures. The shear-driven water film thus created was thereby forced to freeze from below due to convection and evaporation from its surface. Heat conduction lengthwise along the bottom of the channel and perpendicular to it was controlled by measuring the outer surface of the bottom of the channel at several sites. The surface temperature of the flowing water film developing into rivulets, as measured by infrared camera, was found to be negative throughout all the experiments.

INTRODUCTION
A number of atmospheric icing models incorporate, in different ways, the concept of a thin water film which appears and starts flowing when there is an excess of incoming supercooled water onto an icing surface. The precise dynamics of this film, however, and its thermodynamic properties, are still not known clearly. From the time of the first introduction of the concept of a water film on the surface of growing atmospheric ice (Schumann, 1938) and the subsequent introduction of the freezing fraction concept (Messinger, 1953) up to and including late eighties, it was thought that the temperature of this water film should be equal to the equilibrium temperature between the water and ice, or water fusion temperature T_m=273.15 K. Thus, all atmospheric icing models originating from forties onward were based entirely on the heat balance calculation of an icing surface, where the temperature of water fusion was taken as the reference point, distinguishing the solid from the liquid states of water. A series of experiments with artificial hailstones grown in laboratory simulations of natural conditions (List et al.,

[1] NSERC/Hydro-Québec/UQAC Industrial Chair on Atmospheric Icing of Power Network Equipment (CIGELE) and Canada Research Chair on Atmospheric Icing Engineering of Power Networks (INGIVRE), Université du Québec à Chicoutimi, Département des Sciences Appliquées, 555 blvd de l'Université, Chicoutimi, Québec, Canada G7H 2B1

1989; Greenan and List, 1995) confirmed that the temperature of the water film on an icing surface in the wet mode is always below 0 ^{o}C. Yet over 30 years earlier, there was only one theoretical model, proposed by Kachurin (1962), which predicted supercooling of icing surfaces in both icing modes: with and without a water film. This icing model, initially developed for aircraft icing and then applied to the problem of icing of non-rotating cylinders (Kachurin et al., 1974), was based on the dynamics of a supercooled water film flowing over an icing surface and incorporating a Couette shear layer as well as the concept of eddy diffusivity in a flowing water film. Because Kachurin's work was largely unknown in the West, classical run-back icing models, such as the one proposed by Lozowski et al. (1979), continued to adopt the heat balance calculation of an icing surface, and parallel attempts were made to understand and explain theoretically the recorded water supercooling by introducing concept of non-isotropic heat transfer (List, 1990). Simultaneously, Kachurin's idea was successfully applied for computing hailstone growth processes and for explaining experimentally observed supercooling (Gvelisiani, 1968; Karev, 1993). Recently, the experimental data freshly obtained from the parallel fields of thin water film flow gave new birth to the initial idea and made it possible to specify its applicability to the icing processes (Karev et al., 2003a and 2003b). Moreover, a parallel was drawn between the hailstone growth and atmospheric icing processes by recording experimentally the supercooling at the surface of a water-film flowing on icing cylinder (Karev and Farzaneh, 2003). This investigation is an attempt to record water film supercooling by experimentally modeling a Couette shear water layer in plane, which flows on an ice surface at the bottom of a channel and freezes from below. Such an experimental configuration is of scientific interest primarily because of its similarity to all natural icing processes involving the appearance and flow of an aerosol-created water film on an ice surface. The simplifications carried out in relation to the natural icing problem consist in: (i) altering the collection efficiency by applying the corresponding coefficient of the settling of supercooled aerosol particles; (ii) making the shear stress constant lengthwise along the ice-covered bottom of a channel; and, (iii) eliminating the streamwise air pressure gradient. To avoid any inadvertent influence on the ice accretion process, a non-destructive remote sensing technique was applied using an infrared (IR) camera.

THEORETICAL BACKGROUND FOR IR MEASUREMENTS

In our previous studies on atmospheric ice formation on horizontal cylinders (Karev and Farzaneh, 2003), industrial IR pyrometers were used as detectors of electromagnetic waves emitted from the surface under investigation. Such instrumentation, as shown by the results of these studies, is hypersensitive to a number of ambient and geometrical parameters, and mainly to ambient temperature changes. Moreover, calibration adjustment must be made *prior* to taking the measurements by comparing real temperatures, as measured by a reliable instrument such as a thermocouple, with the readout from the IR instrument. The uncertainties in measuring resulted even with 2 ^{o}C errors obtained by using IR pyrometers do not exist for FLIR IR camera SC-2000, for which all ambient conditions, including local emissivity of investigated surfaces, may be adjusted after the IR pictures were taken. The camera covers a 7 to 13 μm spectral range in the long wavelength infrared (LWIR) band which corresponds approximately to an 8 to 14 μm atmospheric window, thus the influence of air humidity, having also been selected between adjustable ambient parameters, is minimal. The seeming problem of angular variation of the IR emissivity of ice and water surfaces in the LWIR band (Rees and James, 1992) may be solved in a simple manner by the adjustment of local emissivity according to the angle of observation using tabulated values of emissivity for

different angles. We refer readers to our previous investigation (Karev and Farzaneh, 2003) for an in-depth discussion of all problems arising during the IR measurement of the ice surface temperatures. A greater part of these problems were solved for this particular IR camera.

EXPERIMENTAL SET-UP

The experiments were carried out at the CIGELE atmospheric icing research wind tunnel which is a horizontal closed-loop low-speed wind tunnel with a total length of about 30 m, including a 3-m long test section with a rectangular cross-section 0.46 m high and 91.5 m wide. Ice was prepared in long narrow open channels prior to each run of experiments. Two different channels were used for this purpose. One was longer than the other with a length of 1.22 m, a width of $6.7 \cdot 10^{-2}$ m, and a wall height of $2.5 \cdot 10^{-2}$ m. The length of the second one was 0.91 m, its width was $7.8 \cdot 10^{-2}$ m and its wall height was 7.6 cm, making it possible to deposit thicker ice in it. The channel was placed in the middle of the test section of the wind tunnel 0.12 m downstream of the water supply. This distance was chosen so that the aerosol cloud might reach the edge of the channel and cover it by half of the cross-section. Water was provided by a single water-dispersing nozzle mounted on an aluminum rake that was fixed to the top of the wind tunnel. The temperature of the ice was measured by six T Type thermocouples that were installed right below the surface of the ice and at the bottom of the channel at three different stations, 0.5 cm, 15 cm and 30 cm behind the leading edge of the channel. During the experiments, additional ice accumulated on the surface of the prepared ice, thus the thermocouples no longer provided the exact temperature of the ice surface, which is why a FLIR SC-2000 IR camera was applied in order to measure the temperature of the water layer flowing on the surface of the ice. The infrared camera was placed 60 cm downstream the leading edge of the channel in a box installed on the top of the wind tunnel. This box might be turned such that the angle of camera to the horizontal direction was 45 degrees, and thus, the entire channel became visible in the camera. Three experiments were performed involving different air velocities, $V_{a1} = 10$ ms^{-1}, $V_{a2} = 20$ ms^{-1} and $V_{a3} = 30$ ms^{-1}, while the following parameters were kept constant: temperature of ambient air, $T_a = -15$ ^{o}C, temperature of supplied water, $T_w = 2$ ^{o}C, , and water flow rate, The longer channel was used for the experiments where the air velocity was 10 m/s and 20 m/s, while the shorter one was applied for the case of 30 ms^{-1} speed. The duration of each run was 15 minutes, while the thermocouples provided data at every second, and images were taken by the infrared camera initially every 15 seconds by the end of the experiment increasing to 30 seconds.

RESULTS AND DISCUSSION

Figures 1 and *2* present the temperatures measured at different designated sites in the bulk ice and on the surface of the water film which flowed on the ice surface. It may be seen in the figures that the start of the ice accretion process influences the temperature measured at all six points. The initial surge of heat flux throughout the ice to the bottom of the channel is recognizable by sudden changes in the temperature at any given site. The first two experiments were performed for the ice thickness h $=2 \cdot 10^{-2}$ m, while the experiment with V_{a3} =30 m/s was performed for thicker ice, h $=5.1 \cdot 10^{-2}$ m, so that the heat surge was greater, but the final temperature at the bottom of the channel at the end of the experiment was lower. Such an anomaly in temperature behavior was always observed at the interface between the prepared ice accretion and the bottom of the channel. At this interface, the oscillations of temperature occur at the beginning of the icing process. These oscillations are related to fluctuations in the main direction of latent heat transfer and go from the one occurring throughout the accreting ice layer to

the one released into the ambient medium. As the ice accretion develops, the oscillations die down and the entire heat flux is directed towards the ambient medium solely as a result of the low value of the coefficient of the heat conduction of ice.

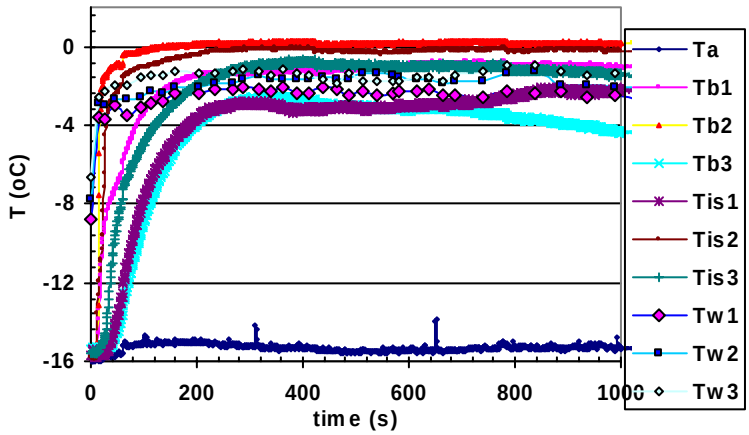

Fig. 1. Typical plot of the temperatures measured by thermocouples and IR camera during the experiment with a small channel and V_a=20 m·s^{-1}: T_a – air temperature; T_b – temperature of bottom of the channel; T_{is} – ice surface temperature; T_w – temperature of the surface of flowing water measured by IR camera. 1,2 and 3 designate chosen sites

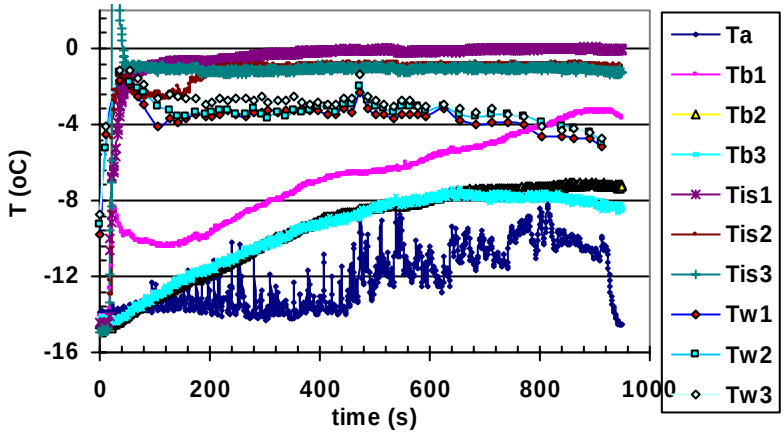

Fig. 2. Typical plot of the temperatures measured by thermocouples and IR camera during the experiment with a large channel and V_a=30 m·s^{-1}: T_a – air temperature; T_b – temperature of the bottom of channel; T_{is} – ice surface temperature; T_w – temperature of the surface of flowing water measured by IR camera. 1,2 and 3 designate chosen sites

Consequently, the icing surface, after initial temperature surge, chills gradually to the ambient temperature. The temperature of the ice surface, even under conditions for water film appearance, remains negative at all times throughout the entire ice accretion process. This temperature displays some weak lengthwise distribution from the leading edge of the channel, where the supercooled aerosol is supplied, to its trailing edge, where the water rivulets form and freeze. From the comparison of the two figures, it may be concluded that the supercooling of flowing water film on the surface of ice depends on the air speed: for V_a=30 m·s^{-1} it is about -4 ^{o}C, as compared to the lower supercooling of -2^{o}C obtained whith the air speed of 20 m.s^{-1}. The investigation should be, however, made in the future concerning the role of initial ice thickness.

During the process of ice formation, the local temperature of a supercooled water film changes slightly over time, displaying a final stabilization depending on the given ambient conditions. It was found that heat transfer throughout the water film to the concurrent air flow is a pivotal factor in maintaining a water film on the ice accretion being formed at the bottom of the channel.

CONCLUSIONS

The results of spatio-temporal remote IR and traditional thermometry measurements were presented and discussed in this investigation into the surface temperatures of an ice-covered channel during the process of ice accretion in an icing wind tunnel. It was demonstrated that the surface temperature of accreting ice, i.e. the surface temperature of flowing water film, remains supercooled at all times during the experiment. The lengthwise temperature distribution in bulk ice accreted at the bottom of the channel and in flowing water film was observed and recorded. In spite of the theory (Messinger, 1955) which proposes the assumption, that the surface temperature is 0^{o}C for the icing regime with a water film on the ice surface, the temperatures of water flowing on the surface of prepared ice were negative even when frozen rivulets were observed at the trailing edge of the channel providing evidence of flowing water. It should be noted that the terminology “wet” and “dry” which since the time of Schumann’s theoretical work (1938) is usually applied in various models in order to distinguish between the ice accretion icing regimes with and without a water film on the icing surface, has now become obsolete and misleading in the light of further research. Finding an alternative to the contemporary distinction between the two icing regimes mentioned should be the main objective of subsequent research in the physics of atmosphere and atmospheric icing. To date, only one theory (Kachurin, 1962), mentioned in the Introduction, satisfies the requirements, and with certain modifications (Karev et al., 2003a and b), should be tested in future experimental work.

ACKNOWLEDGMENTS

This study was carried out within the framework of the NSERC/Hydro-Quebec Industrial Chair on Atmospheric Icing of Power Network Equipment (CIGELE) at the University of Quebec in Chicoutimi. The authors would like to thank all the sponsors of the CIGELE for their financial support. Valuable help provided by CIGELE technician P.Camirand in designing and manufacturing devices for this experimental series is also gratefully acknowledged. We are also most grateful to M. L. Sinclair for editorial assistance.

REFERENCES

Greenan, B. J. W. and List, R. Experimental closure of the heat and mass transfer theory of spheroidal hailstones. *J. Atmos. Sci.* 52 (1995) 3797- 3815.

Gvelisiani, A.I. On ice deposits growing in the flow of supercooled water aerosol on surfaces of different form, *Reports Akad. Nauk GSSR* 51 (1968) 63-68.

Kachurin, L.G. On airplane icing theory, *Izv Akad Nauk SSSR, Ser Geofiz* 6 (1962) 823-832.

Kachurin, L.G., Gashin, L. I., and Smirnov, I. A. The intensity of icing of small fishing vessels under different hydro-meteorological conditions. *Meteor. i Gidrol*. № 3 (1974) 50-59.

Karev, A. Thermodynamic and radar properties of water skin on the surface of growing hailstones, *Russian Meteorology and Hydrology*, № 2 (1993) 37-43 (46-52).

Karev, A.R., Farzaneh M., and Lozowski E.P. Character and stability of a wind-driven supercooled water film on an icing surface I. Laminar heat transfer. *International Journal of Thermal Sciences* 42 (2003a) 481-498.

Karev, A.R., Farzaneh, M., and Lozowski, E.P. Character and stability of a wind-driven supercooled water film on an icing surface II. Transition and turbulent heat transfer. *International Journal of Thermal Sciences* 42 (2003b) 499-511.

Karev, A.R. and Farzaneh, M. Infrared laboratory measurement of ice surface temperatures during experimental studies on the formation of ice accretion. *Proceedings of the 13th Conference of International Society of Offshore and Polar Engineering (ISOPE),* Honolulu, Hawaii, USA, 25-30 May 2003, 390-397.

List, R. Physics of supercooling of thin water skins covering gyrating hailstones. *J. Atmos. Sci*. 47 (1989) 1919-1925.

List, R, Garcia-Garcia, F, Kuhn, R, and Greenan, B. The supercooling of surface water skins of spherical and spheroidal hailstones, *Atmos. Res.* 24 (1989) 83-87.

Messinger, B. L. Equilibrium temperature of an unheated icing surface as a function of air speed. *J. Aero. Sci.* 20 (1953) 29-42.

Rees, W.G. and James S.P. Angular variation of the infrared emissivity of ice and water surfaces, *Int J Remote Sensing*, 13 (1992) 2873-2886.

Schumann, T.E.W. The theory of hailstone formation. *Quart. J. Roy. Meteorol. Soc.* 64 (1938) 3-21.

17th International Symposium on Ice
Saint Petersburg, Russia, 21 - 25 June 2004
International Association of Hydraulic Engineering and Research

METEOROLOGICAL OBSERVATIONS AND METHOD FOR ESTIMATION OF ICE PRODUCTION RATE IN FISH PORT OF HOKKAIDO DURING WINTER SEASON

Shinji Kioka[1], Daisuke Honma[1], Yasuji Yamamoto[1]
Michihiro Nishida[2] and Takashi Terashima[3]

ABSTRACT
Weather observation was conducted at Otsu Fishing Port facing the Pacific Ocean in the eastern part of Hokkaido, which suffers serious damage from freezing nearly every year, in the winter of 2002 to 2003. The negative total heat flux (total heat loss) was the highest from early dawn to dawn, proving the acceleration of freezing early in the morning. Also, in comparing the absolute value of each heat flux at there, that of the net solar radiation was highest, followed by the net long-wave radiation, sensible heat flux and latent heat flux. The percentage of the net long-wave radiation (long-wave backward radiation) was the highest in terms of total heat loss at over 50%. Also, as a result of an on-site survey of the rates of frazil ice production with the intention of removing frazil ice as a measure against port freezing, it was confirmed that frazil ice production was highly dependent on not only heat flux, but also on the physical action of wind that controlled the heat release area of the water surface.

INTRODUCTION
Harbor freezing, a phenomenon in which water in harbors freezes during winter, causes considerable economic damage to ports, harbors and fishing ports in Hokkaido, which is located in the northern part of Japan, due to the impossibility of fishing and anchorage, damage to ships and other problems. The authors are engaged in the development of a multipurpose freezing simulation model that can be used as a tool to provide a relative evaluation of proposed countermeasures for Otsu Fishing Port, which suffers serious damage from freezing nearly every year (Honma et al., 2002). The port is a excavated-type fishing port facing the Pacific Ocean in the eastern part of Hokkaido and situated at the southwest corner of the estuary of the Tokachi River (see Figs. 1 and 3). Figure 2 shows the condition of port freezing that occurred at Otsu Fishing Port in 2000.

[1] Port and harbor eng. division, Civil Engineering Research Institute of Hokkaido, Hiragishi 1-3-1-34, Toyohira-ku, Sapporo, 062-8602, Japan
[2] Hokkaido regional development bureau, Obihiro development and construction department, Minami 8-chome, Nishi 4-jo, Obihiro, Hokkaido 080-8585, Japan
[3] Kumashiro System Frontier Co.,Ltd. Kitabiru-6F, 8, N-7,W-2, Sappro,060-0807, Japan

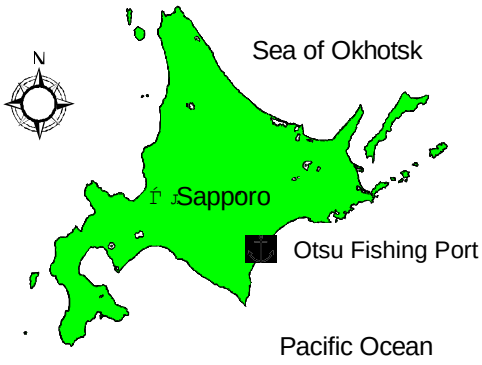

Fig. 1. Map of observation site

Fig. 2. Port freezing in Otsu Fishing Port (in winter,2000)

One of the main factors behind the freezing of this fishing port is the relatively low air and water temperatures in winter. It has also been pointed out that, because the port is excavated, tidal exchange (or heat exchange) with the open sea is unlikely to occur, and also that it is difficult for produced frazil crystals and pancake ice to be removed. Heat fluxes, such as solar radiation and long-wave radiation, necessary for this freezing simulation were obtained by using weather data provided by the Japan Weather Association from weather stations relatively close in proximity to Otsu Fishing Port (Obihiro Weather Station, Otsu AMeDAS, etc.) or estimated indirectly by calculation. It was, however, doubtful whether these heat fluxes truly represented the actual fluxes at the site. Weather observation, including direct, on-site measurement of solar and long-wave radiation, was therefore conducted in the winter of 2002 to 2003.

This study clarifies the weather/heat fluxes at Otsu Fishing Port in winter using field observation data, and compares the heat fluxes estimated from the observation values at the Obihiro Weather Station and/or by calculation using the weather data and data obtained by field observation. Also, an on-site survey of frazil ice production in Otsu Fishing Port per unit of area and time was also conducted, and the relationship with the obtained weather data was studied. This attempt is important for examining the removal of frazil ice, which is one of counter-measures against freezing.

OBSERVATION METHODS

Weather observation

For weather observation, weather observation equipment with instruments to measure wind direction/speed, air temperature, water temperature, net solar radiation and net long-wave radiation was placed on the marsh side, as shown in Fig.3, to collect data between December 2002 and March 2003. Since it was difficult to take direct measurements of the sensible heat flux and the latent heat flux, they were estimated using Kondo's method (1975),

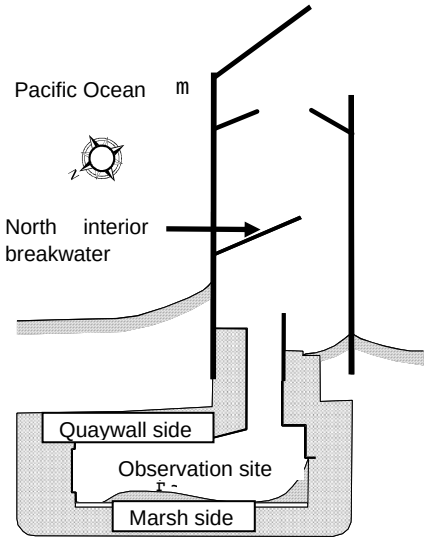

Fig. 3. General view of Otsu Fishing Port

as mentioned below. For relative humidity, data from the Obihiro Weather Station provided by the Japan Weather Association were used.

Survey of frazil ice production

A wooden frame (1 x 3 m) was moored near the area where the weather observation equipment was placed. A net was attached to the bottom of this frame. The wooden frame was moored at one point of the mooring pile on the marsh side, so that its direction changed with the direction of the wind. The survey was conducted starting at 18:35 on December 26, 2002, and lasted until 6:35 on the following day; the amount of frazil ice crystals produced in the frame was measured at intervals of 90 to 120 minutes. We then estimated the rate of frazil ice production.

HEAT BALANCE PROPERTIES OF OTSU FISHING PORT IN WINTER

Figure 4 illustrates an example of the comparison of each heat flux (net solar radiation, net long-wave radiation, sensible heat flux and latent heat flux) per unit of time. To make it easier to understand the figure, the heat flux for three days starting at noon on December 20 is given as an example. Figure 5 presents the changes of total heat flux (net energy flux) in each time period of the day during four different periods (Dec. 20 to Jan. 10, Jan. 10 to Jan. 31, Feb. 1 to Feb. 19 and Feb. 20 to Mar. 12). The total heat flux is shown as the mean value of the total amount per three hours. The total heat flux here is the total of the above-mentioned fluxes. In this case, heat transfer from under the sea was not taken into consideration. These figures show that the total heat flux was positive during the day, with the majority of it produced by solar radiation, and it was negative in the morning, evening and night. Regarding the value per unit of time (total amount per three hours), this heat loss was nearly equivalent to the positive total heat flux (in real terms, the net solar radiation) during the day. This total heat flux would be balanced with latent heat generated by phase changes in ice. It was therefore presumed that freezing/growing and melting were repeated as the increase in ice thickness. Although this particular winter was relatively warm, the positive total heat flux (in real terms, the net solar radiation) per unit of time was equivalent to the heat loss at night, and was unexpectedly high, as mentioned before. Also, the negative total heat flux (total heat loss) was the highest from early dawn to dawn as shown in Figs. 4 and 5, proving the acceleration of freezing early in the morning, which has already been confirmed empirically.

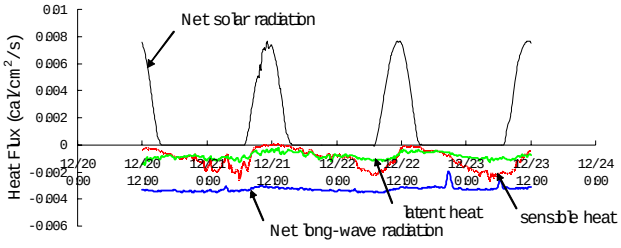

Fig. 4. Example of the comparison of each heat flux

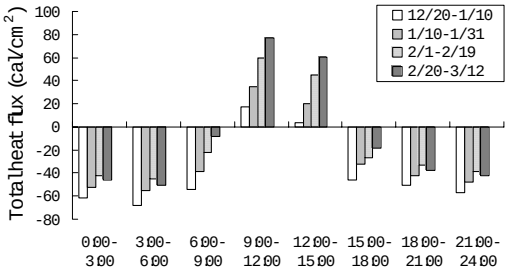

Fig. 5. Changes of net energy flux in each time period of the day

Next, one day was divided into two with the intention of roughly determining the rate of each heat flux (percentage of each heat flux in the total). Figure 6 shows a comparison of each heat flux (total amount per 12 hours) during the day (6:00 – 18:00) and night (18:00 – 6:00) (Jan. 10 to Jan. 31 as an example). The value of net solar radiation was the

highest, followed by net long-wave radiation, sensible heat flux and latent heat flux. The last three fluxes were negative (heat loss) throughout nearly the entire measurement period, and the percentage for the long-wave radiation balance (long-wave backward radiation) was the highest in total heat loss at over 50%. Ishikawa et al. (1984) observed heat balance on the sea ice in Lake Saroma, which faces the Sea of Okhotsk, and reported a similar tendency. The figure also shows the changes in cloudiness (at the Obihiro Weather Station), indicating that the solar radiation and long-wave radiation properties are especially dependent on cloudiness. As is widely known, this causes radiation cooling.

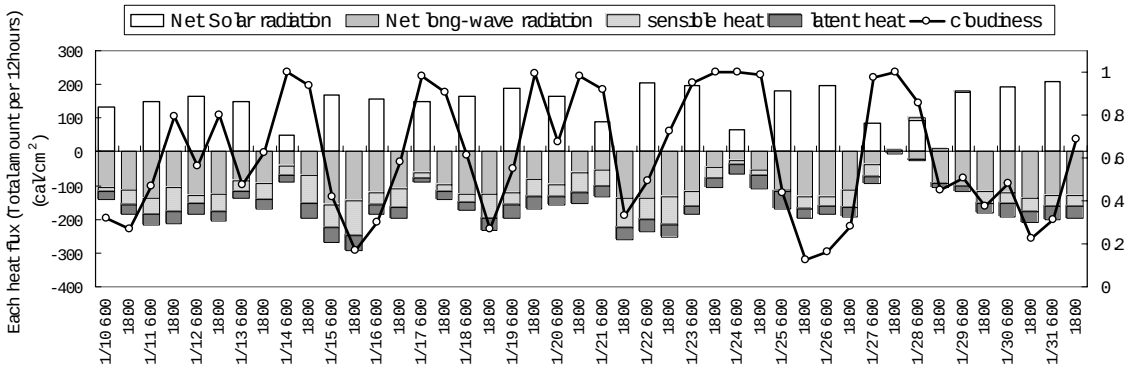

Fig. 6. Comparison of each heat flux (total amount per 12 hours) during the day (6:00 – 18:00) and night (18:00 – 6:00) (Jan. 10 to Jan. 31 as an example)

COMPARISON OF THE ON-SITE MEASUREMENT VALUE OF HEAT FLUX AND THE VALUE CALCULATED USING THE DATA OBTAINED FROM THE NEARBY WEATHER STATION (OBIHIRO)

Heat fluxes, such as solar radiation and long-wave radiation, necessary for the freezing simulation developed by the authors, were obtained by using weather data (solar radiation, cloudiness, water vapor pressure, relative humidity, air temperature, wind direction/speed, etc.) provided by the Japan Weather Association from weather stations in proximity to Otsu Fishing Port or estimated indirectly by calculation. It was, however, doubtful whether these heat fluxes accurately represented the actual fluxes at the site. Another primary purpose of this section is to examine the setting of input information, including weather data necessary for studying the effect of countermeasures by numerical simulation. If there is no significant difference between the heat flux values of the two (on-site measurement data and the data obtained from the weather station and calculated value), we can use weather data of the past several decades accumulated by a nearby weather station. Therefore, the probability year of cold (representative value concerning heat loss, index) can be specified, and quantitative evaluation concerning the effects of countermeasures is possible according to the probability year.

Comparison of solar radiation

As mentioned above, a comparison was made between the two data concerning the solar radiation whose contribution is great as already stated (figure omitted). Obihiro is located in an inland urban area approximately 50 km northwest of Otsu Fishing Port. Although solar radiation depends heavily on cloudiness, the two corresponded well with each other, and the basis for using data from the weather station was determined.

Examination concerning net long-wave radiation

The net long-wave radiation was estimated by calculation because there is no observation data from the weather station. While several estimated formulas have been proposed concerning long-wave radiation, an empirical formula by Clark et al. (1974), which was thought to be most suitable for this case, was used as shown in the equation below. This formula takes the effect of cloudiness and the difference between the surface and air temperature into account based on Brunt's formula, which is frequently used.

$$Q_L = \varepsilon\sigma T_S^{\,4}(0.39 - 0.05e^{1/2})(1 - B_L C^2) + 4\varepsilon\sigma Ts^2(T_S - T_a)\,. \qquad (1)$$

Where ε is the long-wave emissivity of sea ice/seawater (= 0.97), σ is the Stefan-Boltzmann constant, $B_L = 0.51+0.0044$ *lat*(*lat*; latitude), *C* is cloudiness, T_S is the surface temperature of water surface/sea ice (K), T_a is air temperature (K) and *e* is the water vapor pressure of the air. Here, the net long-wave radiation was estimated from the equation given above, using the cloudiness and water vapor pressure of the air obtained from the Obihiro Weather Station and the air temperature obtained from the Otsu AMeDAS, and compared with the on-site observation data as shown in Fig. 7. Although the surface temperature of sea ice/seawater is necessary, it is not usually provided and, in this case, the calculation was conducted on the assumption that it was at the freezing point. In this figure, the two roughly correspond with each other, including variation characteristics. Since this heat flux is presumed to account for the largest percentage of heat loss, the possibility of estimation from weather data by a weather station is considered significant.

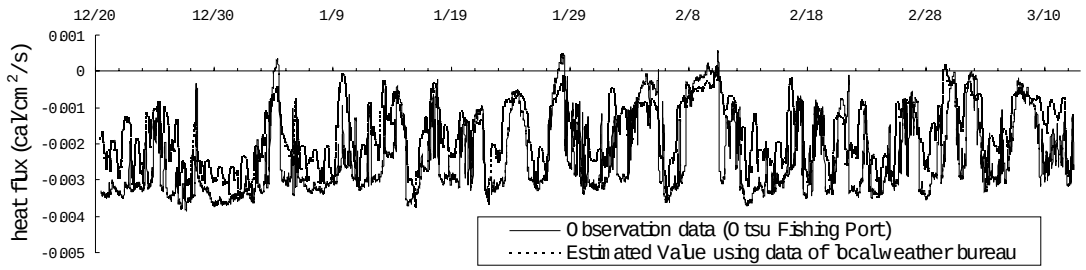

Fig. 7. Comparison of net long-wave radiation between observation data and estimated value using data of Obihiro Weather Station and Otsu AMeDAS

Estimation of sensible and latent heat fluxes

The eddy correlation and other methods are used for direct measurement of latent and sensible heat flux. In this study, estimation was made by the standard bulk aerodynamics method using wind speed, air temperature and other data. The calculation formulas of sensible heat flux (Q_H) and latent heat flux (Q_E) can be expressed by the following equations, respectively:

$$Q_H = \rho c_P C_H V(T_s - T_a)\,, \qquad (2a)$$

$$Q_E = \rho L C_E V(q_s - q_a)\,. \qquad (2b)$$

In these equations, ρ is the atmospheric density, c_p is the specific heat capacity of the atmosphere at constant pressure, *V* is wind speed, *L* is the latent heat of evaporation, q_s is the saturated specific humidity of the air for the water/ice surface temperature and q_a is the specific humidity of the air for the water/ice surface temperature. The water vapor pressure was calculated by first finding the saturated water vapor pressure using Tetens'

formula (1930) and then multiplying this by the relative humidity. The water vapor pressure at the water/ice surface was found as the saturated state. Coefficients C_H and C_E were dependent on the wind speed and atmospheric stability, and Kondo's formula (1975) was employed. Since these are only estimated values, they have not been verified by direct measurement and some ambiguity still remains. It is, however, considered to be sufficient if a certain degree of approximate values can be found because, as was mentioned in the purpose stated at the beginning of this section, the percentage of this amount in heat loss seems not to be large in comparison with that of net long-wave radiation.

DISCUSSION ON FRAZIL ICE PRODUCTION

"Removal of frazil ice" can be considered to be one of countermeasures for port freezing. In other words, it is an attempt to remove and collect frazil crystals in advance using an ice boom or other means before ice forms plates. In this case, it is important to estimate frazil ice production so as to determine the specifications of the ice boom, timing of collection and other factors; therefore, a survey on the frazil ice production rate per unit of time and area was conducted. The observation method was presented earlier. Figure 8 (a) shows the observed and calculated values of the rate of frazil ice production. The observed values in the figure were obtained by converting the frazil ice production obtained in the time period (flat part of each line) into the amount per unit of time and area ($g/m^2/min$), simply by dividing it by the time interval and area of the frame. The calculated value was found by dividing the above-mentioned total heat flux (net energy flux) by the heat of fusion of ice on the assumption that heat supply from the open sea and underwater could be ignored. Figures 8 (b) and (c) present each respective heat flux, air temperature and wind speed during the survey period, respectively. While frazil ice production began to show a tendency to increase at around midnight on the 27th and an increase in heat loss was expected, it was actually observed that each heat flux tended to decrease. In particular, the decrease in net long-wave radiation and the increase in wind speed also began at around midnight on the 27th. Looking at the changes in cloudiness shown in Fig. 8 (b), it was presumed that the

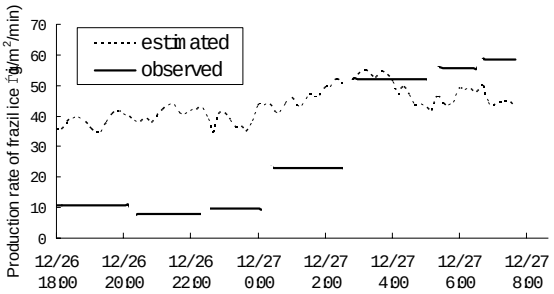

Fig. 8(a). Observed and calculated values of the rate of frazil ice production

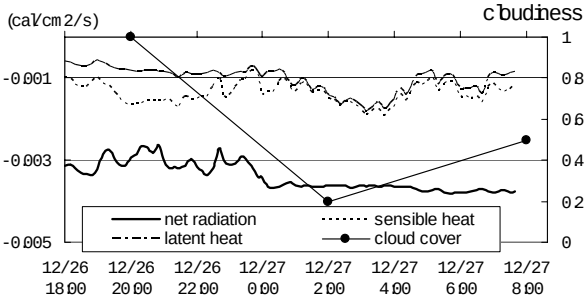

Fig. 8(b). Heat fluxes during the survey period

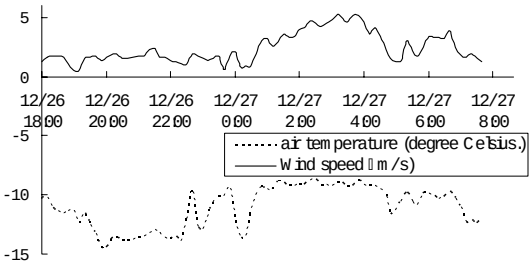

Fig. 8(c). Air temperature and wind speed during the survey period

decrease in net long-wave radiation in this case corresponded with the change from cloudy to sunny weather, and that the decrease in sensible heat flux (negative increase) was caused by the increase in wind speed. Although no particular tendency to decrease was seen for latent heat flux since it was set off by the temperature rise, the total amount of heat flux (net energy flux) tended to decrease and, as shown in Fig. 8 (a), the calculated value of frazil ice production using this total amount of heat flux also indicated this tendency. In the first half, however, the calculated value exceeded the observed value. Although this was probably due to the ambiguity of the observed value (accurate on-site measurement of frazil ice is difficult), it was presumed that it could not be explained with only the calculation formula used for the estimation, or the above-mentioned increase and decrease in each heat flux. This calculation formula is ideally equivalent to the instantaneous value the frazil crystal produced on the water surface, which uniformly reached the freezing point. To examine this, an experiment by Ushi et al. (1993) will be introduced. Ushio et al. (1993) studied frazil ice production, its brine drainage and other factors with a wind speed of 2.2 to 6 m, room temperature of –10 to –30 and water salinity between 0 and 35%, using a water tank measuring 2 m in length, 0.4 m in width and 0.6 m in depth in a cold room. This study was carried out in an attempt to examine radiation characteristics and other factors in an area with an ice-free water surface referred to as a "lead" or "polynyas," which is observed in strong wind zones and very cold zones, in particular. Figure 9 shows an example of the obtained results. According to Ushio et al. (1993), when the water salinity is 25% or higher, or when the temperature with the maximum density is lower than the freezing point, crystals formed on the water surface are transferred to one side (the lee side) by wind under relatively weak wind conditions (2.2 m/s), the area of the open water surface decreases and frazil crystal production is relatively small (frazil crystals cover the water surface quickly and the layer is thin). Under relatively strong wind conditions (6 m/s), on the contrary, the supercooled top of the surface layer sinks into the water due to the forced convection of wind in addition to natural convection, frazil crystals form underwater in large amounts and then form a thick accumulation on the lee side. As a result, a larger open water surface than the former (the case in which wind speed is 2.2 m/s) is maintained, and heat release and frazil crystal production therefore increase. They also indicate that frazil crystal production depends greatly on the salinity of the original water. Here, the above-mentioned changes in observation values for this study will be examined in comparison with this experiment by Ushio et al. (1993). The wind speed in the first half, or when frazil crystal production was relatively low before midnight on the 27th, was approximately 2 m/s and subsequently increased. The time when the wind speed changed corresponds with the time when frazil crystal production increased. In other words, heat release was controlled by frazil crystals covering the water surface in the first half and, to the contrary, frazil crystals are formed underwater by convection of wind and transferred to the lee side in the latter half (some frazil crystals outside the wooden frame must have been trapped by the net under the frame). As a result, a relatively

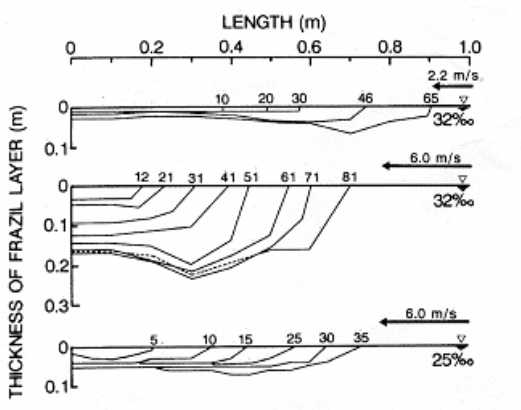

Fig. 9. Cross section of accumulated frazil ice layers [Ushio et al., 1993] Wind is blowing from the right. Contour values above the water surface give the elapsed time (min.) from onset of wind blowing. In all cases, air temp. is equal to -10 deg. Celsius

large open water surface was maintained, and higher heat release continued. Although a significant difference like this one in the open water was not recognized within the wooden frame, it would have been necessary to take the water outside of the frame into consideration as well. It was naturally presumed that heat supply by warm seawater from the open sea might be also influential in the first half. The survey results of Ushio et al. (1993) and the observation values of this study were compared. In the case of Ushio et al., the maximum value was 20g/m^2/min with a wind speed of 2.2 m and at the temperature of -10 (correspondent with the first half of our observation), and was 140g/m^2/min with a wind speed of 6 m and temperature of -10 (correspondent with the latter half of our observation). While it is of course impossible to make a simple comparison of the two due to the differences in various conditions, the ratio was similar to the variation characteristics of frazil ice production in the first and latter half of this observation (the production in the latter half was approximately 7 times as high as that in the first half). It was therefore confirmed that frazil ice production was highly dependent on not only heat flux, but also on the physical action of wind. When adopting frazil ice collection as a countermeasure, the timing of collection was also considered important from a practical standpoint. It has been observed that frazil ice generation on open water surfaces is generally several times higher than ice sheet growth[9)]. It is therefore inefficient to collect frazil crystals constantly every time they are produced because it will increase the heat release area and cause further acceleration of frazil crystal production. On the contrary, the formation of thick ice sheets may lead to difficulty in breaking and removing ice and require extra labor.

CONCLUSION

In comparing the absolute value of each heat flux at Otsu Fishing Port, that of the net solar radiation was highest, followed by the net long-wave radiation, sensible heat flux and latent heat flux. The percentage of the net long-wave radiation (long-wave backward radiation) was the highest in terms of total heat loss at over 50%. From the results of this survey on heat flux, a method for securing the minimum necessary water surface can be proposed as a countermeasure. In other words, heat loss of long-wave backward radiation, sensible heat and latent heat can be controlled while using solar radiation during the day by simply placing floating domes on the water surface to the extent that vessels can travel. Although it is a simple method, considerable effects might be expected. In this case, it is of course assumed that the water surface outside the domes is frozen. Also, as a result of an on-site survey of frazil ice production with the intention of removing frazil ice as a measure against port freezing, it was confirmed that frazil ice production was highly dependent on not only heat flux, but also on the physical action of wind that controlled the heat release area of the water surface. It was also pointed out that timing is important for efficient frazil ice collection.

REFERENCES

Honma, D, Umezawa,D.,Yamamoto, Y., Kioka,S., Kawaguchi,T.: Development of Numerical Simulation Model of Freezing Process in Habor and Demonstration for Its Practical Use, *Proc.of Coastal Engineering,JSCE,*Vol.49, (2000)1261-1265.

Kondo,J.: Air-sea bulk transfer coefficients in diabatic conditions, *Boundary-Layer Meteor*.,9,(1975) 91-112.

Ishikawa N.and Kobayashi,S.: Experimental studies of heat budget of very thin sea ice, *Journal of the Japanese Society of Snow and Ice,* 46,3 (1984) 109-119.

Ushio,S.and Wakatsuchi, M.:A Laboratory Study on Supercooling and Frazil Ice Production Processes in Winter Coastal Polynyas, *Journal of Geophysical Research,* Vol.98, No.C11,(1993) 20,321-20,358.

17th International Symposium on Ice
Saint Petersburg, Russia, 21 - 25 June 2004
International Association of Hydraulic Engineering and Research

A PORTABLE CALORIMETER FOR MEASURING LIQUID FRACTION OF SPONGY FRESHWATER ICE ACCRETIONS

Ryan Z Blackmore[1], Edward P Lozowski[2] and Masoud Farzaneh[3]

ABSTRACT

Atmospheric icing often occurs with the incorporation of unfrozen liquid into the ice. Accurate measurement of the proportions of ice and water is essential for verification of atmospheric icing models. It is also important for producing reliable data for new ice load designs that account for the additional effects of included liquid. A calorimeter has been developed for determining the liquid fraction of freshwater ice accretions, by melting a sample in warm water. The resulting temperature change is measured and is used in a heat balance equation to determine the proportions of ice and liquid in the sample. The calorimeter has been calibrated with a set of controlled experiments. The method has then been validated using an independent data set. The calorimeter is designed for samples in the 5 to 55 g range. Over this range of sample mass, the absolute uncertainty in ice fraction varies from ±0.033 for 5 g to ±0.0092 for 55 g. The calorimeter is inexpensive, easily fabricated, and accurate enough for most purposes.

INTRODUCTION

An atmospheric ice accretion containing unfrozen liquid is said to be spongy. Spongy ice is known to occur in hailstone growth (Gitlin et al., 1968; Knight, 1968) and in aircraft icing (Fraser et al., 1952). It is suspected that spongy ice may also occur during the icing of electrical power network equipment.

Various authors have used calorimeters in their investigation of spongy ice. Lesins et al., (1980) and Blackmore et al., (2002) refer to the use of a calorimeter but give few details. In contrast, Gitlin et al., (1966) give a full description of their calorimeter. However, their approach requires a substantial investment in complex equipment. In this paper, we describe an inexpensive, portable calorimeter which has been carefully calibrated and is currently used to measure the liquid fraction of spongy ice. The

[1] Department of Natural Sciences. The King's University College, 9125-50 Street. Edmonton, Alberta, Canada T6B 2H3. email: Ryan.Blackmore@kingsu.ca
[2] Department of Earth and Atmospheric Sciences. University of Alberta Edmonton, Alberta, Canada T6G 2E3. email: Edward.Lozowski@ualberta.ca
[3] Titulaire de la Chaire CIGELE Université du Québec à Chicoutimi Pavillion de recherche sur le givrage 555, boulevard de l'Université Chicoutimi, Québec, Canada G7H 2B1
e-mail: Masoud_Farzaneh@uqac.ca

calibration process and the uncertainty in the calorimeter's measurement are described here in detail.

THE CALORIMETER AND ITS USE

The calorimeter is depicted in Fig. 1 with its lid and thermometer in place. A cross-section of the calorimeter is shown in Fig.2. The calorimeter body (2 cm sidewall thickness) and lid are fabricated of polystyrene insulation (Styrospan, thermal conductivity, k=0.027Wm^{-1}K^{-1}). This choice is a compromise between cost, compactness and the need to minimize heat loss from the warm water charge. The warm water charge is contained in a styrofoam cup (Canada Cup SM12, 11.5 cm depth) and this container is suspended by its upper rim within the calorimeter body (Fig. 2). The calorimeter lid is inserted snugly into the top of the container.

A partial immersion thermometer (Fisherbrand 15-000A) is used to measure the initial temperature of the warm water charge. The warm water charge should have a mass of about 200 g and an initial temperature in the range 45 to 50 °C. An ice sample is introduced by removing and replacing the calorimeter lid as quickly as possible, while avoiding splashing. The calorimeter is gently swirled to enhance ice sample melting and the mixing of the meltwater with the warm water charge. The temperature of the mixture is then tracked until a steady temperature is reached, typically after a few tens of seconds for a small sample (5g) to a few minutes for a large sample (55g). A mass balance is used to weigh the container, water charge and ice sample (Denver Instruments XP 600 mass balance). Once the mass of the warm water charge, the mass of the ice sample and the initial and final temperatures have been recorded, the liquid fraction of the sample is calculated using an equation derived from the calorimeter's heat balance (developed later).

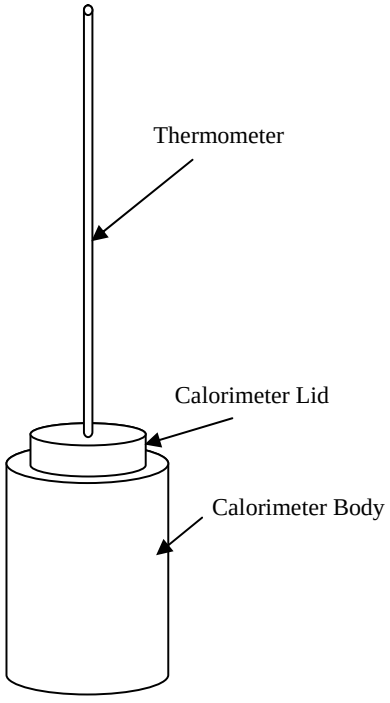

Fig. 1. Schematic of the calorimeter

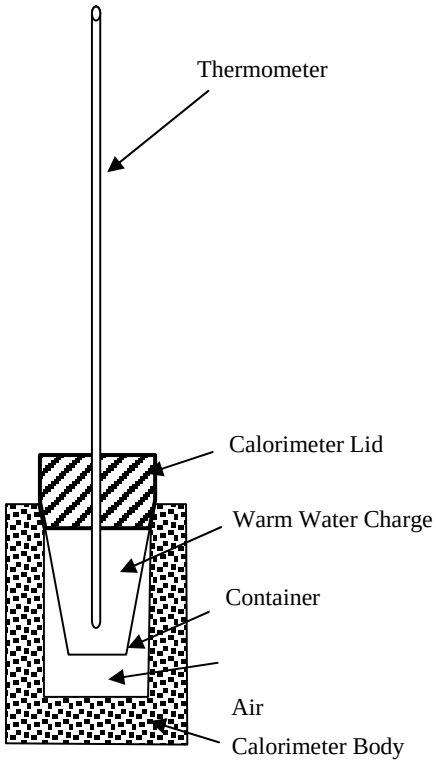

Fig. 2. Calorimeter cross-section

This is a simple and inexpensive calorimeter, which is sufficiently compact that both it and the balance can be readily packed into a small suitcase. The calorimeter's operation is described in the next section.

CALORIMETER OPERATION

The calorimeter setup

A mass balance with 300 g capacity and an uncertainty of ±0.02 g is used to weigh the warm water charge. The thermometer is then inserted through an orifice in the centre of the lid. It should penetrate into the warm water charge container by 7.6 cm, the immersion depth for the Fisherbrand 15-000A thermometer. This thermometer has a measurement range of -1 to +51 °C with a scale resolution of 0.1 °C. If a less precise thermometer is used, the calorimeter will become less accurate in measuring ice fraction.

An insulated thermos is used to store the warm water when a series of calorimeter runs are planned. The initial water temperature must be 45 to 50 °C, since the calorimeter calibration depends on it. The calculation of ice fraction is completed using a spreadsheet programmed with the calorimeter equation.

Steps in a calorimeter run

Here is the procedure for completing a calorimeter run:
1. Using a large syringe, fill the warm water charge container with 200 g (±1 g). Weigh the warm water charge, having tared the weight of the container. 2. Seal the warm water charge in the container by firmly replacing the lid and thermometer. 3 Then place the lid and container into the calorimeter body and tare this combined calorimeter weight on the mass balance. 4. Allow at least one minute for the calorimeter body to come to thermal "equilibrium" with the warm water charge and its container. 5. It is prudent to load the warm water charge (steps 1 to 4) no more than 15 minutes prior to the arrival of the ice sample. This will usually ensure that the warm water charge will not cool below 45 ºC, the lower limit of the initial temperature range for the warm water charge. 6. One minute prior to the arrival of the ice sample, swirl the calorimeter, allowing the temperature of the warm water to stabilize and record the stabilized initial warm water temperature, T_0. 7. Ten seconds before the arrival of the ice sample, loosen but do not remove the calorimeter lid and pull the thermometer up through the lid until the immersion marker is just flush with the top of the lid. 8. When the sample arrives, lift the lid and lower the sample down into the warm water, avoiding splashing. 9. Immediately, replace the calorimeter lid and begin swirling the calorimeter again, at the same time pushing the thermometer downward through the lid to ensure that there is 7.6 cm of thermometer penetration inside the container. To achieve this penetration, push the thermometer down just far enough that a penetration marker that has been fixed to the thermometer stem is flush with the top of the lid. 10. As the ice melts, monitor the temperature. When it stops dropping rapidly, record the final temperature, T_f. This temperature marks the end of the ice-melting phase in the calorimeter run. With a little experience, an operator can observe this transitional temperature because of the rather abrupt change to a nearly constant value of temperature (a cooling rate typically less than 0.1 ºC per minute, compared to 7 to 10 ºC per minute during the melting phase). 11. Weigh the calorimeter with its recently added sample mass. Since the mass of the calorimeter was tared in step 3, the mass of the ice sample can now be read directly from the mass balance and recorded. 12. Enter the two mass and temperature measurements in the spreadsheet programmed to calculate the ice fraction,

f. The formula used to calculate the ice fraction is derived from a model of the calorimeter's heat balance. This heat balance is described next.

CALORIMETRIC HEAT BALANCE

Immersion of the ice sample in the calorimeter's warm water charge melts the sample and warms the resulting meltwater, provided the sample is not too large (the calorimeter is calibrated for sample masses in the range 5g to 55g). Simultaneously, the warm water charge cools. With swirling, the two water masses mix rapidly and reach a nearly constant temperature, after which the temperature drops very slowly as heat transfer occurs into and through the calorimeter walls (typically at a rate less than 0.1 ºC per minute).

We will now formulate an energy conservation equation that takes into account the various heat fluxes that arise both within and without the calorimeter, while the system transits between its quasi-steady initial state (warm water charge and ice sample) and final state (warm water charge mixed with ice meltwater). First we consider the heat sinks.

The energy (J) absorbed in melting the ice sample is:

$$Q_{if} = -fm_s L_f \,, \tag{1}$$

where f is the mass fraction of ice in the sample (dimensionless), m_s is the mass of the sample (kg) and L_f is the specific latent heat of fusion of pure ice at the equilibrium freezing point (3.337×10^5 Jkg^{-1}). The energy absorbed in warming the meltwater from the equilibrium freezing point (0ºC) to the final system temperature, T_f (°C) is:

$$Q_s = c_w m_s (0 - T_f) \,, \tag{2}$$

where c_w is the specific heat of pure water (4.181×10^3 $Jkg^{-1}K^{-1}$).

To maintain generality, we also include a term for the energy absorbed in warming the ice sample to the equilibrium freezing point, should the ice sample initially be non-spongy and at a sub-zero temperature:

$$Q_i = c_i m_s (T_i - 0) \,, \tag{3}$$

where c_i is the specific heat of pure ice (2.080×10^3 $Jkg^{-1}K^{-1}$) and T_i (°C) is the initial temperature of the ice sample. It should be noted that Q_i and T_i are meaningful only for $T_i \leq 0$°C. Each of the heat sink terms in Eq. 1 to 3 is defined to be negative.

Next we consider the heat source. The energy produced in cooling the warm water charge (J) is:

$$Q_w = c_w m_w (T_0 - T_f) \,, \tag{4}$$

where T_0 is the initial warm water charge temperature (°C). Note that this term is positive.

The heat transfer from the warm water charge is largely responsible for melting and warming the ice sample. However, there are several other smaller sources and sinks. For example there is a sink associated with the convective heat transfer and water vapor flux that take place while the calorimeter lid is removed during insertion of the ice sample. Another source or sink is the heat transfer between the warm water charge and the walls of the calorimeter. Finally, there are virtual sources and sinks that arise from unaccounted for measurement errors in the defined terms (Eqs. 1 to 4). We will lump all of these unspecified terms into a single error term, Q_e (J).

Energy conservation can now be expressed as:

$$Q_w + Q_e + Q_{lf} + Q_s + Q_i = 0. \quad (5)$$

Substituting Eqs. 1 to 4 into Eq. 5, and solving for the ice fraction, f:

$$f = \frac{c_w m_w (T_0 - T_f) - c_w m_s T_f + c_i m_s T_i + Q_e}{m_s L_f}, \quad (6)$$

where c_w , c_i and L_f are known and m_w , T_0 , T_f , T_i and m_s are to be measured. Q_e is estimated empirically as described later.

Eq. 6 is quite general, including the possibility that there is no liquid water in the sample and that it is initially at a temperature T_i<0°C. In this case, we assume that the ice sample is fully frozen, ignoring the possibility of embedded supercooled liquid. Later we will use Eq. 6 with solid ice samples in order to check the measured ice fraction against the known ice fraction, f =1.

Normally our purpose in using the calorimeter is to measure the liquid fraction of spongy samples. We will assume that in a spongy ice sample, liquid water and ice are in equilibrium at 0°C. In this case, Q_i vanishes and Eq. 6 reduces to:

$$f = \frac{c_w m_w (T_0 - T_f) - c_w m_s T_f + Q_e}{m_s L_f}. \quad (7)$$

Before we can use either Eqs. 6 or 7, we need to estimate Q_e . The procedure for doing this is developed in the following section.

CALIBRATION

The search for a means of estimating Q_e must proceed under the assumption that it is a systematic parameter in the calorimeter's operation. If it is systematic, it should be possible to predict its value. It is likely to be a function of the manner in which the calorimeter is operated. For this reason the calorimeter's operating procedure must be followed consistently.

Substituting Eqs. 1 to 4 into Eq. 5 and solving for the error term, Q_e , results in:

$$Q_e = f m_s L_f + c_w m_s T_f - c_i m_s T_i - c_w m_w (T_0 - T_f), \quad (8)$$

where all constants and measured quantities, with the exception of either f or T_i , are known for a given calorimeter run. Consequently, Q_e could be calculated for "calibrated" spongy ice samples (T_i = 0°C) for which the ice fraction, f, is already known. Unfortunately, it is not straightforward to produce "calibrated" spongy ice samples. As a result, we have taken an alternate approach and used fully frozen samples of known initial temperature. Hence, T_i is known by measurement and the ice fraction is f = 1, so that Eq. 8 can be solved for Q_e.

We initially hypothesized that the error term, Q_e, might vary with the time required to complete a calorimeter run. However, since the duration of a calorimeter run is not typically measured, another parameter was sought. The mass of the sample, m_s, is likely to bear some relation to the duration of a calorimeter run because it will take longer to melt a larger sample than a smaller sample. But the initial ice temperature could also be a factor in run duration. Hence we have chosen the temperature change during the run, $T_0 - T_f$, which will be influenced by both sample mass and initial temperature.

Fig. 3 shows a scatter plot of Q_e versus T_0-T_f for 42 runs. Each data column represents a different category of ice mass (5g, 15g, 25g, 35g, 45g, 55g). Each column is composed of data points from seven individual experiments, conducted for a particular nominal ice mass, but with slightly different actual masses and different initial temperatures ranging from -8 to -20 °C. The slightly curved data distribution is modelled well by regression using a second degree polynomial. A plot of regression residuals shows an even and random scatter suggesting that this model is appropriate. Also the model fits the data reasonably well with a coefficient of determination of r^2=0.77. The polynomial is:

$$Q_e = -291.3 + 35.15(T_0 - T_f) - 0.5513(T_0 - T_f)^2 . \quad (9)$$

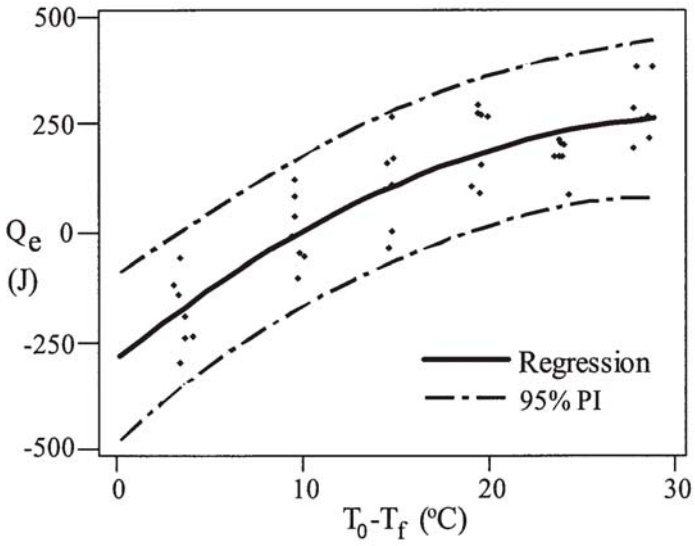

Fig. 3. Plot of the error term Q_e versus the calorimeter temperature difference for the calibration data. The vertically oriented strings of data represent the different mass categories beginning with the 5g data group at about 4°C on the temperature difference axis. The 15 g data is at 10°C, the 25 g data is at 14°C, the 35 g data is at 20°C, the 45 g data is at 24°C and the 55 g data is just under 30°C. The regression line (Eq. 9) is plotted along with the 95% prediction interval curves. The prediction interval gives an indication of the size of error to expect in using Eq. 9 to estimate Q_e

Using this empirical approximation to the error term, both Eqs. 6 and 7 can be used to calculate ice fractions when a calorimeter run gives the required quantities. Estimates of the calorimeter's uncertainty in measuring ice fraction are given in the next section.

SOLID ICE SAMPLE TEST

We established the calorimeter uncertainty by conducting a series of independent experiments, similar to those we used to determine Eq. 9. The initial ice temperatures ranged from -9 to -18 °C, so that the true ice fraction was unity. For these experiments, the ice fraction was calculated using Eq. 6 with Q_e from Eq. 9. At least 15 cases were run, for each of 7 nominal sample mass categories (5 g, 10 g, 15 g, 25 g, 35 g, 45 g and 55 g). The number of data points and 95% confidence intervals for each mass category appear in Table 1. The uncertainties in Table 1 range from a high of ±0.033 for a 5 g sample to a low of ±0.0062 for a 45 g sample.

Table 1. The nominal mass categories, the number of observations for each category, *n*, and the 95% confidence intervals of ice fraction from the solid ice sample tests

Mass Category	5 g	10 g	15 g	25 g	35 g	45 g	55 g
n	17	16	15	16	15	15	15
95% confidence intervals	0.9960 ±0.033	1.0028 ±0.026	1.0045 ±0.013	1.0010 ±0.012	0.9986 ±0.0093	1.0000 ±0.0062	1.0003 ±0.0092

CONCLUSIONS

We have designed, calibrated and tested an inexpensive, easily-fabricated, portable calorimeter to measure the liquid fraction of spongy ice accretions. The calorimeter is designed for ice samples in the 5 to 55 g range. By applying a correction factor dependent upon the temperature change in the calorimeter, we can determine the ice fraction with an absolute uncertainty of less than 0.033. As the liquid fraction is simply *1-f*, the uncertainty in the liquid fraction is similar. Since, for most purposes, a liquid fraction error of ±0.033 or less would be quite acceptable, it appears that the present calorimeter is a suitable instrument for measuring the liquid fraction of spongy ice.

ACKNOWLEDGEMENTS

This research was funded through a grant from the Canadian Foundation for Climate and Atmospheric Sciences.

REFERENCES

Blackmore, R.Z., Makkonen, L. and Lozowski, E.P. A new model of spray icing from first principles. *Journal of Geophysical Research 107(D21):* 4563, doi: 10.1029 / 2001JD001223: AAC9-1 – AAC9-15 (2002).

Fraser,D., Rush,C.K. and Baxter,D. Thermodynamic limitations of ice accretion instruments. *NRC NAE, Canada, Laboratory Report* LR-32, 12pp (1952).

Gitlin, S.N., Fogler, H.S. and Goyer, G.G. A calorimetric method for measuring water content of hailstones. *Journal of Applied Meteorology* 5(10): 715-721 (1966).

Gitlin, S.N., Goyer, G.G. and Henderson, T.J. The liquid water content of hailstones. *Journal of the Atmospheric Sciences* 25(1): 97-99 (1968).

Knight, C.A. On the mechanism of spongy hailstone growth *Journal of the Atmospheric Sciences 25*: 440-444 (1968).

Lesins, G.B., List R. and Joe, P.I. Ice accretions, part I, Testing of new atmospheric icing concepts. *Journal de Recherches Atmospheriques 14*: 347-356 (1980).

17th International Symposium on Ice
Saint Petersburg, Russia, 21 - 25 June 2004
International Association of Hydraulic Engineering and Research

SOME PENDING PROBLEMS IN RIVER ICE RESEARCH

Einar Tesaker[1]

ABSTRACT
Ice research dates back at least 80 years. Many results have been achieved; other topics have been left unsolved. There is a lack of results that can serve as guidelines for practical applications. A few pending topics are reviewed and discussed in this paper: 1) The viscosity and turbulent diffusion of water/frazil mixtures. 2) The formation and release of anchor ice. 3) The conditions for and the timing of disastrous ice runs. 4) Effects of ice cover and hanging dams on movable river beds are now actively studied due to the influence on habitat conditions under ice cover, but yet incompletely understood. 5) An unsolved problem is the correction of winter discharges under ice, obtained from ice free stage recordings. This is closely connected to under-ice friction under varying conditions and also related to the other topics mentioned.

INTRODUCTION
Ice research is much older than the first ice symposium in 1970. Publications by Altberg (1923) and Devik (1931) are examples of classical works on ice formation. The author has been involved since 1964. Outdoor ice research is hampered by frequent weather changes and difficult conditions for instrumentation. Therefore, many outdoor research programs have been aborted before significant results have been achieved. Some aspects of ice, mechanical as well as hydraulic, have therefore been studied in cold rooms or even in room temperature, using substitutes for ice. Many results have been achieved, but there are also topics that have been left unsolved for lack of methods or resources. A few pending topics will be discussed in this paper.

THE VISCOSITY OF FRAZIL/WATER MIXTURES
Ice formation influences on the water flow in various ways. The author's first introduction to ice research was an outdoor study of possible effects of frazil content on the dynamic viscosity and the turbulent diffusion coefficient of water/frazil mixtures. These basic questions were part of an approach 1964-70 to quantify the “winter coefficient”, a correction factor for winter discharges derived from ordinary staff readings (Tesaker, 1970). Since the viscosity of water rises with decreasing temperature, it was assumed that addition of frazil would have observable influence on the shear properties of water near 0°C.

[1] Tesaker Vann AS, Lerkeveien 8B, NO 7072 Heimdal, Norway, einar.tesaker@online.no

In 1964 a secondary channel was blasted parallel to a frazil-producing river reach. Installations were arranged for control of water depth and surface slope with and without notable frazil content. The facilities and methods proved too inaccurate, however, and the outdoor conditions too variable too give reliable results. Later a new attempt was made in an indoor circulating flume, also with meager results for this particular purpose. (Loktu, Roen & Tesaker, 1964).

Some principal effects of frazil/water mixtures were discussed by Gee Tsang (1970). His presentation triggered interesting comments, but since then little has been published to clarify the topic. The flow of water during the freezing process is therefore still ready for further research. It is 100 years since Prandtl (1904) introduced the principles of flows with small viscosity, and it may be time for further progress.

ANCHOR ICE, ITS FORMATION AND RELEASE

Anchor ice is swampy ice accumulations on submerged structures or at the river bed itself. It is common in shallow rivers early in the freezing season, mainly during periods with air temperatures -10ºC or lower and before other ice forms have developed. As soon as an ice cover has formed, further development of anchor ice is halted.

The anchor ice has many implications, such as flooding due to reduced cross sections, and even more flooding when a series of anchor ice dams break, forming so-called ice runs, eventually depositing the ice as jams on flat or narrow reaches. Head loss in power plants is another effect due to constriction of intakes or raised tailwater level.

The formation of anchor ice has been a topic under frequent discussion, while the phenomenon itself is well known, and is precisely described, e.g. in Ashton (1986). Early theory assumed direct nucleation from supercooled water elements, carried by turbulence and nucleated by contact with the solid objects (Altberg 1923; Devik, 1931). Indoor flume experiments have been used as evidence (Tesaker, 1994). This is now to some extent challenged by theories claiming that anchor ice is caused by adherence of suspended frazil particles by impact or deposition (Kerr, Shen and Daly, 1998). Combinations of these effects are probably closer to reality. Both old and new experiments confirm that frazil particles develop and grow inside turbulent flows cooled from the surface (Carstens, 1966: Clark & Doering, 2002). Both references mention suspended mineral particles as possible nucleation cores. Carstens (1966) describes how addition of extra particles or even air bubbles seem to promote the nucleation rate. Local turbulence is another cause of nucleation.

According to Clark & Doering (2002) frazil may form and grow inside the flow even when the ambient water has temperature slightly above 0ºC. This implicates that pockets of supercooled water may exist inside warmer water until being triggered to nucleation by some cause. It seems logical to include the bed and solid structures as triggering causes. The amount of supercooled filaments brought in suspension is limited by the cooling rate. It is therefore less chance of nucleation at solid boundaries the more frazil particles that already exist in suspension. This is in agreement with observations in the field: The more visible drifting frazil, the less anchor ice formation.

Growing frazil particles still in contact with pockets of supercooled water, may attach to any receiving body. The swampy texture of existing anchor ice may filter passive frazil-water mixtures, catching the suspended frazil. Whether passive frazil particles tend to

adhere to structures by impact seems more dubious, since the particles are less dense than the ambient water and therefore without inertia for impact in rotating flow. In conclusion, growth of anchor ice from suspended frazil is possible, but probably not the main cause. The riddle of anchor ice formation seems still open for creative research.

PREDICTION, TIMING AND CONTROL OF VIOLENT ICE RUNS

The conditions for release of anchor ice and timing of disastrous ice runs are still not fully understood. These are problems of great practical importance, since protection against ice runs is difficult and often inefficient if not timed correctly. The key is to avoid formation of big anchor ice dams, or if formed, to avoid sudden collapses starting full clearing of ice from a river reach. Many measures have been proposed and some also tried (Carstens and Tesaker, 1988). Some success has been achieved by construction of thresholds or jetties forming pools with ice cover in stead of supercooled water.

The triggering factors for ice runs are far from clear, and therefore advance warning is difficult and uncertain. Many descriptions of specific ice-run cases can be found in the literature, but attempts to place each into a systematic program for analysis are few. Collapse of anchor ice dams may occur in the middle of cold periods. Because of the damaging effects of major ice runs, investigations for better warning methods and efficient mitigating measures should be continued.

RIVER BEDS UNDER ICE

Effects of ice on the river bed morphology are scarcely described in literature. The reason is obvious: Observation of bed changes through the ice have until recently been difficult, and changes will often be reshuffled by the flood following the ice release. Bank erosion and secondary branching are known effects. Milburn and Prowse (1998) refer to a CRREL report on the morphology under ice (Lawson et al., 1986). Olsson (2000) reports notable increase of local scour at bridge piers due to ice cover. Both the vertical flow profile of the approaching flow, and the special downwards flow motion in front of the piers in open surface flow will be modified by the ice cover. The added scour depth was found to increase with the ratio U/U_c between mean velocity and the critical scour velocity, and was larger for rough covers than for smooth.

Changes in bed pattern may modify the bed roughness and have significant influence on the winter stages discussed below. Rivers with fluctuating or regulated discharges may have problems to adjust the cross sections under ice to match the situation with ice free flow of similar discharge. The most pronounced effects may occur in river outlets to regulated lakes, where the lake level is being artificially reduced through the season.

Under-ice morphology is now being more actively studied as part of increasing interest in fish habitat (Alfredsen, Fjeldstad & Tesaker, 2002), but is still sparsely understood. Instruments for detection of bed level and ice thickness from the ice surface are now available, and will be important in the continued research.

WATER STAGES IN ICE COVERED RIVERS

Nearly all river discharge statistics are referring to stage-discharge relations calibrated by discharge measurements. In ice covered rivers, the observed stages need corrections before being converted to discharges according to ice-free stage-discharge curves. This

correction has been a major obstacle for obtaining reliable winter discharge statistics. Direct discharge measurements by acoustic methods are now to some extent replacing the stage recordings for obtaining discharge data. But the new methods still fail in ice covered reaches due to frequently changing flow conditions and cross sectional shape. Stage-discharge conversion will always be needed, at least for historical data.

The "winter coefficient" $k = Q/Q_s$, relating the actual winter discharge Q with the apparent discharge Q_s from calibrated summer rating curves, depends on many factors, which mostly can be neglected for ice-free recordings. The most important may be:

1. Damming by anchor ice or ice jams at a critical dowstream cross section.
2. Modified cross sections due to anchor ice on bottom and banks, rim ice, and the thickness of the floating ice cover itself.
3. Added friction from the underside of the ice cover.
4. Modified roughness of bed and banks due to anchor ice or other ice accumulations.
5. Effects of frazil etc on the kinematic viscosity and the turbulent energy diffusion.

These factors occur in changing combinations throughout the season. Factor 1 will often be dominant during the initial ice formation. With established ice cover, factors 2 – 4 will add to factor 1, and may often give the most significant effects, but their proportional importance depends on the location of the gauging point in relation to the ice free critical cross section. Factor 5 has been commented above, and may sometimes be important during the ice formation, and during break-up ice runs. Under-ice deposits of frazil will often add to the thickness and the roughness of the ice cover.

The uniform river flow (Q) is usually described by various formulae of which the Manning formula ($Q = A \cdot R^{2/3} \cdot S^{1/2} /n$) is in frequent use in open water courses. In ice free flow the parameters A = area, S = slope and R = A/ P = hydraulic radius, (P = wetted parameter) may be precisely determined for a certain site and water stage. The empirical friction parameter n varies little with stages once determined at a site.
Not so in ice affected flow:

- Added friction from the ice cover etc leads to increased energy slope near a downstream control, increasing the depth and the efficient cross section backwards, until the slope S again approaches the ice free bed slope, but at a higher stage.
- The ice cover adds to the wet perimeter P and modifies the hydraulic radius. In wide rivers with full ice cover, R will be reduced to almost half value by the ice cover.
- Different friction factors apply for bed and ice surfaces, and the bed friction may also be modified by the ice. All ice related friction will vary through the season.
- The measured water levels include about 92 % of the ice thickness, which also is varying through the season.

To approach a method for estimation of the winter coefficient k, it is necessary to gather and correlate long series of different ice related data under varying meteorological situations with actually measured discharges, and then work out functions of k for various combinations of parameters. Some clues already exist:

- An obvious correction is to subtract 92 % of the ice thickness.
- The roughness under the ice has been analysed by many researchers, usually by measuring the velocity profile. The conclusions of a study (Tesaker, 1970) at three local sites in Norway were not promising for the finding of a method useful in general: 'The roughness of the ice cover varied from place to place, and varied in

magnitude between n = 0.03 and n = 0.008, i.e. from that of smooth river bed to glossy surfaces. No simple relationship existed between bed and ice roughness.' Later studies have added to our knowledge, but the vague conclusions remain, as summarised in Ashton (1986):"In general the present state of knowledge of ice roughness for design and operational purposes is poor to that for open channel conditions. A basic problem is the variety of ice covers."

- The 1970 study was combined with weekly determinations of the winter coefficient, which was found to vary between 0.9 and 0.3, with falling trend over the major part of the season, but with larger variations during ice formation and break-up. Anchor ice on the bed may be a main reason for some observed high values of the winter coefficient in the beginning of the season.
- Few studies about hydraulic effects of anchor ice are published. A flume study presentation by Kerr, Shen and Daly (1998) may be a starting point for further investigations.

It should be possible to find working methods for a statistically based reduction of winter stages at locations important for local run-off statistics, at least for the stable periods of ice cover. This will require cumbersome field programs over several years, but may be worth while where winter flow statistics is of economical importance. The program should include direct discharge measurements, and recordings of water level, ice thickness, air and water temperatures, as well as mapping of partial ice cover and registration of special ice events. It may be possible to apply acoustic discharge measurements under ice in periods with stable discharge and ice cover. The complicated transitions in the beginning and end of an ice period may use the adjoining ice free recordings for help in interpretation.

CONCLUSION

Many programs in ice research have been shelved before reaching a conclusion or a satisfactory level of knowledge. Some of these problems invite to renewed interest and research. A few have been reviewed and commented:

- the viscosity and turbulence diffusivity of frazil/water mixtures and its effect on slope and water stage;
- the formation and release of anchor ice;
- prediction, timing and control of violent ice runs;
- changes in river bed morphology due to the ice cover or ice accumulations;
- a working method for correction of discharges calculated from water stages in ice covered rivers, with the purpose to obtain better winter discharge statistics.

REFERENCES

Alfredsen, K., Fjeldstad, H-P & Tesaker, E. Ice effects in artificial habitats. In: *Ice in the environment*, vol. 1, Dunedin (2002) 268-273. ISBN 1- 877139-52-1.

Altberg, W. J. Anchor Ice. On the cause of the formation of ice at the bottom of rivers and lakes. *Quarterly J. of the Royal Met. Soc*., Vol. XLIX No. 205 (1923).

Ashton, G. D., ed. River and lake ice engineering. *Water Resources Publications*, Col, US(1986). ISBN 0-918334-59-4 .

Carstens, T. Experiments with supercooling and ice formation in flowing water. *Geophysica Norwegica*, vol. XXVI, No 9, (1966) 1-18.

Carstens, T. & Tesaker, E. Technical measures for reduction of ice damage. *Nordic expert meeting on river ice. NHP Report No 21*, KOHYNO (1988) 207-216. ISBN 951-715-210-8.

Clark, S. & Doering, J. C. Laboratory obs. of frazil ice. In*: Squire & Langhorn (ed.): Ice in the environment*, vol 1, Dunedin (2002) 127-133. ISBN 1-877139-52-1.

Devik, O. Thermische und dynamische Bedingungen der Eisbildung in Wasserlaufen, auf Norwegische Verhältnisse angewandt. *Geof. Publ. IX*, No. 1 (1931).

Kerr, D. J., Shen, H. T. and Daly, S. F. Evolution and hydraulic resistance of anchor ice on gravel beds. In: *Shen (ed.): Ice in surface waters*, Vol 2, Balkema (1999) 703-710. ISBN 90 5410 973 4.

Lawson, D. E. et al. Morphology, hydraulics and sediment transport of an ice covered river. *CRREL*, Report 86-11(1986).

Loktu, A., Roen, S.& Tesaker, E. Isundersøkelser (Ice research), *Forra 1963/64, Cold Room 1964 (in Norwegian). Report project 600005, SINTEF*, Trondheim (1964).

Milburn, D. and Prowse, T. Observation of the role of an ice cover in sediment deposition in a northern delta. In: *Shen (ed.): Ice in surface waters*, Vol 1, Balkema (1998) ISBN 90 5410 972 6.189-196.

Olsson, P. Influence of ice-cover on local scour at circular bridge piers. *Thesis, Luleå University*, Sweden (2000).

Prandtl, L. On fluid motions with very small viscosity (in German). *3rd Intern. Math. Congr.*, Heidelberg (1904).

Tesaker, E. Measurement of ice roughness and the effect of ice cover on water levels in three Norwegian rivers. *1st IAHR Ice symposium*, paper 3.4, Reykjavik (1970).

Tesaker, E. Ice formation in steep rivers. *12th IAHR Ice symposium*, vol 2, (1994).

Tsang, G. Change of velocity distribution in a cross-section of a freezing river and the effect of frazil ice loading on velocity distribution. *1st IAHR Ice symposium*, paper 3.2, Reykjavik (1970).

17th International Symposium on Ice
Saint Petersburg, Russia, 21 - 25 June 2004
International Association of Hydraulic Engineering and Research

PROPERTIES OF THICK SEA ICE AND OVERLYING SNOW IN THE SOUTHERN SEA OF OKHOTSK

Takenobu Toyota[1], Shinya Takatsuji[1], Kazutaka Tateyama[2], Masashige Nakayama[3], Kazuhiro Naoki[4], Kay I.Ohshima[1]

ABSTRACT

In order to investigate the features of relatively thick ice existing in the southern Sea of Okhotsk, an ice sampling method with a basket was developed for the 2003 winter observation for the first time in this region. This method enabled us not only to efficiently collect thick ice samples, but also to directly examine the properties of overlying snow. The number of sites amounted to 16 and 12 points for ice sampling and snow observation, respectively, during about one week cruise. With ice samples, the profiles of temperature, density, salinity, textural structure, and stable isotopic composition ($\delta^{18}O$) were investigated. From analysis it is found that for ice samples (Hi > 40 cm) frazil ice occupies much more fraction (59%) than columnar ice (30%) and layered structure (averaged unit thickness 9.1cm) is prominent, and that depth hoar and solid-type depth hoar are dominant (69%) for overlying snow. The former result almost coincides with the results for relatively thin ice obtained from 1996 to 2000 and shows that the dynamic processes by rafting/ridging are almost similar to that for thinner ice in this region. The latter is similar to the result obtained in the Antarctic SIZ.

INTRODUCTION

The ice cover in the Sea of Okhotsk, located in the southernmost region in the world, has a significant influence on the interaction between ocean and atmosphere (Honda et al., 1996; Ohshima et al., 2003; Inoue et al., 2003), and it is important to investigate its characteristics and understand the ice growth process. For this purpose, the Institute of Low Temperature Science of Hokkaido University has been conducting the in-situ ice observation in collaboration with Japan Coast Guard, using the P/V Soya in the southern Sea of Okhotsk every winter since 1996. Through this observation, the characteristic of the sea ice in this region has been unveiled to some extent (Toyota et al., 2004). That is,

[1] Institute of Low Temperature Science, Hokkaido University
[2] Sea Ice Research Laboratory, Hokkaido University
[3] Japan Aerospace Exploration Agency
[4] Chiba University

it has been shown that the thickness of undeformed ice ranges from 30 to 50 cm on average, that frazil ice is much more prominent than congelation ice, and that layered structure is frequently found with the averaged layer thickness being 5 to 10 cm. However, it should be noted that the ice samples examined so far were rather biased to the thinner ice (mostly below 50cm) due to the sampling method.

On the other hand, it has recently been revealed from the ice profiling sonar observation that sea ice floes of more than a few meters thick sometimes appear around the coastal regions of Hokkaido, Japan (Fukamachi et al., 2003). Therefore, we need to also examine the properties of relatively thick ice. For this purpose, we developed an ice sampling method using a basket to carry the observers and materials from the ship to an ice surface for the observation in February of 2003. This method provided us with the opportunity not only to collect relatively thick ice cores efficiently, but also to examine the snow properties on sea ice at several sites. In this paper, we describe the results obtained from this observation and compare with the characteristics of relatively thin ice obtained during the period of 1996 to 2000.

Observation

In order to collect thick ice, we introduced a sampling method with a basket which has been used for the Antarctic sea ice observation by the Australian researchers (personal communication with Dr.I.Allison, 2002). We prepared a basket, made from aluminum, with a square base 1.5m on a side and 1m high, which is used to carry two observersand ice sampling materials using a ship crane from a shipboard to ice surface (Figure 1). In our case, we made a 25 cm diameter hole on the base of the basket, through which ice core samples could be collected with an ice auger without the risk of getting out of the basket.

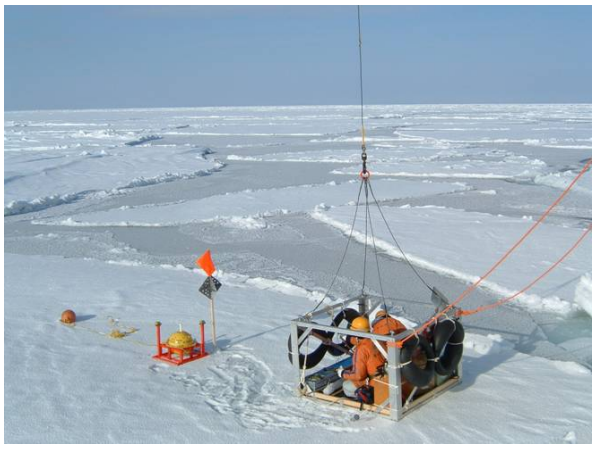

Fig. 1. Ice sampling and snow observation using a basket

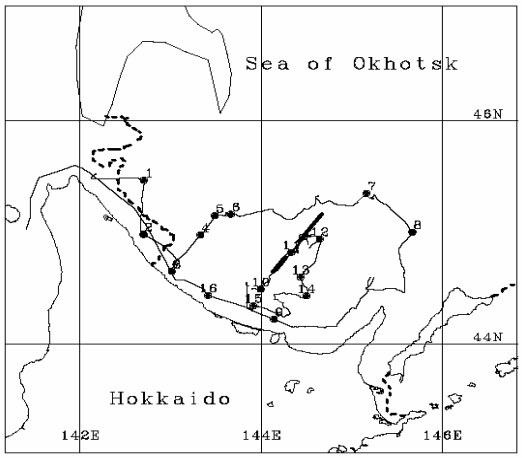

Fig. 2. Cruise track with ice edges (broken lines) and sampling location (circles)

During the basket observation, we firstly collected ice core samples, and then measured the ice thickness, freeboard, snow depth, and the temperature of the ice core at the interval of 5 cm, and examined the snow properties. The observation sites amounted to

16 points for ice sampling and 12 points for snow observation (see Figure 2 for location). It is noticeable that at 10 points among 16 the core lengths were greater than 40cm and the maximum amounted to 167cm whereas the number of first-year ice (Hi>30cm) obtained from 1996 to 2000 had been limited to only 14. Each elapsed time was about 30 minutes to one hour. In addition, it seems to be significant that this sampling method enabled us to directly examine the snow properties. Because most of sea ice floes are covered with snow, the snow properties on sea ice are requisite to derive the characteristics of sea ice from satellite data. However, there has been only a few observations for the Sea of Okhotsk (e.g. Toyota et al, 2002), and the snow properties on sea ice have been little known to date in this region. The sampled ice cores were kept in the freezing room (-15) during the cruise, and carried to the cold room (-16) of ILTS immediately after the cruise. For each ice sample, the density, salinity, and isotopic composition were measured basically at the interval of 3 cm and the vertical crystal structure was examined through this section analysis.

RESULTS

Sea ice

As one example of the ice core analysis, the vertical profiles of crystal structure, temperature, density, salinity, and $\delta^{18}O$ of the ice sample with 91cm core length and 6cm snow depth are shown in Figure 3. This figure shows that the vertical profile of temperature is almost linear, while the other profiles show variation, suggesting that this ice sample was formed by the piling-up of several ice floes.

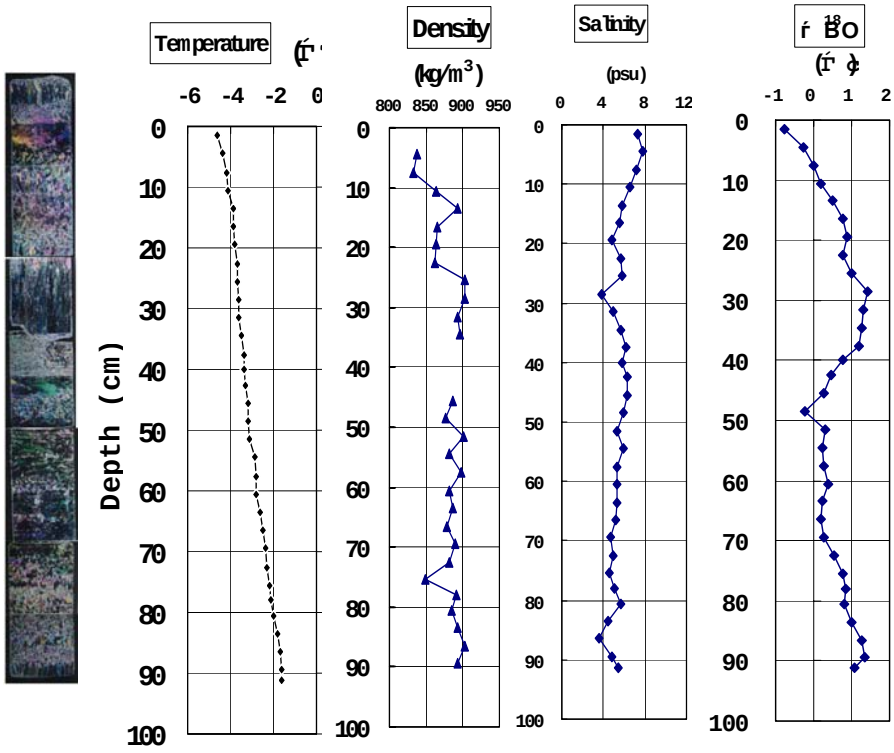

Fig. 3. One example of the ice sample analysis (at No.12 in Figure 2)

From the left, the vertical profile of textural structure, temperature, density, salinity, and $\delta^{18}O$ are shown. Ice density 881±19kg/m3, Ice salinity 5.54±0.9psu, Mean layer thickness 7.0cm, Fraction of granular ice 76%. At observation air temperature was -3.8 .

From the arrangement of textural structure and the vertical profiles of density, salinity, and $\delta^{18}O$, the number of the layers is estimated to be 12. Since granular ice and $\delta^{18}O<0$ can be the indicator of snow ice in this region (Toyota et al., 2004), this sample is recognized to contain snow ice at the depth of about 50cm. This fact also verifies the occurrence of a piling-up process. In addition, the textural structure shows that granular ice is much more prominent than columnar ice. In this case, about 90% of granular ice is composed of frazil ice. These results suggest that the frazil ice accumulation and the sequent piling-up process are much more significant than congelation process during the growth of this ice sample. As for the snow properties of this sample, the snow types are new snow for the upper 1cm, lightly compacted snow for upper 1 to 4cm, and solid-type depth hoar for the lower 2cm. The salinity is 0.11, 0.71, and 4.97 psu, respectively. From this result, the effect of sea water flooding is detected within the lower 2cm of snow.

The same analysis was carried out for all the 16 ice samples (mean core length 50cm). The statistics shows that the fractions of snow ice, frazil ice, and columnar ice are 7, 60, and 30 %, respectively (Table 1). All the ice samples have layered structure, and the averaged layer thickness (the value obtained by dividing the total thickness except snow ice by the total number of layers) is estimated to be about 9cm. These features almost hold true for the 10 ice samples with thickness greater than 40cm (Table 1), and almost coincides with those derived from thinner ice (mostly below 50cm) so far (Table 2). This result suggests that in this region relatively thick ice (about 40 to 100cm thick) is also formed by the piling-up of ice floes with 5 to 10 cm thickness as well as thinner ice. In addition, it is shown that bulk ice salinity has a good correlation with ice thickness while the salinity is by a few psu lower than that for the polar regions, which is compiled by Kovacs (1997) (Figure 4). This feature is also similar to the result obtained for the thinner ice (Hi<80cm) by Toyota et al.(2000). Furthermore, we calculated the profiles of brine volume fraction using the formula by Cox and Weeks (1983) from the temperature, density, and salinity. As a result, it is found out that the brine volume fraction ranges from 5 to 12% except the bottom layer within ice, and that the bulk brine volume fraction has a further better correlation with ice thickness than bulk salinity (Figure 5). This is probably because mean ice temperature is also correlated with ice thickness and the brine volume fraction, including both effects of salinity and temperature, has better correlation with thickness than either.

Table 1　Statistics of ice types and layer thickness for 2003 winter

	Type	si	f	c	g/c	H_L
Total (16 samples)	Fraction (%)	7.0	59.8	29.6	3.5	8.6 cm
	Thick (cm)	3.7	6.2	7.1	1.4	
Hi > 40cm (10 samples)	Fraction (%)	7.3	58.9	30.2	3.5	9.1 cm
	Thick (cm)	4.2	6.5	7.7	1.5	

In the table, si, f, c, and g/c denote snow ice, frazil ice, columnar ice, and the mixture of granular and columnar ice. The H_L means the averaged layer thickness calculated for all the samples.

Table 2. Statistics of ice types and layer thickness for 1996-2000 ice samples

(Cited from Toyota et al. (2004))

Type	N	c	g	c/g	etc	H_L
First-year ice (Hi > 30cm)	14	21	76	2	1	
Young ice (10<Hi<30cm)	33	24	68	2	5	
Total	47	22	74	2	3	8.2 cm

(Unit: %)

In the table, N is the number of ice samples, and c, g, and c/g denote columnar, granular, and the mixture of granular and columnar ice. H_L is the same as Table 1.
It should be noted that total granular ice (74%) is composed of 10 % snow ice and 64% frazil ice.

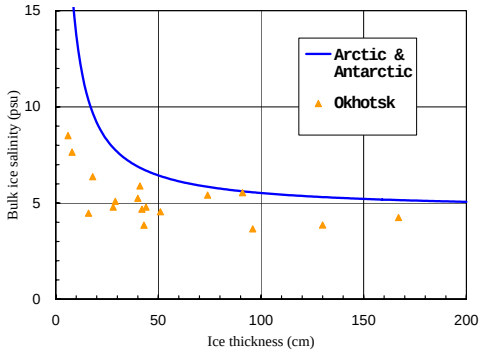

Fig. 4. Bulk ice salinity as a function of ice thickness. Thick line is for the polar region, compiled by Kovacs (1997)

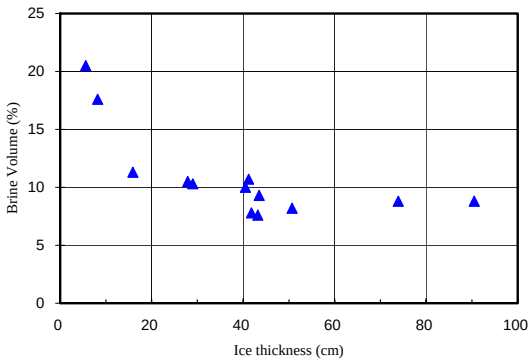

Fig. 5. Bulk brine volume fraction as a function of ice thickness

Snow

The statistics of all the 12 snow observation sites show that the average of snow depth is 8.9 cm and that among snow types depth hoar and solid-type depth hoar occupied about 70% of the total depth and are much more prominent than compacted snow (Table 3).

Table 3. Statistics of snow types overlying sea ice for 2003 winter

ns	cs-l	cs	gs	dh-st	dh	sh
19.3	7.5	0.0	19.2	12.6	55.9	0.9

(Unit: %)

In the table, ns, cs-l, cs, gs, dh-st, dh, and sh denote new snow, lightly compacted snow, compacted snow, granular snow, solid-type depth hoar, depth hoar, and surface hoar.
It should be noted that one snow layer can contain more than one type of snow, and therefore the summation of the individual types in the table exceeds 100%.

This result indicates the significance of morphological development due to a large temperature gradient within snow layers. This feature matches with the result by Toyota et al. (2002). Sturm et al. (1998) reported the similar result for the snow properties on sea ice in the winter Antarctic SIZ. In their case, depth hoar occupies about 30% and is the most prominent. We consider that the prevalence of depth hoar is caused by the fact that over relatively thin ice snow depth is limited and thereby the vertical temperature gradient tends to be large, and may be one of the characteristics of snow overlying sea ice in the seasonal ice zones where relatively thin ice prevails. The granular snow was found only at the bottom layer of snow and the height was 5cm at most. This suggests that granular snow is formed mainly through sea water flooding from sea ice surface and the effect comes up to several centimeters.

CONCLUSION

In 2003 winter season, relatively thick ice samples and snow overlying sea ice were collected with a basket in the southern Sea of Okhotsk and their properties were examined. The number of sites amounted to 16 and 12 points for ice sampling and snow observation, respectively, during about one week cruise. From analysis it is revealed that for ice samples thicker than 40 cm frazil ice occupies much more fraction (59%) than columnar ice (30%) and layered structure is prominent with the averaged thickness being 9.1 cm. This result almost coincides with the results for relatively thin ice obtained from 1996 to 2000 and shows the importance of similar dynamic processes by piling-up to the ice growth for relatively thick ice (40-100cm thick) in this region. In addition, it is shown that bulk brine volume fraction has further better correlation with ice thickness than bulk ice salinity. As for overlying snow, it is found that depth hoar and solid-type depth hoar are dominant (69%), similar to the result obtained in the Antarctic SIZ. This indicates the strong vertical temperature gradient within sow layers. Considering that snow depth is limited over relatively thin sea ice due to isostasy balance, this may be one of the characteristics of sea ice in the SIZ. The effect of sea water flooding was observed to come up to several centimeters at the lower layer of snow.

ACKNOWLEDGMENTS

We are sincerely grateful to the crew of P/V *Soya* of the Japan Coast Guard and our co-workers, Jun Inoue and Yuji Mukai, of ILTS for their kind corporation throughout the cruise. This observation was partly supported by the fund from Research Revolution 2002 (RR2002) of Project for Sustainable Coexistence of Human, Nature and the Earth of the MEXT of the Japanese Government.

REFERENCE

Cox, G.F.N., and Weeks, W.F. (1983): Equations for determining the gas and brine volumes in sea-ice samples, *Journal of Glaciology*, Vol.29(102), 306-316.

Fukamachi, Y., G.Mizuta, K.I.Ohshima, H.Melling, D.Fissel, and M.Wakatsuchi, Variability of sea-ice draft off Hokkaido in the Sea of Okhotsk revealed by a moored ice profiling sonar in winter of 1999, *Geophysical Research Letters*, 30(7), 1376, doi: 10.1029/2002GL016197, 2003.

Honda, M., Yamazaki, K., Tachibana, Y., and Takeuchi K. (1996): Influence of Okhotsk sea-ice extent on atmospheric circulation. *Geophysical Research Letters*, 23(24), 3595-3598.

Inoue, J., Ono, J., Tachibana, Y., Honda, M., Iwamoto, K., Fujiyoshi, Y., Takeuchi, K. (2003): Characteristics of heat transfer over the ice covered Sea of Okhotsk during cold-air outbreaks, *Journal of the Meteorological Society of Japan*, Vol.81(5), 1057-1067.

Kovacs, A. (1997): The bulk salinity of Arctic and Antarctic sea ice versus thickness, 1997 OMAE-Volume IV, Arctic/Polar Technology ASME.

Ohshima, K.I., T. Watanabe, and S. Nihashi (2003): Surface heat budget of the Sea of Okhotsk during 1987-2001 and the role of sea ice on it, *J. Meteor. Soc. Japan*, 81, 653-677.

Sturm, M., Morris, K. and Massom, R. (1998): The winter snow cover of the West Antarctic pack ice: its spatial and temporal variability. Antarctic Sea Ice: Physical Processes, Interactions and Variability, edited by M.O.Jeffries. Washington,DC,American Geophysical Union,1-18(Antarctic Research Series, 74).

Toyota, T., Kawamura, T., Ohshima, Kay I., Wakatsuchi, M. (2004): Thickness Distribution, Texture and Stratigraphy, and a simple probabilistic Model for Dynamical Thickening of Sea Ice in the Southern Sea of Okhotsk, *Journal of Geophysical Research* (in press).

Toyota, T., Kawamura, T., and Wakatsuchi, M. (2000): Heat budget in the ice cover of the southern Okhotsk Sea derived from in-situ observations, *Journal of the Meteorological Society of Japan*, Vol.78(5), 585-596.

Toyota, T., Baba, K., Hashiya, E., and Ohshima, Kay I. (2002): In-situ ice and meteorological observations in the southern Sea of Okhotsk in 2001 winter: ice structure, snow on ice, surface temperature, and optical environments, *Polar Meteorology and Glaciology*, No.16, 116-132.

17th International Symposium on Ice
Saint Petersburg, Russia, 21 - 25 June 2004
International Association of Hydraulic Engineering and Research

NEW DYNAMIC ASPECTS OF CONTEMPORANEOUS CONCEPTS IN ATMOSPHERIC ICING MODELLING

Anatolij R. Karev[1], Masoud Farzaneh, Laszlo Kollar and Sandy Vaslon

ABSTRACT

This article addresses several heretofore unexplored aspects of modern concepts in the theory of atmospheric ice accretion on the surface of a test body placed within a supercooled aerosol cloud. The air velocity of a flowing aerosol cloud in experiments carried out in an icing wind tunnel is considered as a vector which forms angles with the cylinder axis in the vertical plane passing in both streamwise and lateral directions. This complicates both momentum- and heat-transfer from the icing surface, introducing different types of water film instabilities and modifying the accreting ice mass. Under conditions modeling freezing rain (ZR) and in-cloud icing (CI), the ice mass accreted on the experimental cylinder oriented streamwise was always found to be smaller than the mass accreted on the cylinder oriented perpendicular to air flow.

INTRODUCTION

All contemporaneous icing theories make use of a cylindrical body set horizontally with its axis perpendicular to a supercooled aerosol flow. Such a spatial disposition leads to a frequently used tendency of simplifying natural icing processes by presenting them in a two-dimensional (2-D), mostly circular form. Under extremely cold ambient conditions, when aerosol droplets freeze upon contact with the icing surface without spreading over it, a simplified 2-D representation of the icing process for theoretical and experimental investigation is recommended. Such a step would save computation time and would not forego any significant feature of the process, provided the spatial uniformity of the LWC of the aerosol cloud in the experiment is preserved. The 2-D consideration fails, however, under ambient conditions favorable to the appearance of a supercooled water film on the surface of a growing ice accretion, since the dynamics of this film, which is pivotal to heat- and mass-exchanges, is not adequately addressed. If the cylinder axis forms some angle streamwise of the aerosol flow in the horizontal or vertical planes, thereby setting the water film in motion under the influence of air flow or gravity, then additional aspects will appear of the ice accretion process occurring underneath the

[1] NSERC/Hydro-Québec/UQAC Industrial Chair on Atmospheric Icing of Power Network Equipment (CIGELE) and Canada Research Chair on Atmospheric Icing Engineering of Power Networks (INGIVRE), Université du Québec à Chicoutimi, Département des Sciences Appliquées, 555 blvd de l'Université, Chicoutimi, Québec, Canada G7H 2B1

flowing film. This type of complex flow does not resemble accepted notions of water film flow in icing models. Examples of simplified concepts of water film flow in icing models include: (i) circular flow around the cylinder concurrent with strong air flow, as in water run-back models of icing of a non-rotating horizontal cylinder (Kachurin, 1974; Lozowski et al., 1979); (ii) circular flow counter-current to a weak air stream on the upper half of the cylinder towards the lower half, as in models for pendant ice formation (Szilder and Lozowski, 2000); (iii) lengthwise on a vertical cylinder, as in current models for ice sponginess (Blackmore et al., 2002). In the second instance, by excluding airflow influence and considering gravity only by reformulating the 2-D problem of water flow in the vertical plane passing through the cylinder axis, it is possible to define icicle spacing (de Bruin, 1999; Farzaneh et al., 2003) as a feature affected by the *Rayleigh-Taylor instability* between the layers of two fluids of different densities (Taylor, 1950). In this experimental sequence, the icing body is a non-rotating cylinder tilted with the horizontal plane either streamwise or lateral to the air flow. The corresponding water film flow is, thus, a combination of the three simple types presented earlier. Based on theoretical considerations, the introduction of an additional flow of one of the two superposed fluids, at a relative horizontal velocity, would create a different type of oscillation, the *Kelvin-Helmholtz instability* at the boundary between the fluids (Chandrasekhar, 1961). By introducing the thermal factor as a uniform transverse temperature gradient, *thermocapillary instability* (Chandrasekhar, 1961) would arise. Furthermore, in a flowing transitional water film, the introduction of heat transfer from below would result in stabilizing laminar flow due to an increase in the *indifference Reynolds number* (Strazisar et al., 1977). The issue of water flow on icing surfaces is, thus, more complex than it seemed initially. The main goal of this investigation is to evaluate the potential significance of water flow direction in the final mass and shape of ice accretions for different inclined angles of a cylinder.

A subsidiary goal is imposed by the different droplet size distributions (DSD), and by different manners of water supply to the icing surface in three atmospheric icing phenomena: in-cloud icing (CI), freezing drizzle (ZL) and freezing rain (ZR). In the cloud droplet range, which is set at droplet diameters of 10 μm to 50 μm (Jeck, 1996), the droplets are not generally affected by gravitational forces and may float or be wafted by in-cloud main drafts in any direction. Since horizontal movements in stratified winter clouds predominate, the CI may be successfully modeled in a wind tunnel by the horizontal flow of a supercooled aerosol cloud streaming over an experimental cylindrical body set in any position. In the ZR droplet range, which covers diameters from several tens of microns to several millimeters, the droplets are already noticeably affected by gravitational settling. Thus, the vertical component of rain droplet velocity may be considered a major factor during the impinging and spreading of droplets on an icing surface, to be taken into account throughout experimental modeling. The factors promoting drizzle production should exist during formation and development of the ZL droplet range which forms a part of the ZR range (Jeck, 1996) and which conventionally covers diameters from 50 μm to 500 μm. Since the presence of air turbulence or wind shear is one of those drizzle-promoting factors, either of two the manners of supercooled water supply to an icing surface mentioned earlier may be considered in ZL. This simplified division of droplet cloud ranges and the categorization of types of water supply to an icing surface cannot be other than conventional, since air turbulence or wind shear may exist in all three ice-producing phenomena, depending on prevailing thermodynamic conditions. The preceding categorization contributes, however, to defining a second goal of this research: to investigate how the obvious differences in (i) DSD within a droplet cloud of various ice-producing phenomena, and, (ii) the

application of corresponding manners of water supply, influence the results of experimental modeling of icing on an inclined cylinder.

EXPERIMENTAL SET-UP

Facilities and Designing of Experiments

The experiments were carried out at the CIGELE atmospheric icing research wind tunnel, a horizontal closed-loop low-speed wind tunnel 30 m total length, including a 3 m test section with a rectangular cross-section 0.46 m high and 0.915 m wide. For this series of experiments, special devices were designed to fix the experimental cylinder rigidly in various inclined positions either perpendicular or streamwise to aerosol flow direction. Cylinder dimensions were 0.915 m in length and $3.81 \cdot 10^{-2}$ m in diameter.

Two means of water supply were applied in this investigation. The first was a standard single spray-bar system with three air-assisted nozzles mounted at the tunnel center-line, and 0.2 m left and right of this line. The system modeled CI by producing an aerosol cloud with a DSD characterized by a median volume droplet diameter (MVD) of approximately 30 μm. Regular tap water at room temperature was used for atomization 4.4 m upstream from the icing cylinder, which is sufficient for droplets several tens of microns in diameter of to cool down to ambient air temperature and even slightly lower due to the relative humidity factor. The liquid water content (LWC), w ($g \cdot m^{-3}$), of the modeled aerosol cloud was kept constant throughout all experiments. The second means of water supply, for modeling ZR, was a single water-dispersing nozzle mounted on an aluminum rake attached to the ceiling of the test section and movable horizontally. The nozzle produced a droplet cloud with an ellipsoidal cross-section and a wide spectrum of droplet sizes as shown by a MVD of approximately 400 μm. Under corresponding ambient conditions, for the larger droplets in the DSD the distance from the ceiling to the icing object is not sufficient for any significant cooling if the water at room temperature is used. This fact involves working with a commercially designed machine manufactured by CIMCO and capable of cooling flowing water down to 1-2 ^{o}C. The water flow rate in the entire series was kept constant at 0.9 l/min. The temperature of the water used in this dispersing system was, thus, deemed a significant parameter and measured by an Omega T Type thermocouple at a distance of $2.54 \cdot 10^{-2}$ m from the nozzle edge inside the water line. The same type of thermocouple was used for measuring the air temperature.

Selecting Experimental Conditions

In order to maintain constant the influence of the thermal or dynamic factors mentioned in the introduction, it was decided to keep air temperature, T_a (^{o}C), and air speed, V_a($m \cdot s^{-1}$), constant at $T_a = -10$ ^{o}C and $V_a = 20$ $m \cdot s^{-1}$ throughout the experimental series. This choice was dictated mainly by the potential for adequately modeling ZR in this icing wind tunnel configuration, which the frequently used value of air temperature for ZR $T_a = -5$ ^{o}C did not originally allow. Jeck (1996), however, reported that the value $T_a = -10$ ^{o}C is also fairly frequent in ZR, especially when it occurs aloft. The LWC of a flowing aerosol cloud should be in a range which covers the water supply rate characteristic of natural CI conditions (up to 1.3 $g \cdot m^{-3}$), but one of the goals of this research involves the application of the same thermodynamic conditions (T_a and V_a) for both the icing phenomena modeled: CI and ZR. With a pre-chosen $T_a = -10$ ^{o}C for modeling ZR, the LWC should be at least doubled to obtain flowing water effects similar to those for $T_a > -5$ ^{o}C. The chosen value for LWC of 3.2 $g \cdot m^{-3}$ for experimental modeling of CI may seem unrealistic since it approaches the range of the LWC for

convective clouds. It may be simply shown, however, that the pair of variables chosen for these experiments (w = 3.2 g·m^{-3}; T_a= −10 ^{o}C) will have the same effects on the formation of excess water on an icing surface as the pair representing natural conditions (w<1.3 g·m^{-3}; T_a> −5 ^{o}C). The duration of each experimental trial was set at a constant 15 minutes.

RESULTS AND DISCUSSION

Experimental Output

The following data were collected as the output of the experimental series: (i) ice mass per unit of cylinder length, dM/dl (g·cm^{-1}); (ii) ice shape; (iii) state of ice surface and size of surface roughness elements; (iv) ice accretion profiles along the cylinder length. A thin preheated aluminum cutter was used to cut the ice specimens for weighing. The selected length and position at which all data were collected were 10.2 cm left and right of the cylinder centre. Ice shape and the size of surface roughness elements were examined through digital photography of ice specimens extracted from various locations. Ice accretion profiles were collected in two ways: by drawing the profiles manually on cardboard and by processing the data gathered from photographs of the profiled specimens. Only the ice mass data will be presented due to a shortage of space.

Mass of Modeled In-cloud Ice Accretion

The data presented in *Figure 1a* were obtained through experimental modeling of CI of a horizontal cylinder set at different orientations relative to a flowing supercooled aerosol cloud. The results of two different series of experiments with an inclined cylinder are presented: (i) a variable inclined angle, α, formed between the horizontal plane and the axis of the cylinder set perpendicular to the air flow; and, (ii) a variable inclined angle, β, formed between the horizontal plane and the axis of the cylinder set parallel to the air flow. In the first series, the experiments were carried out for an inclination to the right hand side only, assuming that symmetry exists around the centerline of the test section. In the second series, the inclination of the icing cylinder was examined on both sides. Conventionally, the positive inclined angle β corresponds to the exposure of the lower half of the experimental cylinder to the air flow, while the negative inclined angle β corresponds to the exposure of the upper half to the air flow. An interesting finding emerges from the series with the inclined cylinder set perpendicular to the aerosol flow: a maximum of ice growth mass appears for a small inclined angle formed between the axis of the cylinder and the horizontal plane. This effect may be ascribed to the increased mass transfer of supercooled water on the surface of the cylinder from the raised edge to the center due to gravity. For the combination of thermodynamic parameters used in the entire series of experiments, this inclined angle, which is optimal for the redistribution of water on an icing surface, was found to be around $\alpha \approx 8^o$. As compared to the standard experimental configuration of a horizontal cylinder, *i.e.* for $\alpha \approx 0^o$, this positioning brings about an 11%-increase in ice mass. If the inclined angle is greater than this, the effects of gravity dominate over the effects of air shear stress, and the mass of the local ice accretion decreases, since the excess water flows faster along the cylinder. It may be assumed that for other combinations of thermodynamic parameters, the maximum of ice mass may be obtained for various inclined angles. The shapes of ice pendants in the experiments with inclined cylinders are also considerably different compared to standard configuration, while the variety of their shapes increase, when $\alpha \approx 8^o$. The same may be said about roughness elements since their shape and volume seem to reach maximal development for this

configuration. With a further increase in the inclined angle, the variety of roughness elements and ice pendants decreases considerably, and a certain amount of uniformity in their distribution may be observed. The shape of ice accretions, however, will never be similar to the ones obtained for standard cylinder orientation. The closer the orientation of the cylinder is to standard orientation, the more uniform the shapes of ice accretions along the cylinder are. A further conclusion, which may be drawn from the study of Fig. 1a, concerns the potential minimum of ice mass for the cylinder parallel to the aerosol flow. In this series, experiments with $\beta=0^o$ were not carried out due to the possible influence of cylinder support on the results of experimental modeling. The low minimum may be assumed for this position, however, as regards the gravitational droplet settling process even for the air speeds accepted in this series. All ice accretions for the grazing angles investigated here have the shape of white feathers as observed on cylinders with a standard orientation at some angle from the stagnation line, since effective LWC in such a position is relatively low.

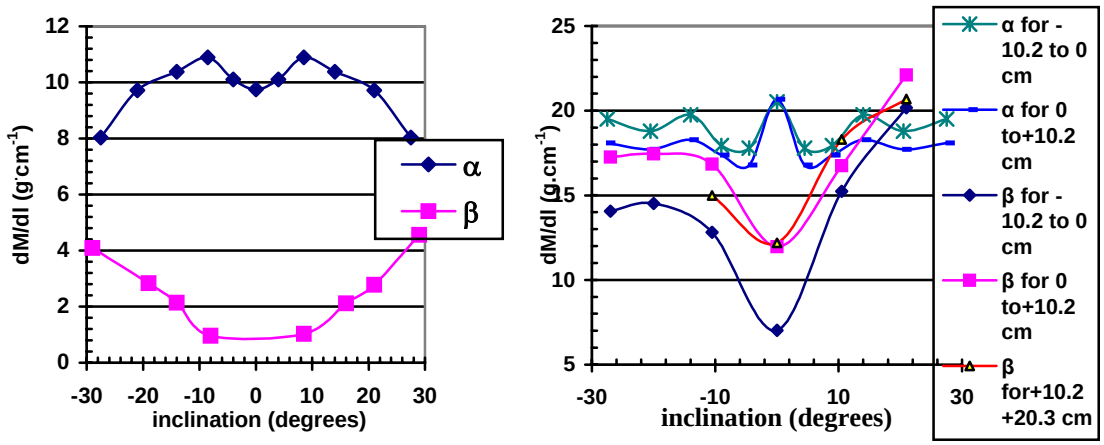

Fig. 1. Ice mass obtained with the inclined cylinder for a) CI (left); and b) ZR (right)

The series of experiments for $\beta = 29^o$ was repeated for doubled LWC and a higher air temperature, T_a=-5°, to attain conditions with water flowing on the cylinder surface. The results, however, were always negative. From Fig. 1a it is clear that the ice mass increases with the increase of angle β in the whole range of measurements for positive and negative angles starting from $\beta = 0^o$, i.e. there is no maximum. A further difference between the two sets of results presented in Fig. 1a is that there is no symmetry around $\beta = 0^o$, the mass increase with the increase of β occurs more rapidly if the lower half of the cylinder is exposed to the flow.

Mass of Ice Accretion during Freezing Rain Modeling

Fig. 1b presents the results obtained for the second type of water supply to the cylindrical icing surface for modeling ZR conditions with a single water-dispersing nozzle mounted on an aluminum rake. The same two sets of cylinder orientation were used in the experiments, as shown in Fig. 1a. The temperature of cooled water in the nozzle kept constant between 1.2 and 1.8 °C. For the perpendicular cylinder orientation with a variable α angle, results are very similar to those obtained for modeling CI and presented in Fig. 1a, except for $\alpha=0^o$, which will be the subject of additional investigation at a later date. One surprising result of the research is the dependence of ice mass on the inclined angle β as found for the streamwise orientation of a cylinder. In

spite of a significantly different type of water supply, as compared to the double series modeling CI (Fig.1a), and the different type of ice deposit observed in both cases, the dependence of ice mass on the inclined angle is remarkably similar for both the icing phenomena modeled. There is a minimum of ice mass at 0^o inclined angle with two increasingly divergent branches for positive and negative β. Furthermore, as in CI modeling, the increase of the mass for positive β angles is steeper than that for the negative β. This difference is even more striking than in the case of CI.

CONCLUDING REMARKS

The dependence of ice mass accreted on an inclined cylinder on the inclination angle to the air flow was investigated by modeling CI and ZR conditions. In spite the different types of water supply and the different DSD used to model both icing phenomena, as well as different ice accretion shapes obtained for a streamwise oriented cylinder, a distinct resemblance exists between both sets of results as regards the dependence of ice mass on the inclined angle. Furthermore, ice mass accreted on the inclined cylinder oriented perpendicular to the air flow is mostly greater than the mass accreted on the inclined cylinder oriented streamwise, at least for the range of inclination angles used in this investigation. The dynamics of water film flow should be scrutinized in depth (3-D) to explain theoretically the results obtained. A further dynamic aspect to be investigated at a later date may be related to the varying directions and absolute values of the air velocity.

ACKNOWLEDGMENTS

This study was carried out within the framework of the NSERC/Hydro-Quebec Industrial Chair on Atmospheric Icing of Power Network Equipment (CIGELE) at the University of Quebec in Chicoutimi. The authors would like to thank all the sponsors of the CIGELE for their financial support. Valuable help provided by CIGELE technician P.Camirand in designing and manufacturing devices for this experimental series is also gratefully acknowledged. We are also most grateful to M. L. Sinclair for editorial assistance.

REFERENCES

Blackmore, R.Z., Makkonen, L. and Lozowski, E.P. A new model of spongy icing from the first principles. *J. Geophys. Res*. 107, D21, paper 9, 4563, AAC 9.1-9.15 (2002).

Farzaneh, M., Karev, A.R. and Mousavi, M. The Rayleigh-Taylor instability as an influence in the spacing of icicles on a horizontal cylindrical body. *Proceed. 13th Int. Offshore and Polar Eng. Conf.*, Honolulu, Hawaii, USA, May 25-30, (2003) 382-389.

Chandrasekhar, S.Hydrodynamic and Hydromagnetic Stability.*Oxford Univ.Press*, London(1961) de Bruyn, J.R. On the formation of periodic arrays of icicles. *Cold Regions Sci Technol*. 25 (1997) 225-229.

Jeck, R.K. Representative values of icing-related variables aloft in freezing rain and freezing drizzle. *FAA Int. Conf. On In-Flight Icing*, DOT/FAA/AR-96/81, II (1996) 57-68.

Kachurin, L.G., Gashin, L.I. and Smirnov, I.A. Icing intensity of small fishing vessels under different hydro-meteorological conditions. *Meteorol. i gidrologiya*, n3 (1974) 50-59.

Lozowski, E.P., Stallabrass, J.R. and Hearty, P.F. The Icing of an Unheated Non-rotating Cylinder in Liquid Water Droplet – Ice Crystal Clouds. *National Research Council of Canada, Division of Mechanical Engineering, Rep.LTR-LT-96*, Feb. 1979.

Szilder, K. and Lozowski E.P. Numerical simulations of pendant ice formations. *Cold Reg. Sci. Technol.* 31 (2000) 1-11.

Strazisar, A.J., Reshotko, E. and Prahl J.M. Experimental study of the stability of heated laminar boundary layers in water. *J. Fluid Mech*. 83 (1977) 225-247.

Taylor, G.F.R.S. The instability of liquid surfaces when accelerated in a direction perpendicular to their planes I. *Proc. R. Soc. London, Ser. A* 201 (1950) 192-196.

17th International Symposium on Ice
Saint Petersburg, Russia, 21 - 25 June 2004
International Association of Hydraulic Engineering and Research

SEA ICE EFFECTS ON THE LOCAL CLIMATE OF THE SURROUNDING LAND

Nobuyoshi Ishikawa[1], Yuji Kodama[1], Toshiyuki Kawamura[1] and Kunio Shirasawa[1]

ABSTRACT

Long-term meteorological observations have been carried out around the Saroma-ko Lagoon on the northeastern coast of Hokkaido for describing the local climate before and after sea ice formation. During early winter the northerly wind was warmer than the other directions, which was due to the higher water temperature of the ice-free Okhotsk Sea as compared to the inland surface temperature. A surface temperature inversion was frequently observed after sea ice formation and in the late spring, which was explained by the radiation cooling in the sea ice season, and cold water deposit in the late spring. The climatic sensitivity was introduced for evaluating the influence of sea ice on the climate and high sensitivity was obtained during sea ice season. For eliminating the advection effect, the difference of the temperature lapse rate before and after high sea ice coverage was analyzed and the effect of sea ice was found to be dominant to the daily minimum temperature.

INTRODUCTION

Big lakes and oceans have the capacity to modify the climate over the surrounding land due to high specific heat capacity. However, once they freeze up, the effect will become smaller because of the small specific heat capacity of ice. Further, with snow deposits over the ice, the heat stored in the water would not transfer to overlying atmosphere because of its low heat conductivity. These might change the local climate conditions (Nakamura, 1996). Many heat balance studies have been carried out on sea ice in the Polar Regions (e.g. Weller, 1968, Allison et al., 1982, Perovich et al., 1998). Heat balance components such as radiation and turbulent heat fluxes were said to change drastically after sea ice formation. So the change of heat exchange processes just after

[1] Institute of Low Temperature Science, Hokkaido University, N-19, W-8, Sapporo, Japan

the freezing of water must be quantified in spite of logistic difficulties. Recently, heat balance studies just after sea ice formation were examined and the change of heat balance with sea ice thickness was reported (Pegau et al. 1996, Ishikawa et al., 2003). The aim of this study is to clarify the sea ice effect on the local climate of the surrounding land.

OBSERVATION SITES AND INSTRUMENTATIONS

In order to investigate the characteristics of the local climate, long-term meteorological observations have been carried out around the Saromako Lagoon on the northeastern coast of Hokkaido, Japan since 1995. The area of the lagoon is 149.2km^2 and the mean water depth is 14.5m. The lagoon is connected to Okhotsk Sea by two narrow channels and the salinity is 3.1%. The lagoon and neighboring ocean (the southern part of Okhotsk Sea) usually freeze up from mid-January to mid-March. Three sites were established at different places around the lagoon (Fig.1); Wakka site was located at the second inlet of the lagoon on the sandbank between Saroma-ko and Okhotsk Sea (EL. 10m), Kimuaneppu site was just 4.5km south of Wakka across the lagoon (44°06.08′N, 143°56.12′E, EL. 5m) and Horoiwa site was at the highest peak near the lagoon (EL. 376m). The highest site was assumed to be a reference point because it was less affected by the surface condition change. All meteorological factors were recorded at every hour and stored in data acquisition system (Intelligent Data-Stocker DS-64K2, KONA Sapporo Co. and EXL-009C, LOG ELECTRIC Co.).

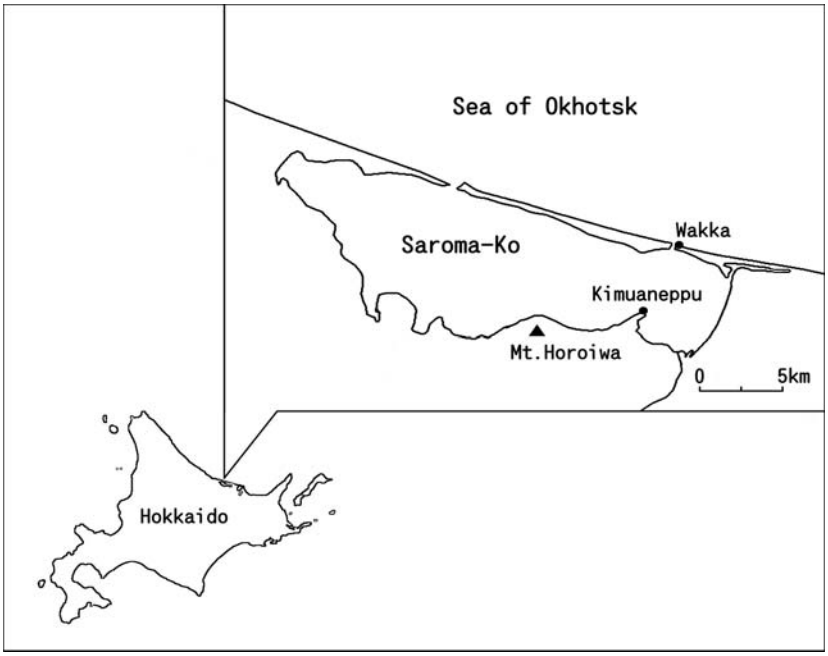

Fig. 1. Observation sites around the Saroma-ko Lagoon

Observation items at each site are air temperature, wind speed, wind direction and humidity. Solar radiation was measured at Kimuaneppu site. Sea ice concentration of the southern part of the Okhotsk Sea was estimated from pictures of radar images taken by Sea Ice Radar Network belonged to the Sea Ice Research Laboratory, Hokkaido University, which covered 50km from the coastline (Ishikawa et al., 1998).

OBSERVATIONAL RESULTS

The relationships between air temperatures at two sites are seen in Fig.2 (Wakka and Kimuaneppu) and Fig.3 (Wakka and Horoiwa). The altitude difference of the former is none and the latter is 370m. The air temperatures at the lake surface level show almost the same values, however with elevation increase the temperature difference became larger.

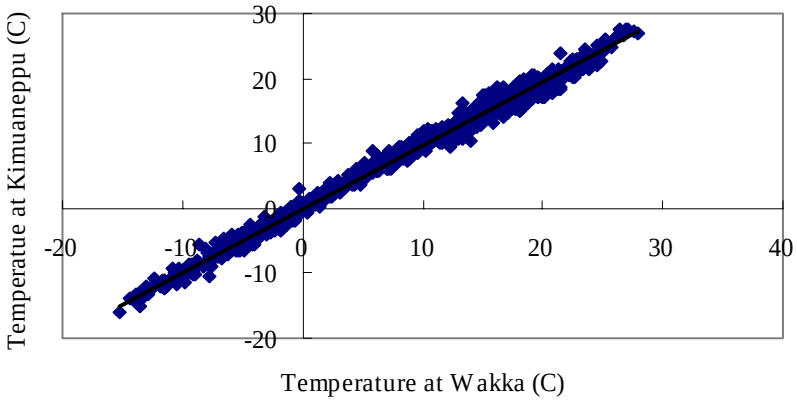

Fig. 2. Relationship between daily mean air temperature at Wakka and Kimuaneppu. (surface level)

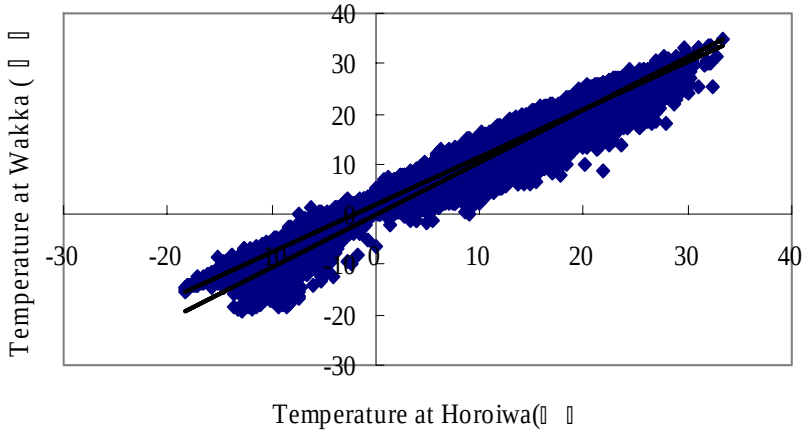

Fig. 3. Same as Fig.2, but at Wakka and Horoiwa (elevation difference: 370 m)

Air temperatures at Wakka were sometimes lower than at Horoiwa throughout the whole year. The monthly mean temperatures at Wakka and Horoiwa were compared. From August to January, the temperatures at Horoiwa were about 2.5°C lower than at Wakka, owing to 370 m elevation difference (the lapse rate was 0.68 °C/100 m), which was nearly the lapse rate of the standard atmosphere. But from February to July the temperature differences between two sites were small, especially in February and May.

Figure 4 shows the frequency of surface temperature inversion for every month, i.e. the percentage of temperature inversions occurring in a month. It is clearly shown that the occurrence of inversion was high during the period of February to July. Usually the temperature inversion occurs due to the surface radiation cooling. Under the conditions of fine and calm weather night, the temperature near the ground surface starts to go down and temperature inversion forms. This phenomenon becomes dominant when the surface is dry soil or snow. In mid-winter, the Saroma-ko lagoon and neighboring Okhotsk Sea totally freezes and snow covers the surface. After April, the sea ice melts away and the water surface appears, so radiation cooling hardly occurs. Further, cool water due to sea ice melt tends to stay, so the air temperature at the surface maintains lower values than the upper site, which results in a temperature inversion.

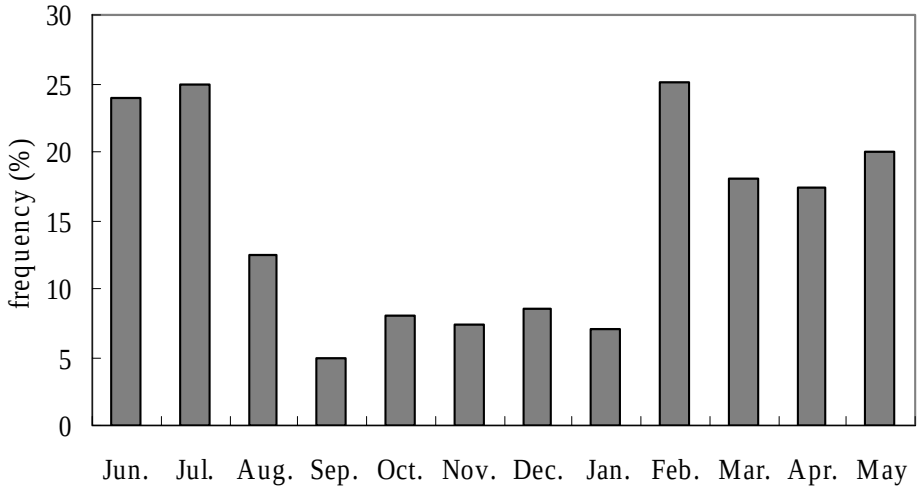

Fig. 4. Frequency of the surface temperature inversion for a month

The daily temperature range, which is the difference between the daily maximum and minimum temperature, expresses the degree of radiation effects. Figure 5 displays the monthly means of the daily temperature range at Wakka and Horoiwa in 1998 to 2001. From December to March the temperature range of Wakka was larger than Horoiwa, and from April to August it became smaller. These results indicate that the cause of the temperature inversion at the lagoon was by radiation cooling due to the lake water freezing in February and March, and was due to the presence of cold water from April to July.

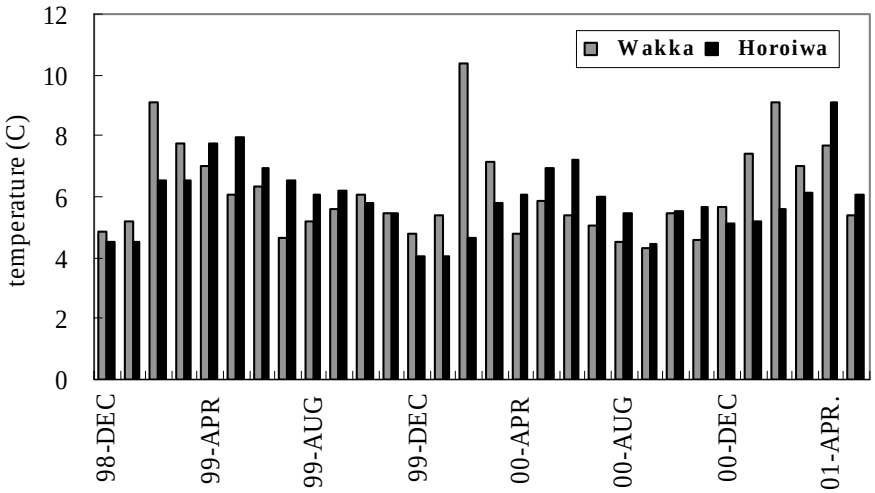

Fig, 5. Monthly means of daily temperature range

The daily mean air temperature for each wind direction was examined for a year. From December to February, the northerly wind was warmer than the other wind directions for both sites. It might be due to warmer water temperature of the ice-free Okhotsk Sea as compared to inland winds. From March to August, air temperatures were lower for northerly winds and higher for southerly winds. No apparent difference was found from September to November.

In order to evaluate the influence of the surface change on the local climate, the idea of climatic sensitivity (Schneider and Dickinson, 1974, Takeuchi et al., 2002) was examined. The climatic sensitivity is defined as the change of a variable indicating the climatic condition to the change of the external condition. In this study, the clearness index (Cx) was regarded as the external condition, the daily air temperature range (TR) was the variable of the climatic condition, and the climatic sensitivity (β) was obtained as the ratio of those two quantities, which is expressed by

$$\beta = TR / Cx. \quad (1)$$

The clearness index was defined as the ratio of daily sum of global radiation observed at Kimuaneppu site (SR) to the daily sum of extraterrestrial radiation (SR_0). When weather was clear throughout the day, the index was about 0.8, and for cloudy day it was closed to 0. The climatic sensitivity defined here indicates how much the air temperature rises for a unit increase of clearness index. Therefore, the seasonal change in surface condition of Saroma-ko Lagoon would change the climatic sensitivity surrounding.

The climatic sensitivities at both sites show the same annual variation, namely, during the sea ice season the values became larger compared with summer water season (Fig.6).

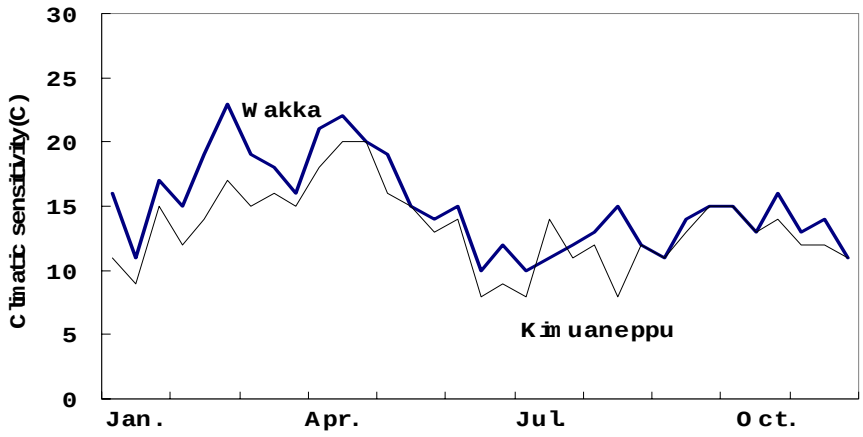

Fig. 6. Variations of climatic sensitivity of Wakka and Kimuaneppu

To examine the influence of sea ice on the change of air temperature, we focus attention on the period before and after high sea ice concentration. Figure 7 shows the sea ice coverage off the coast of the lagoon, obtained by a Sea Ice Radar Network of the Sea Ice Research Laboratory.

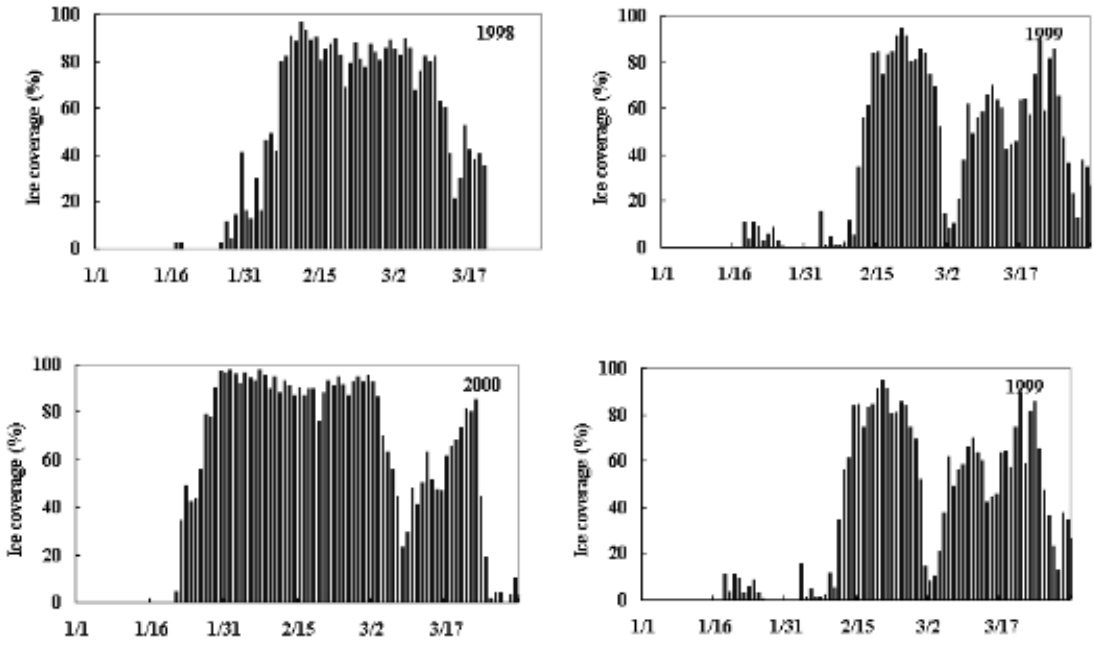

Fig. 7. Time series of sea ice coverage in the Okhotsk Sea from 1998 to 2001

Using these data we compared two different periods; ice-free or low ice concentration period (Period I), and high ice concentration period, which was the period of more than 80% ice coverage (Period II). The difference of 10 days' mean temperature (ΔT) between Period I and Period II at each site was expressed by

$$\Delta T_m(i) = T_m(i)_{II} - T_m(i)_I , \qquad (2)$$

where i means site name (Wakka, Kimuaneppu, Horoiwa), m shows daily mean air

temperature, daily maximum and daily minimum temperature, I and II correspond with Period I and Period II. We can see the clear temperature change before and after the high ice concentration, especially the large temperature drop appeared at the lower level sites, and the dominant influence of sea ice on the daily minimum temperature (Fig.8).

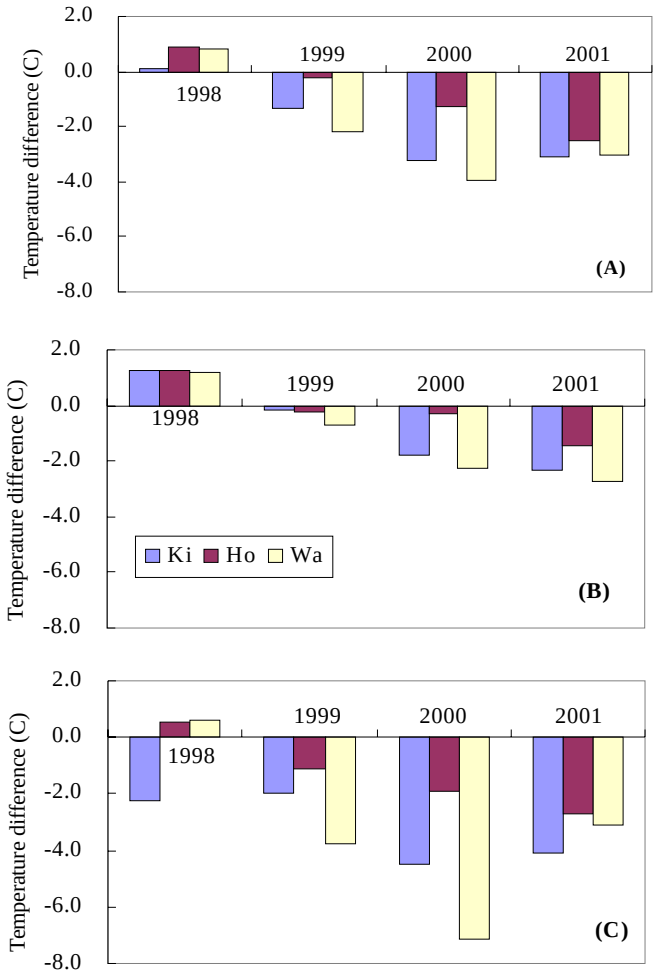

Fig. 8. Differences of 10 days mean air temperature in Period I and II at three sites. (A): daily mean temp. (B): daily maximum temp. (C): daily minimum temp

In this study we examined the air temperature itself to determine whether the cause of temperature drop is due to the surface condition change (water to ice) or synoptic scale cold air mass advection, which brings sea ice from north. In order to see the effect of sea ice on the local climate, we must eliminate the advection effects. The air temperature at higher elevation would reflect the synoptic scale air mass condition rather than the surface condition change. We assume that the temperature difference between Period I and Period II at the Horoiwa site ($\Delta T(Ho)$) was the temperature change of advection air mass. Therefore, the difference of ΔT at lower sites and higher site (ΔM)

would reflect the sea ice effects.

$$\Delta M_m(i) = \Delta T_m(i) - \Delta T_m(Ho), \quad (3)$$

where m is the same index in eq.(2), i: Wakka or Kimuaneppu. This leads to the following equation,

$$\Delta M(i) = \{T(i)_{II} - T(i)_I\} - \{T(Ho)_{II} - T(Ho)_I\} =$$

$$= \{T(i)_{II} - T(Ho)_{II}\} - \{T(i)_I - T(Ho)_I\} \quad (4)$$

namely, ΔM(i) shows the change of the temperature lapse rate between the lower and higher sites before and after high sea ice coverage. Figure 9 shows the magnitudes of lapse rate between Wakka and Horoiwa, and Kimuaneppu and Horoiwa, using the daily mean temperature and the daily maximum and minimum temperature, respectively. The large temperature drop after high ice coverage is shown, especially the effect of sea ice influenced on the daily minimum temperature.

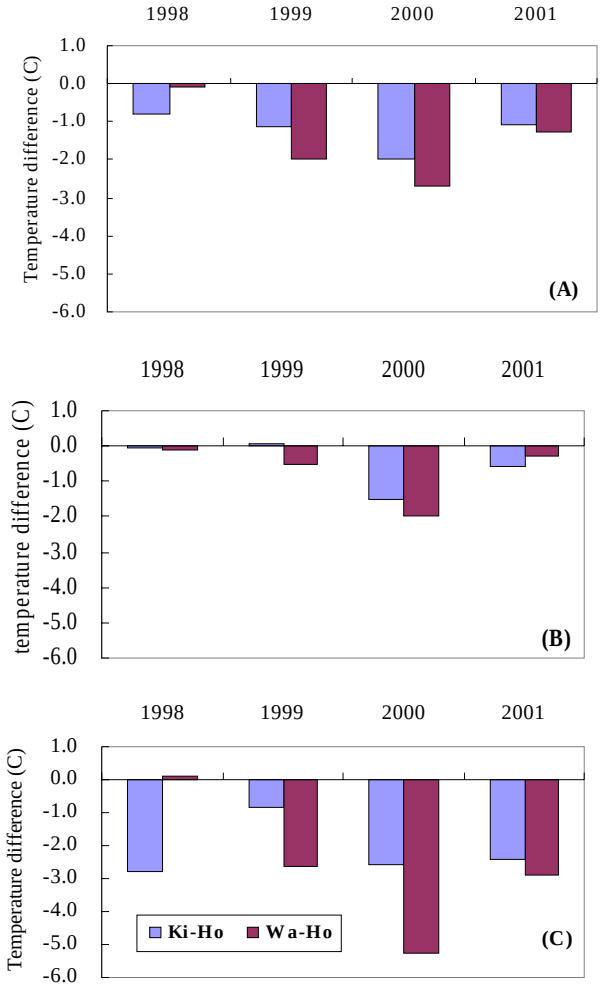

Fig. 9. Differences of lapse rates before and after high sea ice coverage. (A): Daily mean temperature (B): Daily maximum temperature, (C): Daily minimum temperature

The magnitude of ΔM between Wakka and Horoiwa was larger than ΔM between

Kimuaneppu and Horoiwa. The reason was that Wakka was located on the sandbank between lagoon and Okhotsk Sea and the lagoon was usually frozen earlier than the offshore sea, so the air temperature at Wakka was substantially influenced by open water before the high ice concentration developed. But after high sea ice coverage, Wakka was surrounded by sea ice, so the temperature change became dominant at Wakka. ΔM was changeable year by year; the magnitude in 2000 was largest, which is explained by the difference of the duration of high ice coverage. The sea ice coverage in 2000 suddenly increased and the duration of the high ice coverage lasted for a longer time (see Fig.7), so the sea ice effect might become dominant in this year. However, Horoiwa Mt. is not at a high enough elevation to eliminate some amount of daily temperature range. So another observation point with higher elevation is needed for more precise analysis.

CONCLUSIONS:

For examining the sea ice effects on the local climate surrounding land, the long-term meteorological observations have been carried out around the Saroma-ko Lagoon. In early winter the northerly wind was warmer than the other wind directions, which was due to warmer water temperature in the ice-free ocean as compared to the inland winds. The probability of occurrence of surface temperature inversion was high from February to July. During the sea ice season, the inversion occurred by the surface radiation cooling and in late spring it was due to cold water of the lagoon. The climatic sensitivity term was introduced to evaluate the influence of sea ice on the local climate and high sensitivity was obtained during sea ice season.

The temperature change at the sea surface level reflected the synoptic scale air mass effect and interaction with the surface condition. To eliminate the advection affect, the difference of the temperature lapse rates before and after high sea ice convergence was analyzed, and the effect of sea ice was found to be dominant on the daily minimum temperature.

ACKNOWLEDGEMENT

The authors are grateful to the technical staffs of the Monbetsu Sea Ice Research Laboratory, Hokkaido University and graduate students of the Institute of Low Temperature Science who supported the field observation and data compilation. Prof. L.D. Hinzman, University of Alaska read the manuscript. Part of this research was supported by a Grant-in-Aid for Science from Ministry of Education, Science, Sport and Culture of Japan government.

REFERENCES

Allison, I., Tivendale, C.M., Akerman, G.J., Tann, J.M. and Wills, R.H.: Seasonal variations in the surface energy exchanges over Antarctic sea ice and coastal waters. *Annals of Glaciology 3*: 12–16(1982).

Ishikawa, M., Takatsuka, T., Ikeda, M., Shirasawa, K., and Aota, M.: Distributions of pack ice in the Okhotsk Sea off Hokkaido observed using a Sea Ice Radar Network, Jan.-Mar. 1998. *Low Temperature Science, A, 57*, 45-61(1998).

Ishikawa, N., Takizawa, A., Kawamura, T., Shirasawa, K. and Lepparanta, M.: Changes in radiation properties and heat balance with sea ice growth in Saroma Lagoon and the Gulf of Finland. *Proceedings of the 16th IAHR International Symposium on Ice. Dunedin, New Zealand, 2-6, Dec. 2002, 3,* 194-200(2003).

Nakamura, K., Quantitative understanding of the cooling effect of sea ice on the air temperature in the coastal area of the Sea of Okhotsk in Hokkaido. *Tenki (J. of the Meteorological Society of Japan), 43, 6,* 21-28(1996).

Pegau, W.S., Paulson, C.A., Zaneveld, J.R.V.: Optical measurements of frazil concentration. *Cold Region Science and Technology 24*: 341–353 (1996).

Perovich, D.K., Roesler, C.S. and Pegau, W.S. Variability in Arctic sea ice optical properties. *Journal of Geophysical. Research 103*(C1): 1193–1208 (1998).

Schneider, S.H. and Dickinson, R.E., Climate modeling. *Reviews of Geophysics and Space Physics, 12,* 447-493(1974).

Takeuchi, Y., Kodama, Y. and Ishikawa, N.: The thermal effect of melting snow/ice surface on lower atmospheric temperature. *Arctic, Antarctic, and Alpine Reseach, 34,* 1, 20-25(2002).

Weller, G., Heat budget and Heat Transfer Processes in Antarctic Plateau Ice and Sea Ice. ANARE *Science Report A(IV) Glaciology,* 102, 155p (1968).

17th International Symposium on Ice
Saint Petersburg, Russia, 21 - 25 June 2004
International Association of Hydraulic Engineering and Research

SEA ICE PROPERTIES AND UNDER ICE HYDROGRAPHY IN A SHELTERED BRACKISH WATER BASIN

Jari Uusikivi[1] and Kunio Shirasawa[2]

ABSTRACT
In Santala Bay, a small sheltered bay close to Hanko in the Gulf of Finland area in the Baltic Sea, ice properties were investigated during three winters from winter 1998-1999 to winter 2000-2001. Santala Bay freezes every winter and is in a coastal landfast ice region. Measurements include ice cover structure and evolution, ice temperature profiles, under ice water temperature profiles and currents and meteorological data. Heat flux from water through ice cover to atmosphere was calculated and how it was affected by different ice cover properties. Also ice surface albedo variations under different conditions were calculated from short wave radiation measurements.

INTRODUCTION
In a Finnish-Japanese cooperative project, entitled "Ice climatology of the Okhotsk and Baltic Seas" the seasonal evolution of the properties of landfast sea ice in the Baltic Sea was studied during three winters, 1999-2001. Ice Station experiment was performed as a part of that project at the Santala Bay, Hanko Peninsula, Gulf of Finland, the Baltic Sea. A seasonal monitoring part and an intensive field campaign part were included. This experiment focused on the structure and properties of the Baltic brackish ice, under ice currents, heat budget, and solar radiation.

The Baltic Sea is a semi-enclosed brackish water basin where sea ice occurs annually. On the average the maximum annual ice extent is 45 percent of the sea area and in the north the average length of ice season is six months. Interannual variations in the characteristics of ice seasons are quite large. During the last 100 years the maximum ice extent has ranged from 12 to 100 percent and the length of ice season from 4 to 7 months (Haapala and Leppäranta, 1997).

METHODS
Each winter before freezing of Santala Bay, an automatic station was deployed on a floating platform for the surface layer meteorology. Meteorological parameters were

[1] Division of Geophysics, Department of Physical Sciences, University of Helsinki, Finland
[2] Sea Ice Research Laboratory, Institute of Low Temperature Science, Hokkaido University, Mombetsu, Japan.

collected at a 2-m level for air temperature and wind direction and at about 1.5 m and 2m for wind speed. Also surface radiative temperature, humidity, and short-wave and long-wave radiation were included. At the same time a current-meter (ACM32M, Alec Electronics Co. Ltd, Japan) was deployed nearby the floating platform for the temperature, salinity and 3D-flow of the water beneath the ice. When the ice had formed and grown to a safe working thickness, a thermistor string was deployed in the ice. Also a three-month time series of ice samples was collected each winter from Santala Bay, the sampling interval was one week (Ehn et al., 2003).

ICE COVER PROPERTIES

Maximum ice thicknesses were measured each year during March and quite notable variance was observed between years. Winter 1999 had maximum total ice thickness of 0.52 m and it was measured on March 24, winter 2000 had 0.275 m on March 20 and winter 2001 had 0.47 m on March 12 (Ehn et al., 2003).

The composition of ice cover also varied between the years. Every year columnar ice showed similar crystal structure, typical for sea ice, but the proportion of granular ice differed significantly from year to year (Garnskog et al., 2004). In 1999 maximum granular ice thickness was 0.225 m, in 2000 it was 0.07 m and in 2001 it was 0.08 m. Proportions of granular ice from maximum total ice thickness were in 1999 43 percent, in 2000 25 percent and in 2001 17 percent.

In this area snow cover on ice has high variance between years. Winter 1999 had continuous and relatively constant snow cover of 0.05- 0.2 m through the entire ice growth period (Ehn et al., 2003). As winter 2000 had almost no snow on ice during the whole season. And winter 2001 had very variable snow cover and it decayed completely once during the ice growth period.

ALBEDO

Ice cover surface albedo measurements were recorded through winters 2000 and 2001. Daily average (10-14 hours local time) albedo varied between 0.2 and 0.99 during ice cover period. Albedo variation correlated highly with daily average temperature. Occurrence of snow cover had some influence but temperature was the dominating factor during both winters. Diurnal albedo cycle had some interannual variation. Winter 2000 had nice diurnal cycle after beginning of March with highest albedo in the morning and gradual decrease during day and the lowest albedo at the time of sunset. Morning albedos were in some cases five times higher that evening albedos (Figure 1). Some cloudy days had quite constant albedo during the whole day. Winter 2001 had no notable diurnal cycle in the albedo and remained constant throughout the day. From the beginning of March until the end of ice cover season, winter 2001 had lower average incoming radiation and air temperature than winter 2000.

ICE TEMPERATURE

Chain of thermistors was fixed to the ice cover during winters 2000 and 2001. In winter 2000 thermistors were installed 22nd of February in 5 cm intervals and retrieved in the beginning of April. In winter 2001 thermistors were fixed to the float during mounting of the float in December. Thermistors had 10 cm intervals, but only two top ones froze into the ice mid-February. Energy flux through ice to atmosphere was calculated from

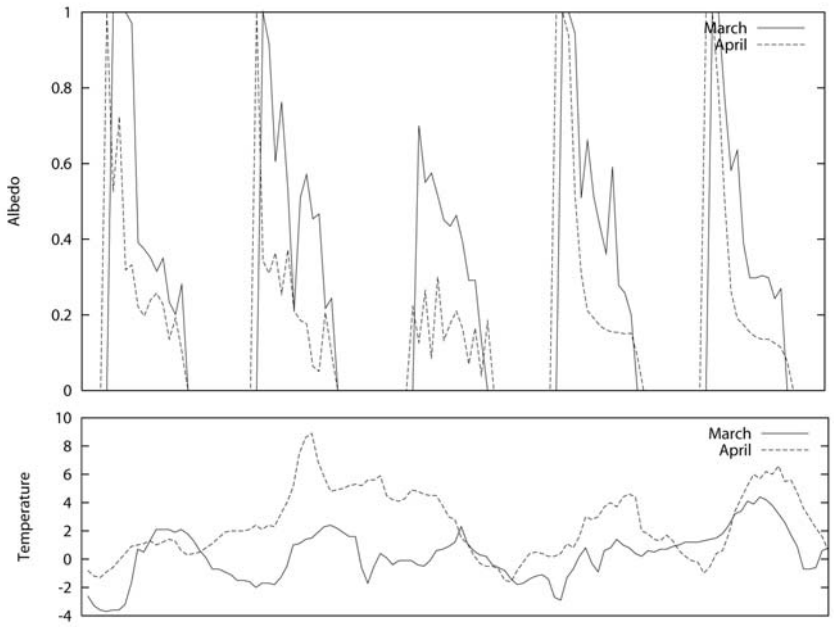

Fig. 1. Albedo and temperature in spring 2000 during March (15-19) and April (2-6)

these ice temperatures. Ice cover surface radiative temperature was recorded during all three winters and energy flux through ice could also be calculated from these observations. When comparing both of these methods in winters 2000 and 2001 it was obvious that surface radiative temperature was accurate method for calculating energy flux through ice to atmosphere. During initial ice formation energy flux through ice to atmosphere was largest, for short periods up to 200 w/m^2 and consistently over 150 w/m^2. After initial ice growth energy flux was smaller and had maximum of 70 w/m^2 during ice growth periods. Energy flux had diurnal cycle so that maximum flux to atmosphere was usually around midnight. Ice growth was very consistent with calculated energy fluxes in the first half of the winter before any melting took place.

HYRDOGRAPHY

Local hydrography and current field was recorded with a three-dimensional electromagnetic current meter with temperature, conductivity and depth sensors and small conductivity-temperature sensor (CT). They were deployed near the ice-station in a place where the water depth exceeded 6 m. In winter 2000 current meter was deployed to the depth of two and half meters and in winter 2001 to the depth of two meters. CT sensor was in three meters depth during both of the winters.

Salinity and temperature measurements have clear signals from ice formation and ice brake-up periods. Both winters have minimum measured water salinity at the moment of initial ice formation. After that water salinities increase through the winter, until right before ice melting commences salinities begun to decrease. Immediately after ice broke-up water salinity was lower than during open water and ice cover season. During ice cover period water salinity had very little fluctuations until the beginning of intense spring melt (Figure 2). Exception being the beginning of February 2001, during a very cold spell in the weather associated with rabid ice growth, water salinities increased rapidly but decreased to preceding values after two days.

Water temperature had annual minimum value during initial ice formation. Temperatures decreased close to the freezing temperatures even in three meters depth. In winter 2000 just before initial ice formation water temperature was at freezing point all the way to the depth of 2.5 meters. After ice cover has formed temperatures were stable and increased gradually during ice cover period.

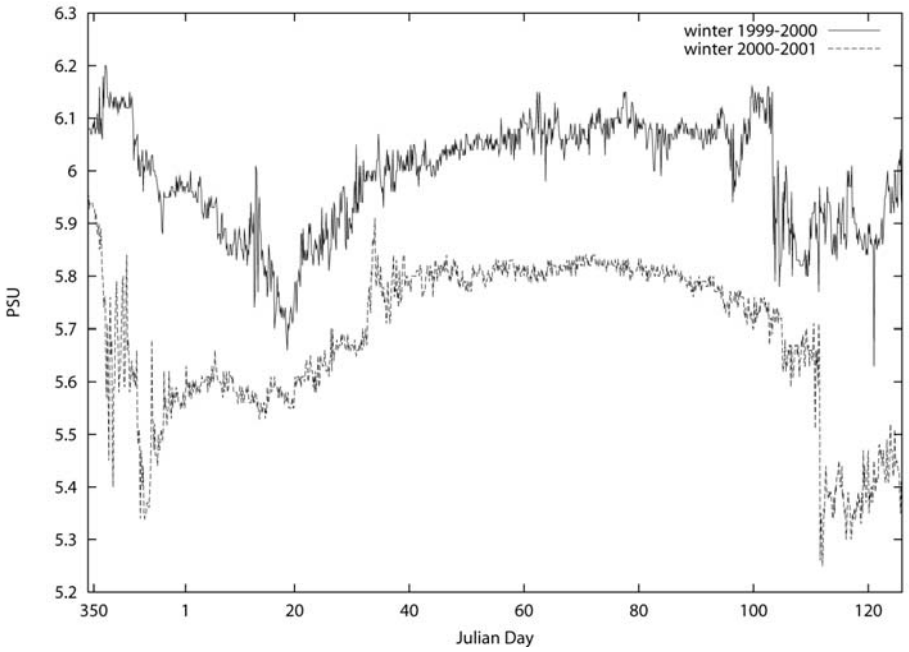

Fig. 2. Water salinity in three meters depth during winters 1999 – 2000 and 2000 – 2001

Winter 2001 had one occasion of fluctuating temperatures at the beginning of February, simultaneously with salinity fluctuations and rapid ice growth. Temperature difference between those two depths was very small and at some occasions even inversed, in particular during two days at the beginning of February 2001. Temperature gradient in the water body was very small, but salinity gradient was sufficient to keep the water body stratified during the whole measurement period.

During winters 2000 and 2001 thermistor chain was mounted to the float for the whole winter season. Most of the ice cover period under ice water temperature was lowest nearest to the ice bottom. Associated with colder air temperatures and intense ice growth were periods with inversed temperature gradient near the ice bottom. During these periods temperature was usually lowest 20 cm under the ice bottom, but there were occasions with lowest temperature 60 or 80 cm under the ice bottom. There were also few cases with uniform temperature between 20 cm and 80 cm under the ice bottom (Figure 3). This indicates that brine expulsion has formed saltier and colder water and that has made this temperature structure possible (Shirasawa and Ingram, 1997). In winter 2001 there were very cold weather and rapid ice growth for eight days in the beginning of February. And by 6th of February the whole under ice water layer, to the depth of 80 cm under the ice bottom, was in the freezing temperature for a short period of time. There were four more situations with similar temperature structures during the two winters but those situations were shorter in duration and were associated with initial ice formation.

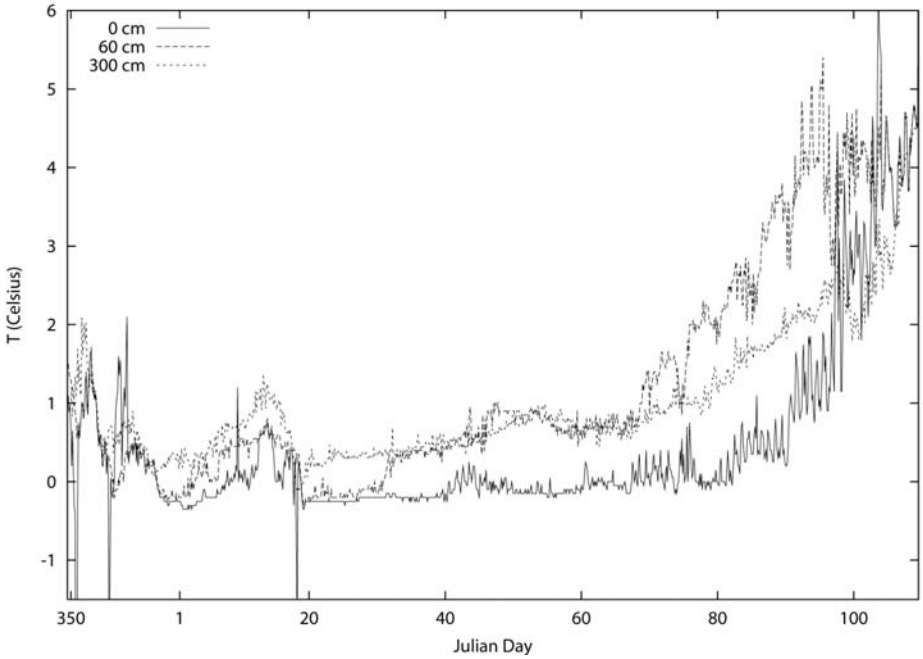

Fig. 3. Water temperature, ice bottom (0 cm), 60 cm and 3 meters below ice bottom

CURRENTS

Three-dimensional current field was recorded with 30 minutes intervals. Average current velocity during ice cover was 3.60 cm/s in winter 2000 and 2.58 cm/s in winter 2001 and maximum measured velocities being 40.4 cm/s and 20.2 cm/s respectively (Figure 4). The 99th percentile from the recorded current velocities in winter 2000 was 18.3 cm/s and in 2001 it was 9.6 cm/s. That makes these very high velocity situations not so uncommon during winter 2000. With 30 minutes measurement intervals the high velocity cases did not usually last long enough to be measured at two consecutive measurements, but there were some (5 and 6 per winter respectively) situations with two successive high velocity measurements. During winter 1999 current measurements were recorded only during March and during that time current velocity did not exceed 4.1 cm/s. During both winters 2000 and 2001 current velocities greater than 99th percentile were all in the same directions, between 73 and 140 degrees and between 261 and 311 degrees, making those directions approximately opposite. Almost 40 percent of all current measurements had current direction between 261 and 311 degrees in winter 2000 and in the next winter almost 50 percent. After ice brake-up until the current meter was retrieved in May average open water current speed was higher, but no high (over ice cover period 99th percentile) current velocities were measured.

CONCLUSIONS

The seasonal evolution of landfast sea ice properties and under ice hydrography was studied during three winters (1999-2001) in the Gulf Finland, the Baltic Sea. The focus was on the ice cover surface albedo, energy flux through ice and under ice temperature, salinity and currents.

Average daily albedo was highly dependent on daily average temperature. Diurnal albedo cycle was very prominent during spring time. Morning albedo was even five times higher than evening albedo.

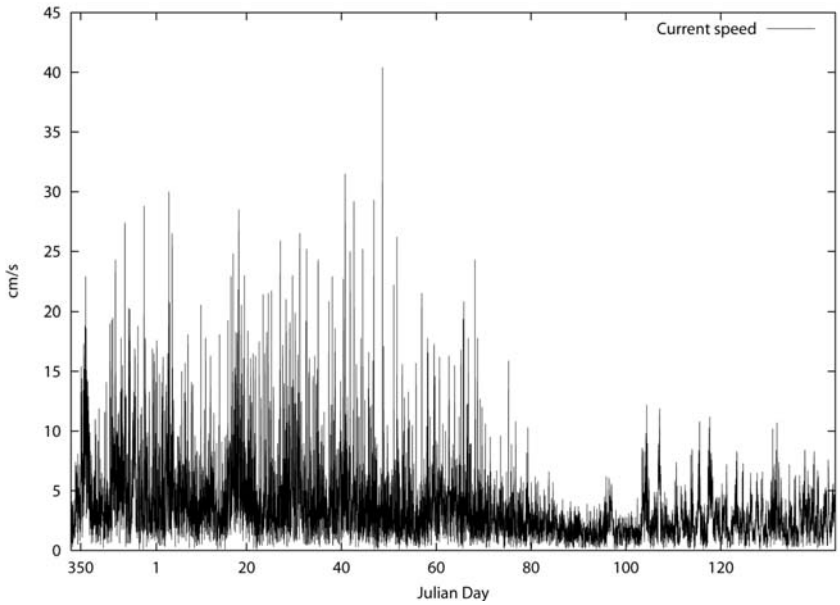

Fig. 4. Current speed (cm/s) during winter 1999 – 2000 at 2.5 meters depth

Calculations of energy flux through ice cover showed that ice surface radiative temperature was good estimate for energy fluxes when compared to ice temperature profile based calculations. Energy flux trough ice cover was highest during and right after initial ice formation. Otherwise energy flux had diurnal variation and maximum energy flux to atmosphere was during night time.

Water salinity and temperature both show clear signals from ice formation and brake-up. Water salinity minimum was during initial ice formation. During the rest of the ice cover period water salinities were very stable.

Water temperature minimum was also during initial ice formation. Water was in the freezing point to the depth of 2.5 meters in the location where water depth was six meters. During ice cover period temperature gradient in the under laying water was very small, in some cases temperature was uniform from 60 cm depth to three meters depth.

Average current velocity at 2.5 meters depth during ice cover was between 3.6 cm/s and 2.6 cm/s and maximum velocities were between 40.4 cm/ and 20.2 cm/s. These high current velocity situations were short in duration, less than 1.5 hours. All the high velocities were measured from same directions.

REFERENCES

Ehn, J., Granskog, M., Ishikawa, M., Ishikawa, N., Kawamura, T., Leppäranta, M., Lindfors, A., Rasmus, K., Shirasawa, K., Takatsuka, T. and Takizawa, A. Data report of the sea ice experiment Hanko-9012. *Report Series in Geophysics 99*, University of Helsinki (2003).

Garnskog, M.A., Leppäranta, M., Kawamura, T., Ehn, J. and Shirasawa, K. Seasonal development of the properties and composition of landfast sea ice in the Gulf of Finland, the Baltic Sea. *J.Geophys. Res., 109*, C02020, doi:10.1029/2003JC001874 (2004).

Haapala, J. and Leppäranta, M. The Baltic Sea ice season in changing climate. *Boreal Environment Research, 2*, 93-108 (1997).

Shirasawa, K. and Ingram, R.G. Currents and turbulent fluxes under the first-year sea ice in Resolute Passage, Northwest Territories, Canada. *Journal of Marine Systems 11*, 21-32 (1997).

17th International Symposium on Ice
Saint Petersburg, Russia, 21 - 25 June 2004
International Association of Hydraulic Engineering and Research

GLACIERS OF CENTRAL ASIA: PAST, PRESENT, AND FUTURE

Malik A. Sattarov[1]

ABSTRACT

This paper is devoted to a generalization of the investigations of glaciers of Central Asia in 1870-1990. An estimate of changes in the hydrological-glaciological characteristics of the glaciation areas and volumes and their influence on the flow-off formation of large Tajikistan rivers is given. A prediction of the state of these parameters due to a climate warming by 1-2^{o}C until 2050 is presented.

The determining role of the orography and orientation of Central Asia mountain ranges in the accumulation of the moisture brought by western and south-western winds was established on the basis of analysis of the data of many years.

A new model of the "ice+water" system in wide rivers is developed. It makes it possible to estimate the hydrological characteristics of the two-phase flow in the period of intensive ice drift.

DYNAMICS OF GLACIER FLOW-OFF OF TAJIKISTAN MOUNTAIN RIVERS.

Now mountainous Tajikistan is the largest glaciation zone in Asia. From the total glaciation area of Central Asia of 17000 km^2, more than 50% is in Tajikistan territory. A large glaciation zone is the mountainous Pamir plateau, whose glaciation area within CIS constitutes 8 thousand km^2. Tajikistan glaciers are the main source of river alimentation in hot dry summer months, when the demand for fresh water in the national economy of Central Asia is maximum (see Table 1).

The history of stage-by-stage investigation of Pamir and Tien Shan glaciers can be conventionally divided into three stages: first, many glaciers of this region were opened and described in 1870-1890. As a result of the second stage of the investigations (1906-1914), in particular, a noticeable change in the location of the end parts of some glaciers of the Peter the Great Ridge was detected. The third stage of more detailed investigations took place in the years of Soviet power, until 1990. For instance, it was shown that in this period, from 1950 to 1990, the area of Gissaro-Alai glaciers reduced by almost one third and the ice volume decreased by a factor of 2. Systematic instrumental measurements of the morphometric characteristics of the Abramov and

[1] Institute of Hydrodynamics SB RAS, prospect Lavrenteva 15, Novosibirsk 630090 Russua
e-mail: msattarov@mail.ru

Skogach glaciers (Bulletin No. 3, SARNIGMI 1999) revealed considerable changes in their spread area and volume in the second half of the XXth century. However, it was found that the largest Fedchenko glacier, whose length, area, and volume are 77 km, 651 km^2 and 130 km^3, respectively, degrades much slower than glaciers of Gissaro-Alai ridges: Over the past hundred years, this Fedchenko glacier retreated by not more than a kilometer, and its area and volume decreased only by 1,7% and 0,8%, respectively. A similar slow retreating of glaciers is also observed in eastern Pamir with a severe arctic climate. This is caused by the orography and the orientation of high mountain ranges of the region with respect to moisture-carrying western and south-western winds (Galtsev, 1964).

Table 1. Hydrography of Tajikistan rivers and glaciers by river basins (Shults, 1965)

River basin	Area, thou. km^2	River flow rate	Total river length, km	Glaciers		
				Number	Area, km^2	Ice volume km^3
Syr-Darya	13,4	(15.9); 0,5	4069	–	–	–
Zeravshan	12.3	5,10	5770	1225	575	30
Karatag,Sherkent	1,6	≈1,1	1098	80	25	0,7
Kafernigan	11,6	5,11	5947	380	85	2,6
Vakhsh	31,2	19,1	12308	2595	3150	264
Pyandzh	65,0	31,9	34867	4700	2960	130
Flow-off free area	8,5	-	5150	575	555	29
Total for TR	143,1	62,8	69189	9555	7350	456

In accordance with some investigations of glaciologists, the main volume (95-97%) of glacier flow-off of Pamir-Alai rivers is formed in the July-September period. Therefore, to estimate the character of change in the glacier flow-off over a long period, it was proposed (A.S. Shchetinnikov, 1977) to take the ratio between the flow-off volume in July-September and the annual flow-off volume in percent, that is, $W_{VII-IX}/W_{год}$ % in the period up to 1990. Here, the glacier flow-off means not the total flow-off from the glacier surface, which also includes the melting of seasonal snow of a given year, but only the melting of ice and firn reserves of many years. Firn is «old snow» that remained from previous years, an intermediate structure between snow and ice. On the basis of this formulation, the glacier flow-off constitutes 35% of the total river flow-off during the July-September period. This share, which constitutes, for rivers of glacier-snow and snow-glacier alimentation, 15-20% and 10-15% of the total annual flow-off, respectively, is in agreement with the relations between the glacier and total flow-off found experimentally (at the partition of hydrographs) (Table 2).

Table 2 Change in the glaciological and hydrological factors of the region in 1957–1980

Change factors	Geographical region	
	Gissaro-Alai	Pamir
1. Altitude interval of the greatest glaciation: a) km (above sea-level) б) in % to the total glaciation area	 3,70 – 4,40 70,4	 4,40 – 5,40 68,1
2. Altitude interval of the greatest glacier flow-off: a) km. (above sea-level) b) m^3/year c) in % of the glacier flow-off volume from the entire area	 3,70 – 4,40 2,8 90	 4,00 – 5,00 4,6 70
3. total glaciation decrease in 1957-80, %: a) in the entire glaciation area b) at Tajikistan territory	 15,6 17,1	 10,5 10,8

To predict the change in the glacier and total river flow-off over a long period, up to 2050, at an increase in the average summer air temperature by 1^0C - 2^0C, the calculation model developed by G.E. Glazyrin et al. (1986) was used. It is based on the dependence W= F(S; ΔT), where W, S, and ΔT are the changes in the flow-off volume (in %), glaciation areas (in %), and deviation from the norm (1990) of the average summer air temperature (in ^{0}C), respectively, in the period (Table 3).

Table 3 Prediction of the influence of climatic factors on glaciation areas and share of glacier flow-off

Change of climatic factors	Change of glaciation area, in %	Change of glacier flow-off, in %
Change of summer temperature:		
а) by +1°C	–30,3	–25
б) by +2°C	–57,6	–45
Change of precipitation:		
а) by +20%	26,9	44
б) by +10%	14,2	23

The change in areas of the glaciation and glacier flow-off in the Pamir-Alai plateau in the second half of the XXth century and first half of the XXIst century at different climatic scenarios, including a strong warming (by 2^0C), was investigated by G.E. Glazyrin et al. (1986). Table 4 shows the total flow-off decrease in percent in comparison to its norm for 1990 and the flow-off decrease in large Tajikistan rivers in every 15 years, until 2050.

Table 4. Prediction of decrease in total river flow-off* (in %) at a warming to+2^0C versus the share of glacier alimentation in comparison with 1990.

River – station	Average annual flow-off volume in years, km^3				
	1990	2005	2020	2035	2050
Zeravshan –Pendgikent	5,10	4,96	4,88	4,79	4,70
Kafernigan – Tartki	5,11	5,05	5,01	4,98	4,94
Vakhsh –Komsosolabad	19,1	18,6	18,3	17,9	17,6
Pyandzh – Nizhni Pyandzh	31,9	31,1	30,7	30,2	29,7
Total	61,2	59,6	58,9	57,9	56,9
Decrease in 1990 – 2050	–	1,50	2,30	3,30	4,30
In % from 1990 norm	–	2,45	3,76	5,39	7,03

*The calculation was made with allowance for the transboundary flow-off from Kirghizstan and Afganistan

RHEOLOGY OF THE «ICE+WATER» SYSTEM AND ITS MODEL DESCRIPTION

The rheological state of the ice cover of most rivers can be divided into the following three stages: spring and autumn ice drift, and winter freezing-over. Let us assume that the joint motion of an ice layer of thickness h_1 and liquid water of thickness h_2 takes place in a river of width B ($B>>h_1 + h_2$). In contrast to liquid water, whose motion is described by the Newtonian rheological model, the ice layer is an elastically viscous body, whose motion is described by rheological models of the Shvedov-Bingham type (Riner, 1965). From the hydrodynamical point of view, the Reynolds averaged particle velocity of the «ice+water» body consists of two parts. These are the ice layer motion with at a constant maximum speed (since there is no relative motion of ice particles

inside the layer) and the particle motion of liquid water, which takes place in accordance with the conventional laws of motion of viscous liquids. The shearing of glaciers (for instance, of the Medvezhiy glacier) in natural conditions takes place under gravity in accordance with the laws of dry friction. At the breakage of the glacier structure under the action of a natural phenomenon, such as an earthquake, the ice mass flow differs essentially from the mechanics of sliding of a solid body over a rigid surface. In this case, the flow of the broken glacier mass, under which a liquid water layer has been formed, can be represented in the same way as the scheme of «ice+water» motion.

To describe the flow dynamics of the «ice+water» system, let us use the model theory (Sattarov, 1972). The equation of the steady homogeneous flow is written as follows:

$$\left.\begin{array}{l} d\left[\nu\left(-u_z + N(z/H)\right)\right] = gIdz, \\ Q = U\omega = const. \end{array}\right\}, \quad \tau_0 = \mu N(z/H), \quad H = h_1 + h_2 . \tag{1}$$

Here, the *Oz*-axis is directed vertically downward from the ice layer lower surface, *u(z)* is the velocity of a Reynolds averaged water particle, τ_0 is the additional shearing stress, which appeared at the pulsation of particles of the liquid, μ and ν are the dynamic and kinematic viscosities of the system, g is the acceleration of gravity, $I = \sin\alpha$, α is the slope angle of the bottom, Q and U are the flow rate and average velocity, and ω is the area of the flow effective cross-section.

Let the velocity profile of the liquid flow in the channel be a smooth surface with extreme points ξ_*. Then we obtain from the first integral (1) (Sattarov, 1972):

$$z_*\left[gI/\nu - N(z_*/h_2)/z_*\right] = 0 , \tag{2}$$

Based on the hydrodynamic meaning of the roots of equation (2), we divide the set of moving liquids into two groups.

Let the velocity profile surface of liquid water have a maximum point $z_*=0$. Such liquids, which include classical Newtonian liquids, can be called generalized Newtonian liquids (GNL). The velocity maximum condition at the point $z_* = 0$ for the function $N(z/h_2)=M^*(z/h_2)^n$ demands that the inequality $n>1$ be satisfied. Then the second root (2) is a minimum point. For a nondeformable bed, this point $z_* = h_2$ and , where τ_c is the stress at the flow bottom. We consider that the «ice+water» system belongs to GNL. The upper ice part of the ($-h_1<z<0$) system, as well as the velocity of liquid water at the ice layer lower surface at the point $z = 0$ moves at the maximum speed. In accordance with the classification presented, the solution to equation (1) describes the law of flow of the «ice+water» system:

$$u_{ice}(h_1) = \text{const} = u_{w.\max}(0) \tag{3}$$

$$u(z) = \frac{gI}{2\nu_w}\left(h_2^2 - z^2\right) - \int_z^{h_2} N(z/h_2)dz \equiv u_l - u_{tr} . \tag{4}$$

Formula (4) is a self-similar velocity distribution of the GNL flow, which consists, in accordance with the principles of similarity theory (A.A. Townsend, 1956), of the following two parts: u_l is the velocity profile of the laminar flow and u_{tr} is the correction of the profile due to the pulsation of liquid particles in the bed. Thus, depending on the nature of the additional stress $N(z/h_2)$, velocity profile (4) is flat if $N(z/h_2) > 0$ or

stretched if $N(z/h_2) < 0$. At $N(z/h_2) = 0$, the Poiseuille-Stokes parabola follows from (4). Let us consider the case of additional stress of the following form:

$$\tau(z/h_2) = \mu N(z/h_2) = \mu M(z/h_2)^n \equiv \rho g I h_2 (z/h_2)^n, \qquad n > 1. \tag{5}$$

Then, from (4) and (5), we have for the velocity profile $u(z)$ and the average velocity U of GNL:

$$u(z) = \frac{gIh_2^2}{2\nu_w}\left[\frac{n-1}{n+1} - \left(\frac{z}{h_2}\right)^2 + \frac{2}{n+1}\left(\frac{z}{h_2}\right)^{n+1}\right], \tag{6}$$

$$u_{w.\max}(0) = u_{ice}(h_1) = \frac{gIh_2^2(n-1)}{2\nu_w(n+1)}, \tag{7}$$

$$U_w = \frac{(n-1)gIh_2^2}{3\nu_w(n+2)}. \tag{8}$$

The total flow rate of the «ice+water» system is determined by the formula

$$Q_{i+w} = U_i h_1 + U_w h_2 = \frac{(n-1)gI(H-h_1)^3}{3\nu_w(n+2)}\left(1 + \frac{3(n+2)k}{2K(n+1)}\right), \tag{9}$$

where $\kappa = h_1/h_2$, $K = \nu_{ice}/\nu_w$.

Hence, as $n \to \infty$, we have the laminar flow law of the «ice+water» system. In the absence of ice ($k = 0$), we have the law of homogeneous turbulent water flow in channels of comparatively large width (Sattarov, 2003).

CONCLUSION

Step-by-step statistical processing of the data obtained by I.A. Shiklomanov (UNESCO, 1998; UNESCO 2000, Paris) has shown that in the period from 1961 to 1985, in comparison with that from 1921 to 1960, the water resources in Central Asia (CA) countries decreased by 5-6%. At the same time, a similar comparative analysis of the dynamics of water resources of Ukraine and Azerbaijan gave the opposite result: it turned out that in the period investigated, the water resources of these countries increased almost by 10% and 7%, respectively. The predicted decrease in the total annual flow-off volume of Tajikistan rivers by 7% by 2050, at an amplitude of its oscillations equal to (+30%; -24%), seems insignificant (Sattarov et al., 2002).

A considerable reduction of the glaciation areas, as well as a decrease of the role of glaciers in the change of the annual river flow, have a negative impact on the most vulnerable branches of economy, agriculture, and hydro-electric engineering. Total modernization of the irrigation farming agriculture system and the completion of constructing a complex of large water reservoirs in CA mountain gorges, which allow us to regulate the flow-off of mountain rivers for many years, are deciding factors of adaptation measures, mitigating the unfavorable consequences of changes in the climatic conditions.

Improvement of the basic physics of the rheology of shearing and breakage of glaciers, calculation of the hydrological, hydrophysical, and hydrothermal characteristics of

motion of the «ice+water» system, as well as the dynamics of the enforced water flow in the freezing-over period, is an important problem of modern glaciology.

REFERENCES

Galtsev A.P. Dependence of precipitation in Central Asia mountains on the irrigation of submountain plains, *Izv.Akad. Nauk SSSR, Ser. Geogr*, No. 2, (1964).

Glazyrin G.E. et al."Change in the glacier flow-off of Central Asia rivers due to a possible climatic *change Proc. of SANNIGMI, Goskomgidromet, issue* 117 (198), (1986) 59-70.

Climatic change and surface water resources of the Aral Sea. *Bulletin No.3, V.A. Bugayev SARNIGMI*, Tashkent (1999).

M.Riner. Rheology (translation from English).M.*: «Nauka»*, (1965) 223 p.

Sattarov M.A. et al. Water resources and water industry of the Tajikistan Republic (ed. by M.A.Sattarova). Report on the vulnerability of water resources and water industry of Tajikistan at the change of climatic factors. *UGMS of the Tajikistan Republic, Dushanbe*, (2002) 52 p.

Sattarov M.A. Some Models of Filtration in Porous Media. *Dokl. Akad. Nauk SSSR*. V.203, No.1, (1972) 54-57.

Sattarov M.A. A model method to calculate turbulent characteristics of the flow in rectilinear channels. *J. « Kishovarz – Agriculture»*, Dushanbe, (2003) No. 4.

A.A.Townsend. The Structure of Turbulent Shear Flow. (translation from English) *Izd. Inostr. Lit, M.:* (1959) 400 p.

Shiklomanoov I.A. Water resources of the World at the Beginning of 21st Century. UNESCO, Paris (1998).

V.L.Shults. Rivers of Central Asia. *L.*, (1965) .

Shchetinnikov A.S. The Morphology of Glaciation of Pamir-Alai River Basins as of 1980 (Reference book) Tashkent (1997), 18-35.

Water Related Vision for the Aral Sea Basin. UNESCO, Paris, (2000) 237p.

17th International Symposium on Ice
Saint Petersburg, Russia, 21 - 25 June 2004
International Association of Hydraulic Engineering and Research

HELICOPERBORNE MULTI-FREQUENCY, MULTI-POLARIZATION SCATTEROMETER MEASUREMENTS DURING ARK XIX/1

Stefan Kern[1] **and Martin Gade**[1]

ABSTRACT
Sea ice type classification based on active microwave remote sensing can be improved using multi-frequency, multi-polarization data. We present results of a first analysis of such data acquired by the helicopterborne multi-frequency (five different frequency bands), multi-polarization (all like- and cross polarizations) scatterometer HELISCAT during ARK XIX/1 around Svalbard. HELISCAT C band data were compared to almost coincident Envisat ASAR imagery yielding a correlation of 0.496 and 0.745 for two selected flight legs and a good agreement in the relative C band backscatter variation along the flight track. Changes in L, (C), and K_u band data are in good agreement with changes in sea ice thickness from electromagnetic thickness sounding, laser altimetry of the sea ice freeboard, and CCD-camera imagery.

INTRODUCTION
Spaceborne remote sensing sensors such as the synthetic aperture radar (SAR) aboard, e.g., the European Remote Sensing Satellites ERS-1/2, the Canadian RADARSAT-1, and the recently launched Envisat ASAR provide high-resolution information about different surface properties by means of backscatter measurements. Among other application fields, SAR data is used for high-resolution sea ice mapping, and has improved our knowledge about sea ice type distribution. However, the incidence angle dependency of the SAR signature of both sea ice and wind-roughened open water, the camouflaging effect of a snow cover, and the often very small changes in sea-ice backscattering properties of significantly different sea-ice types hamper sea ice type discrimination and lead to ambiguous results of classification methods used for sea ice mapping. Such ambiguities can be effectively reduced and the sea ice type discrimination can be improved if backscatter measurements of different frequencies and different polarizations are combined (Rignot and Drinkwater, 1994; Dierking et al., 2003). We present and discuss first sea ice backscatter measurements done with the helicopter-borne multi-frequency, multi-polarization HELISCAT instrument over Arctic sea ice in winter during the expedition ARK XIX/1 in 2003. The paper is organized as

[1] University of Hamburg, Centre for Marine and Climate Research, Institute of Oceanography, Bundesstrasse 53, D-20146 Hamburg, Germany

follows. An introduction of the HELISCAT system is given in the next section, followed by a brief description of the two flights considered here. The second section is about the results and is followed by some discussion and conclusion.

THE INSTRUMENT

The HELISCAT (HELIcopter SCATterometer) was developed and built at the University of Hamburg and is flown on a Messerschmidt-Bölkow-Blohm BO-105 helicopter. It operates at 1.25 GHz, 2.4 GHz, 5.3 GHz, 10.0 GHz, and 15.0 GHz (L, S, C, X, and K_u band, respectively) and is capable of performing radar backscatter measurements quasi-simultaneously at the four polarization combinations VV, VH, HH, and HV (the first and the second letters denote the polarization of the transmitted and of the received microwave, respectively; V means vertical and H horizontal polarization). HELISCAT uses a single broad-band 96cm parabolic dish antenna both for transmission and reception. The antenna is aft-looking and can be tilted mechanically during the flight in such a way that the *nominal* incidence angle covers the range between 23° and 65°. The *effective* incidence angle, particularly at L and S band, horizontal polarization, may be slightly smaller, because of the antenna beam geometry. The system parameters of HELISCAT are given in table 1. Numerous experiments were carried out with the HELISCAT (primarily over open water) to help interpreting spaceborne data as, for example, of SIR-C/X-SAR (Gade et al., 1998; Wismann et al., 1998). However, the measurements shown and discussed in this paper are the first taken with the HELISCAT in its present form over Arctic sea ice and during winter conditions.

Table 1. Specifications of the HELISCAT system

Scatterometer Type	Superheterodyne Doppler Scatterometer				
Antenna Type	Parabolic Dish, 96 cm Ø				
Polarization	HH, HV, VV, VH				
Nominal Flight Altitude [m]	150				
Nominal Ground Speed [m/s]	50				
Nominal Incidence Angle [°]	23–65				
Pulse Repetition Frequency [kHz]	40				
Radar Band	**L**	**S**	**C**	**X**	**K_u**
Frequency [GHz]	1.25	2.4	5.3	10.0	15.0
Output Power [mW]	150	100	40	10	10
Antenna Beamwidth (2-way; 3 dB) [°]	17.0	7.1	3.2	1.7	1.1
Antenna Footprint at 23° incidence angle [m × m]	53.1×24.4	22.0×10.1	9.9×4.6	5.3×2.4	3.4×1.6
53° incidence angle [m × m]	128.9×37.3	51.7×15.5	23.2×7.0	12.3×3.7	8.0×2.4

All measured data were stored on tape and were digitized after the campaigns. Because of the limited number of recording channels and since the two cross-polarization channels at a single radar band contain the same information, only time series at VV, HH, and HV polarization were recorded. In addition, time series of the helicopter's pitch and roll measured by a gyre were recorded simultaneously. Images acquired by a CCD-camera looking at the footprint of the antenna were also recorded on tape and complete the data set, together with GPS information and digital photographs taken at selected waypoints along each flight track.

For the investigations presented herein only the variations in the backscattered radar power from different ice (and snow) surfaces are of interest. Therefore, HELISCAT was not absolutely calibrated (thus yielding the relative backscattered power, RBP, instead of the normalized radar cross section, NRCS). For each radar band time series at the three polarization combinations, HH, HV, and VV were sampled at a frequency of 10 kHz. From these time series radar Doppler spectra (of length 4000) were calculated, and the integral of the spectral Doppler peak (within its 6 dB limits) was used for the computation of the RBP time series with a sample rate of 2.5 Hz (time steps of 0.4 s). Note that, because of the wider beamwidths at L and S band, at a nominal ground speed of 50 m/s and at a nominal flight altitude of 150 m consecutive data points in the RBP time series at L and S band represent the backscattered radar power from overlapping surface areas. Only data with a signal-to-noise ratio exceeding 3 dB have been used, in order to avoid any influence of the instrumental noise on the obtained results. For this reason, we restricted our investigation on HH and VV polarization data.

THE EXPERIMENT

The presented data were acquired during two (April 15 and 19, 2003) of a total of 14 flights which took place during the cruise of the research icebreaker *Polarstern* ARK XIX/1 in the framework of the Winter ARctic Polynya Study (WARPS) and CRYOsat Validation EXperiment (CRYOVEX) between Feb. 28 and Apr. 24, 2003, near Svalbard. On April 15, the *Polarstern* was on drift station anchored to a large multiyear ice floe at about 81.81°N/10.22°E. The helicopter flight took place between 9:20 and 9:50 UTC along a triangle of about 60nm length, heading 180°, 60°, and 300°. Flight altitude was about 80 m; the speed above ground was 50 m/s. The sky was clear, wind speeds were around 5 m/s, and air temperatures were around –18°C. Prevailing ice was multiyear ice with overfrozen leads.

On April 19, the *Polarstern* was slowly heading south. The flight started at 81.26°N/ 10.60°E, took place between 18:30 and 19:10 UTC along a triangle of about 80 nm length, heading 270°, 150°, and 30°. This flight was a tandem flight together with the helicopter-borne electromagnetic ice thickness sounder (EM-Bird) of the Alfred-Wegener Institute (AWI) mounted on a second helicopter flying about 100 m ahead of the helicopter carrying the HELISCAT. Therefore, flight track and speed above ground (60 m/s) are essentially the same. Flight altitude was again 80 m. Weather conditions: little high cloud, wind speeds around 5 m/s, and air temperatures around -15°C. There was no change in the prevailing ice type to April 15.

RESULTS

April 15

Data of this flight are presented here, because of the ability to compare relative variations in HELISCAT C band HH polarization backscatter with a quasi-coincident Envisat ASAR wideswath image (C band, HH polarization) acquired at 12:30 UTC, same day. A comparison was made for two specifically, i.e. by means of GPS data and digital images, selected legs along the flight track of the helicopter. Figure 1 shows a subset of the Envisat ASAR wideswath image superimposed by the two legs. Bright areas in this image correspond to high backscatter values as caused, e.g., by a rough surface (in case of surface scattering), or by porous or comparable ice/snow properties (in case of volume scattering). This can be rough and/or deformed first-year ice and/or

multiyear ice. Dark areas correspond to low backscatter values as caused, e.g., by a smooth surface – which can be level and/or young ice or a calm open water area.

A correction was applied to the flight track taking into account a possible drift of the *Polarstern* attached to the multiyear ice floe within the three hours between the HELISCAT flight and acquisition of the ASAR image. Here it was assumed that the movement of this ice floe corresponds to the drift of the *Polarstern* during the three hours period mentioned, and that this movement is representative for the drift of the entire sea ice region covered by the helicopter flight. The *Polarstern* drifted by about 50 m towards north and by about 700m towards east between HELISCAT flight and ASAR image acquistion. Moreover, the ASAR image was corrected for the incidence angle variation across the subarea shown in figure 1 a), assuming that the sea ice incidence angle dependency can be neglected over this lateral distance (50 km).

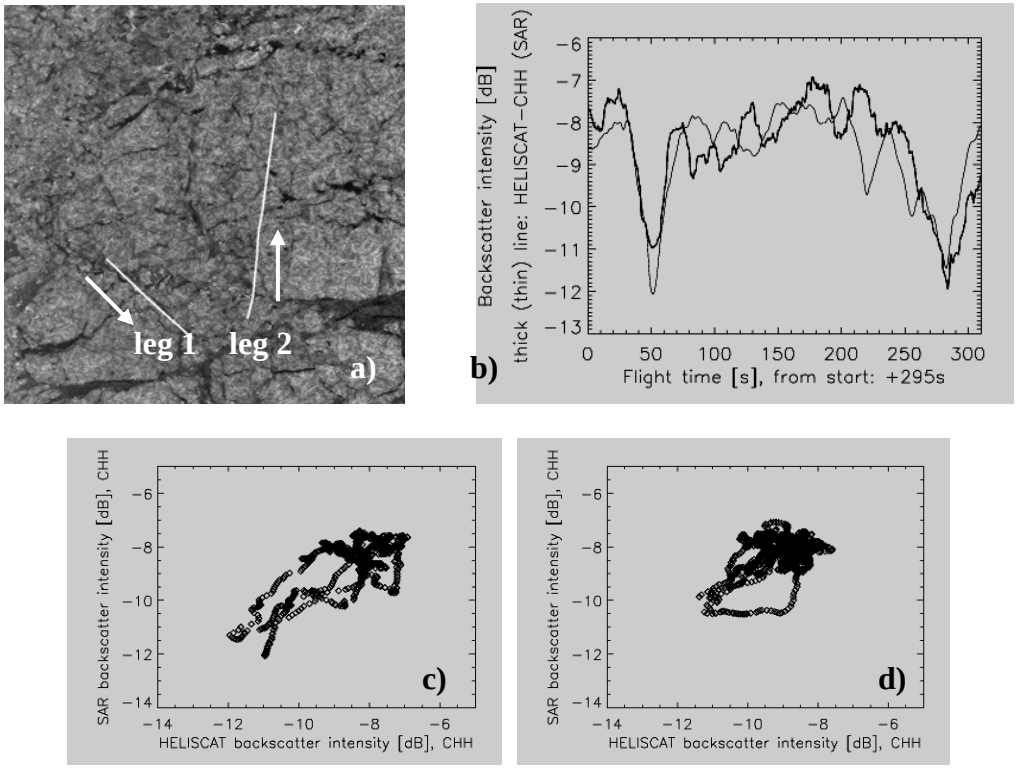

Fig. 1. a) Zoom of a near-range (25° incidence angle) subarea of an Envisat ASAR wideswath image acquired at 12:30 UTC on April 15, 2003, superimposed with two legs (white lines) of the flight track of the helicopter (flight direction is indicated by the arrows); pixel size is 75 m x 75 m; b) comparison of HELISCAT (thick line) and Envisat ASAR (thin line) C band HH polarization backscatter along leg 1, averaged over 500 m; c) scatterplot of backscatter values shown in b); correlation of both data sets is 0.745; d) same as c) but for leg2; correlation of both data sets is 0.495

The good agreement between HELISCAT and Envisat ASAR data puts some confidence to the HELISCAT measurements of which one more example is shown in figure 2. This figure 2 shows a comparison of C and K_u band data: profiles of the relavite backscatter and the polarization ratios, i.e., the ratio of VV and HH polarization backscatter.

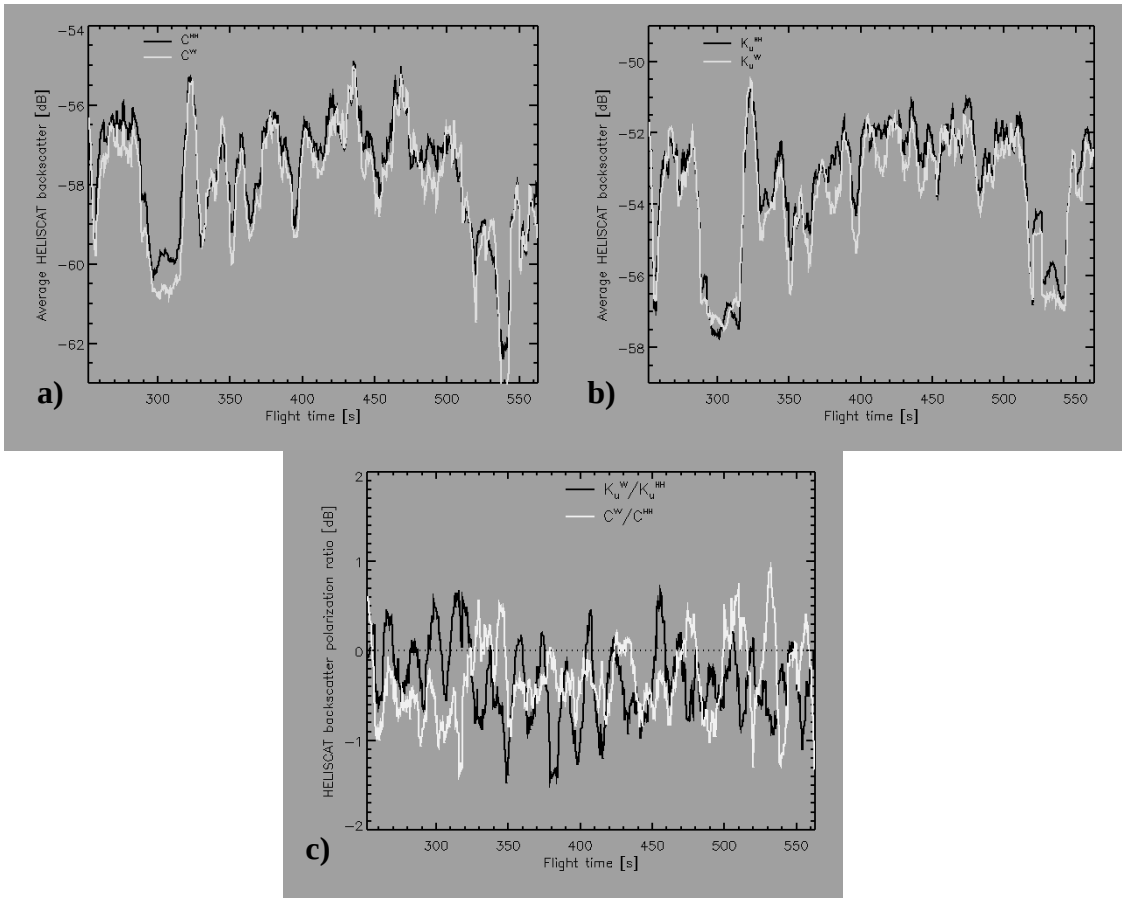

Fig. 2. a) HELISCAT C band backscatter along leg1; b) same as a) for K_u band;
c) C and K_u band polarization ratios along leg1

April 19

Data of this flight were selected, because it is the only flight which was carried out together with the EM-Bird of the AWI, and therefore, HELISCAT data can be related to ice thickness measurements. Moreover, an analysis of the CCD-camera imagery was carried out. For this purpose, the CCD-camera movie was digitized and split into single images (25 images per second). For a footprint equivalent subarea (the CCD-camera viewed a larger area than the HELISCAT, even at L band) gray levels of each single image were averaged and stored together with the variance and extreme values. Finally, data of a laser altimeter carried by the helicopter with the EM-Bird were analysed yielding the sea ice freeboard along the flight track with high resolution (100 Hz). In the following we show a comparison of L, C, and K_u band HELISCAT data acquired at HH and VV polarization with EM-Bird sea ice thickness, laser sea ice freeboard, footprint equivalent CCD-camera mean gray level and its standard deviation. These images are discussed in the following section. Note that the sea ice thickness values represent the total thickness of the sea ice floating in the water, i.e. thickness variations which can be identified in the profile are not necessarily caused by rigdes only but by keels also.

DISCUSSION AND CONCLUSIONS

Backscatter values acquired by the HELISCAT in C band, HH polarization, during the flight on April 15 have been compared to Envisat ASAR imagery along the flight legs.

This first comparison, although limited, yielded encouraging results insofar as the HELISCAT was able to i) identify smooth ice areas at approximately the same locations as the ASAR and to ii) provide relative changes in backscatter values which are consistent with those measured by the ASAR. In order to improve the quality of this comparison several steps are suggested: i) a correction of HELISCAT backscatter values for incidence angle variations, ii) the consideration of the difference in incidence angle and look direction between HELISCAT and ASAR, iii) an improved estimate of the sea ice drift between flight and ASAR image acquisition, and iv) the calibration of the HELISCAT data. At a first glimpse there is no evidence for a difference between the relative C and K_u band backscatter along leg 1 (figure 2). However, the polarization ratios given in figure 2 c) show that while relative backscatter values reveal similar variations the polarization ratio can differ a lot. Between flight time 310-330 s, and 470-540 s changes in C band polarization ratio seem to oppose changes in K_u band polarization ratio. Since no supplementary data (CCD-camera and laser altimeter) of this flight have been analyzed so far, no suggestion about i) the significance of these opposing changes, and ii) their origin can be made.

Backscatter values acquired by the HELISCAT on April 19 have been compared to footprint equivalent CCD-camera mean gray levels (GL) and corresponding standard deviations (GLSD), EM-Bird ice thickness data and laser altimeter sea ice freeboard data. The backscatter values reveal clearly the different ice types associated with the change in thickness between multiyear ice (around 3 m) and thin first-year and young ice (below 0.5 m) as is typical for leads (see figure 3 a) to f)). Especially in L and K_u band the agreement between low backscatter and thin ice on the one hand, and high backscatter and thick ice on the other and is striking (see arrows in figure 3 g)). The agreement between ice thickness variations and changes in the polarization ratio is less pronounced and limited to L and C band (figure 3 g)) and lead 2. Note that due to the missing absolute calibration the given polarization ratios are not necessarily correct. This is evident from figure 3 a) wherein the L (C) band polarization ratio is below (above) zero over multiyear ice but should be zero in both cases, because of the isotropic character of volume scattering in multiyear ice. The polarization ratio at K_u band seems to be not affected by the change in sea ice thickness at all (figure 3 h)).

No agreement was found between GL and the sea ice thickness – except that significant drops in the gray levels are observed where the EM-Bird indicates open water or thin ice (see figure 3 g), leads 1+2). However, some agreement was found between the GLSD and the laser altimeter sea ice freeboard: the GLSD tends to be low for a small sea ice freeboard and large for a large sea ice freeboard. But in lead 2 (figure 3 g)) a small sea ice freeboard (and thin sea ice) corresponds to a large value for the GLSD. The same is observed in leads 3 and 4 (figure 3 g)). According to the flight log the latter was covered by frost flowers that might have caused the large variability. Note in this context the HELISCAT C band backscatter measured over lead 2 (figure 3 c),d), figure 4). While L and K_u band backscatter values decrease (increase) by about 5 to 8 dB at the start (end) of this lead, the C band backscatter first decreases but then sharply increases at both HH and VV polarization. There is no evidence for this behaviour in the sea ice freeboard (figure 4 a)) or the sea ice thickness (figure 4 b)), however, a peak can be identified in the GLSD (figure 4 c)). This needs further investigations.

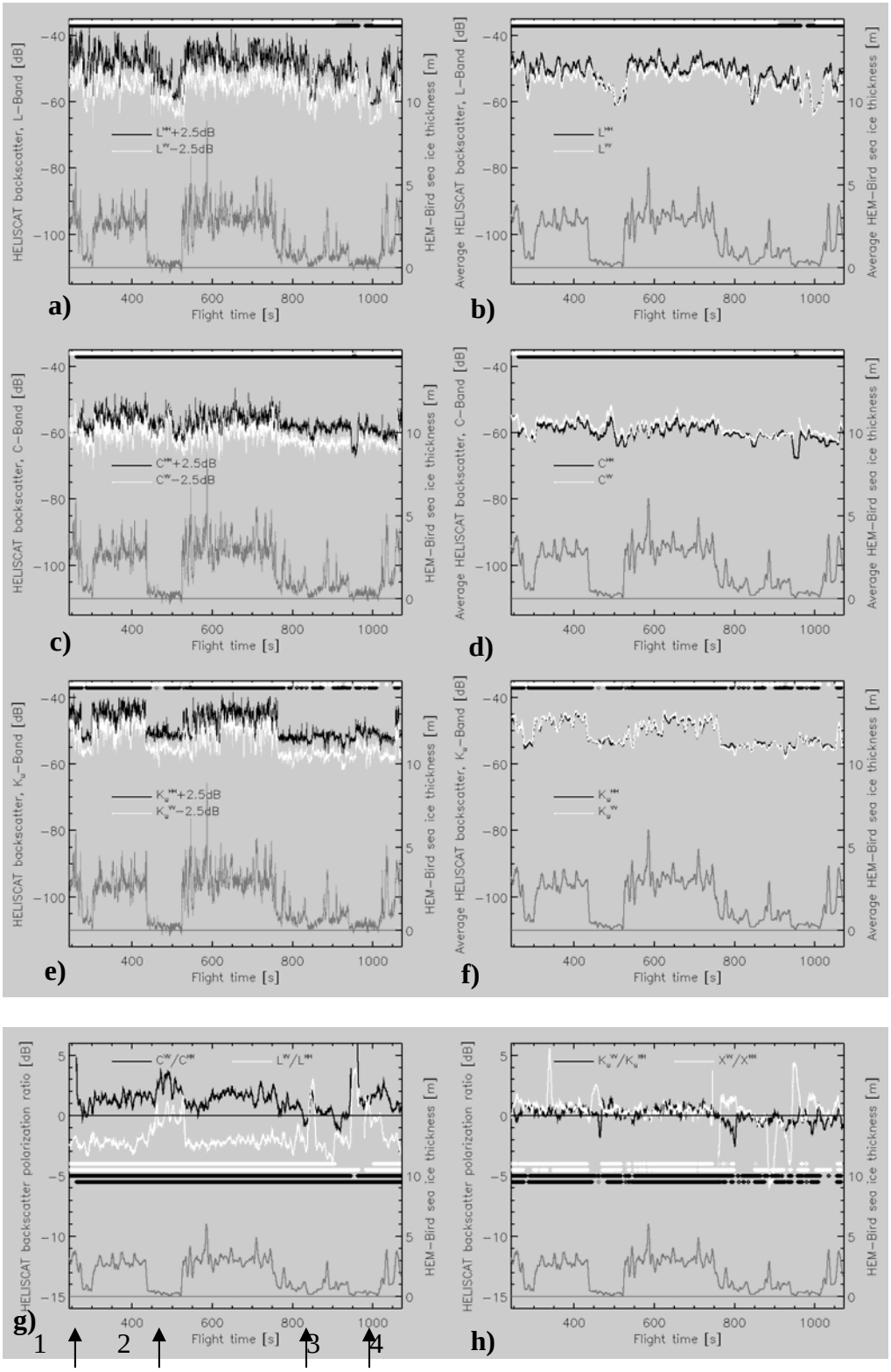

Fig. 3. From top to bottom: L, C, and K_u band backscatter at HH (black) and VV (white) polarization (left y-axis) (a to f), and polarization ratios (g,h) together with EM-Bird sea ice thickness (gray, right y-axis); l.h.s.: raw data and L (white) and C (black) band polarization ratio, r.h.s.: 200 m-average and X (white) and K_u (black) band polarization ratio. Backscatter values have been shifted by ±2.5 dB in the left column. Black arrows in g) denote leads mentioned later

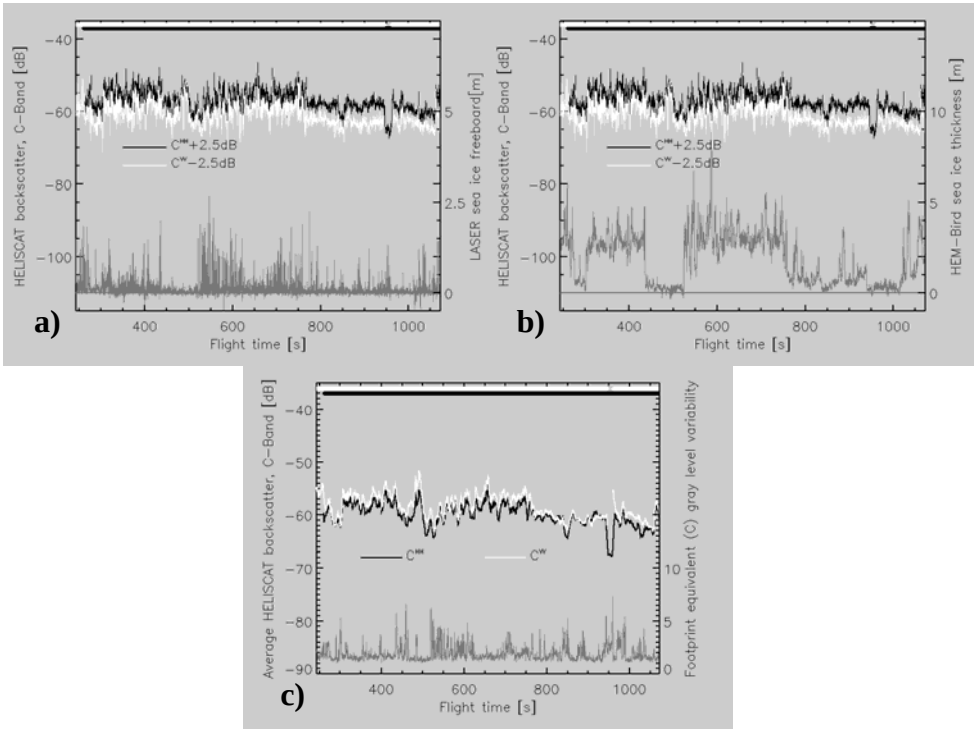

Fig. 4. a) HELISCAT C band backscatter, HH (white) and VV (black) polarization (left y-axis) together with laser altimeter sea ice freeboard (right y-axis); b) same as a) but with sea ice thickness; c) same as a) but with 200m-average backscatter and foot-print equivalent CCD-camera gray level standard deviation

Main conclusions for any forthcoming experiment involving HELISCAT and for the continuation of the analysis of ARK XIX/1 data are: i) calibration of HELISCAT data; ii) consideration of as many supplementary data as possible; iii) carrying out an extensive in-situ measurement program.

ACKNOWLEDGEMENTS

The authors thank the crew of the *Polarstern* and of the company *Helicopter Service Wasserthal* for the support on board the ship and the perfect collaboration concerning the helicopter flights, Steffen Schulz for his help in finalizing the equipment and for his data analyzing efforts, and Christian Haas, Torge Martin, and many more people from Alfred-Wegener Institute, Bremerhaven, Germany, for support on board, and analysis and provision of EM-Bird, laser altimeter, and PODAS data.

REFERENCES

Dierking, W., Skriver H. and Gudmandsen, P. On the improvement of sea ice classification by means of radar polarimetry, Workshop ESRIN Frascati, Italy, *ESA Special Publication* SP-529 (2003).

Gade, M., Alpers, W., Hühnerfuss, H. and Wismann, V. On the reduction of the radar backscatter by oceanic surface films: scatterometer measurements and their theoretical interpretation. *Remote Sensing of the Environment* 66: 52-70 (1998).

Rignot, E. and Drinkwater, M.R. Winter sea-ice mapping from multi-parameter synthetic-aperture radar data. *Journal of Glaciology* 40(134): 31-45 (1994).

Wismann, V., Gade, M., Alpers, W. and Hühnerfuss, H. Radar signatures of marine mineral oil spills measured by an airborne multi-frequency multi-polarization microwave scatterometer. *International Journal of Remote Sensing* 19: 3607-3623 (1998).

17th International Symposium on Ice
Saint Petersburg, Russia, 21 - 25 June 2004
International Association of Hydraulic Engineering and Research

A STUDY ON ICE PROCESSES FOR THE WATER DIVERSION PROJECT FROM SOUTH-TO-NORTH DURING THE WINTER REASON

GAO Peisheng, JIN Guohou, LU Binxiu[1]

ABSTRACT
This paper briefly introduces the ice processes for the water diversion project from South-to-North in China. According to the one-dimensional heat balance equation the water temperature in channel, the starting time of frazil ice, discharge of frazil ice, become time of the ice cover, forecasting the position of ice jam, the flowing capacity under ice cover etc. been simulated. Moreover, the possibility of safe water transfer in the winter reason also has been given.

INTRODUCTION
The Water diversion project from South to North means water transfer from Yangtze River to Northern provinces in China, it is a big water project for the purpose of resolving water use problem for living and agriculture. This article, based on one part of the engineering project, researches the feasibility of safe water transmission in winter and measures to prevent ice. As the channel water flows from warm area to cold regions, so during winter time, the water flow of the channel in north of the Yellow River will be influenced by cold temperature and the factors of adjustment and control, and the development and changes of ice regime will be different, and this will influence the channel transmission and water supply operation in the regions along the channel. This article has analyzed, based on analysis and research of the real meteorological data, the cold year, average year temperature, the temperature changes of a warm year, ice flow rate, the predicted development of ice regime and the discharge of ice flowing, etc.

THE STATISTICS AND ANALYSIS ON CLIMATE CHARACTERISTICS ALONG THE CHANNEL
The main channel from Danjiangkou reservoir to Beijing is in the continental climate region of semi-humid, semi-humid+semi-dry climate. The climate in the region north of Yellow River along the channel, is influenced by Siberia and Mongolian high pressure control in winter, and there are more northwest winds, and the climate is dry-cold. The ice

[1] P.O130X.366, No.20, Chegongzhuang Xilu, Beijing 100044 TEL:010-68711905 Email: slxb@iwhr.com

regime of the rivers along the channel has different ice disasters because of abnormal climate and different river channels and water flow conditions.

Taking January as an example, from Nanyang to Beijing, there is 5°N latitude difference, but the temperature difference is 6.5 ℃ the average temperature statistics in each month and each 10-days of all regions in winter can be seen in table (1). From table (1), we know the temperature of all stations in January is lower than zero degrees. From the statistics data, we select 3 typical temperature year, they are cold year, average temperature year and warm year. So in the channel, the preliminary ice and ice flowing dates are early in north and late in south; the dates for melting of the rivers are early in south and late in north; in history there used to have ice blocking. Since more than 40 years, the rivers are dry with less ice in winter, quite seldom there are cases of ice disaster and flood because of inconvenient water transmission in winter.

Table 1. The average temperature statistics of each month and each 10-days in all regions in winter

Stations	Dec.				Jan.			
	Early period	Mid period	Last period	Month average	Early period	Mid period	Last period	Month average
Zhenzhou	3.52	1.64	0.29	1.82	0.11	-0.28	-0.35	-0.17
Xinxiang	3.02	1.14	-0.23	1.31	-0.35	-0.43	-0.65	-0.48
Anyang	2.34	0.58	-0.97	0.65	-1.27	-1.31	-1.49	-1.36
Xintai	1.46	-0.36	-2.04	-1.31	-2.40	-2.36	-2.48	-2.42
Shijiazhuang	1.28	-0.48	-2.40	-0.53	-2.66	-2.57	-2.88	-2.70
Baoding	-1.15	-1.75	-3.53	-1.81	-3.78	-4.01	-3.85	-3.88
Beijing				-2.7				-4.9

Stations	Feb.				Total average
	Early period	Mid period	Last period	Month average	
Zhenzhou	0.58	2.44	2.84	1.95	1.2
Xinxiang	0.35	2.24	2.85	1.81	0.88
Anyang	-0.32	1.45	2.37	1.17	0.15
Xintai	-1.42	0.57	1.56	0.23	-0.83
Shijiazhuang	-1.86	-0.03	1.11	-0.26	-1.16
Baoding	-2.82	-0.97	0.10	-1.23	-2.31
Beijing				-2.3	-3.3

SIMULATION OF WATER TEMPERATURE IN THE CHANNEL

The authors have simulated use heat balance equation the water temperature change along the channel, and forecast the starting time of ice river and the water temperature change under ice conditions in 1987. Use wendroff hidden format center differential method to solve the equation [1].

$$\frac{\partial}{\partial t}\left(\rho C_p A T_w\right)+\frac{\partial}{\partial x}\left(Q\rho C_p T_w\right)=\frac{\partial}{\partial x}\left(AE_x\rho C_p\frac{\partial T_w}{\partial x}\right)+B\sum Q_t, \qquad (1)$$

in where, Cp is water heat ratio, A is cross section area, Tw is water temperature, Q is flow rate, Ex is water flow vertical dispersing coefficient, B is water surface width,

ρ is water density, $\sum Qt$ is the total heat exchange volume, t is time: v is average velocity: X is river length. given $C = \frac{B\sum Q_t}{\rho C_p d}$; d is average water depth. So we get

$$\frac{1}{2}\left[\frac{T_w^{(i+1,j)}+T_w^{(i,j)}}{dx}+\frac{T_w^{(i+1,j+1)}-T_w^{(i,j+1)}}{dx}\right]+\frac{V}{2}\left[\frac{T_w^{(i,j+1)}-T_w^{(i,j)}}{dt}+\frac{T_w^{(i+1,j+1)}-T_w^{(i+1,j)}}{dt}\right]=C, \quad (2)$$

in where, dx, dt are calculated distance and step length of time separately. From formula (2) we get the proximate solution of the water temperature at different time along the channel sections:

$$T_w^{(i+1,j+1)} = T_w^{(i,j)} + \frac{v-p}{v+p}\left[T_w^{(i+1,j)} - T_w^{(i,j+1)}\right] + \frac{2Cdt}{v+p}, \quad (3)$$

in where, P, $\frac{dt}{dx}$, in order to satisfy the calculation weakening and calculation format stability, given p<1.0, here we take dt = 864 s, dx = 1000 m.

From formula (3) and when we simulate the calculation of the water changes of each channel section, we always follow channel design parameter, the real measured materials from all regional meteorological station as basis, to set the water temperature at time of water flowing-out from Danjiangkou Reservoir at all typical years, and also consider the channel linen surface temperature as the preliminary conditions and boundary conditions of calculation. The water temperature and boundary temperature in different years are as following:

Cold year: the preliminary water temperature is 4.0ºC, the boundary temperature is 5.0ºC, up to northern channel sections, ice appears, water surface temperature is 0.0ºC ~ –0.05ºC;

Average year: preliminary water temperature is 4.5ºC the boundary temperature is 6.0ºC, up to northern channel sections, the water temperature is about 1.0ºC;

Warm year: the preliminary water temperature is 5.0ºC the boundary temperature is 8.0ºC, up to northern channel sections, the water temperature is about 2.0ºC.

THE ICE FLOWING RATE AND THE FORECAST OF THE POSITION FOR ICE JAM

After channel water temperature has reduced to 0ºC, if the temperature keeps low continuously, and it reduces the water temperature to below 0ºC, then it is in too cold status. In too cold water, ice crystal starts to form, and it develops very fast. For the given river section, the ice flowing rate during ice flow period can be estimated according to following formula:

$$\frac{dQ_i}{dt} = \frac{\sum Q_t A_s}{\rho_i L_i}, \quad (4)$$

in where: Qi^{n+1} and Qi, are the ice flow rates for times of n+1 and n separately, $\Sigma Q^n As$ is at n time, the algebra sum of each branch volume of water (ice) surface heat balance; As is the water surface of calculated channel section; dt is the step length of time. For convenient calculation, we carry it out in north and south regions separately.

The estimation of ice regimes in north of the Yellow River

The simulation calculation on the ice production volume in the main channel, the ice status happening, development and changes are as following:

(1) During the water transmission in winter, there is only ice flowing in cold years, the ice flowing rate is bigger than the cross section of this section of channel. Ice flowing ability. Usually in winter, the temperature is below zero, the lowest average day time temperature is -8.5°C. The water flow velocity is between 1.4 – 1.2 m/s. When there is low cold temperature, the water surface temperature is zero, the ice will flow downstream to the front of slots and piles up, and the ice flowing rate is bigger than ice flowing ability. With the increase of ice, the ice pile will become thicker, and it will influence the flow. In the average year and relatively warm year, as the temperature is high, the water temperature is always above 0°C. In these years, the water transmission in this channel section will have no big amount of ice.

(2) In No. 283~327 km section, for water transmission in cold year or average year, the water temperature is about 0°C, on water surface, there is flowing ice already. With the continuous low temperature, the density of river surface ice becomes higher, and ice is flowing towards the cross section of narrow channel sections, and in front of the siphonage, there will be blockings.

Forecast for the position of ice jam

In the process of water transmission, there are two possibilities of ice jam: one is that ice flowing volume during ice flowing season is bigger than the maximum ice flowing capacity; the other is that the continuously formed ice covers are broken under exterior conditions, and a big volume of ice jam are moving downwards. For the transmission and piling-up of ice during ice flowing period, in the evenly flowing river channel, the max. Ice flowing capacity at the cross-section of the river channel L_i is:

$$\frac{L_i}{b} = K \frac{t_i^{1.16}}{D^{0.33}} b^{0.13} S_0^{0.32} q^{0.36}, \qquad (5)$$

in where b is the bottom of trapezoidal-shape channel; D is the diameter of the ice jam; K is experience coefficient (the value at all channel sections have relations with climate conditions and water temperature changes); q is unit width flow rate at the cross section of channel, $q=Q/b$ S is bottom slope of channel; t_i is ice jam thickness.

The flow velocity at all sections along the channel are all bigger than the conditions that form stable ice covers. See Fig. 1 for the max ice flowing ability at all sections of river channel.

At the channels north of the Yellow River, as water has to be transmitted during cold climate year, the ice volume is high at large in the open channel, and it may possibly produce ice at certain cross section and ice may pile up and form ice jam. So, in the channel of north of the Yellow River, we must pay attention to take measures to prevent from ice jam, so as to secure the normal water transfer operation in all channel.

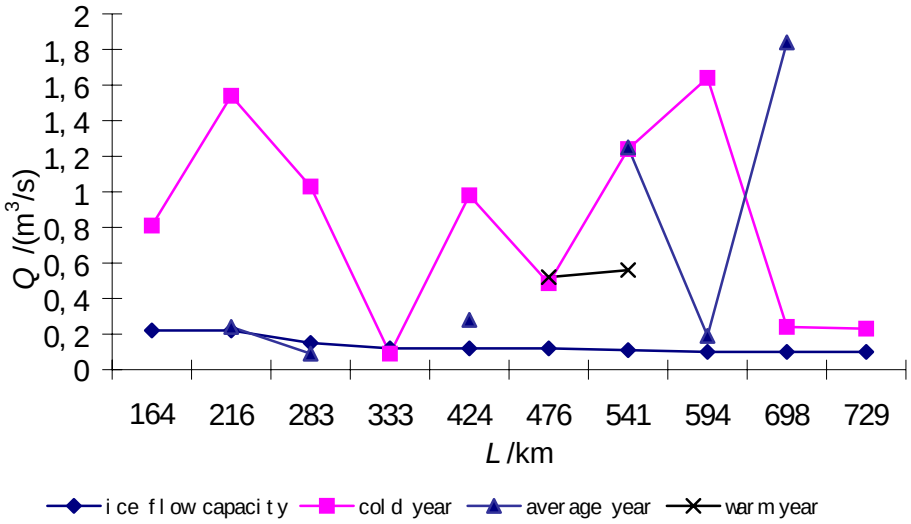

Fig 1. The max. discharge of ice flowing in the north channel of The Yellow River

THE INFLUENCE OF ICE REGIMES AND ICE DISASTER PREVENTION MEASURES

The influence of ice flowing period to the water discharge

At normal years with the designed water flow conditions, at all channel sections in the north of the Yellow River, no ice covers can be formed. The ice with its own weight at the water surface is moving downstream with the water flow. When the rive channel is transmitting water with max. ice carrying capacity, the water line of the river channel is almost the same as the water line without carrying ice. The flow velocity distribution at the river channel is not changed, so during the ice flowing season, ice has no influence to the water discharge, in cold years, the ice flowing at north channels is serious, sometimes ice covers can be formed, and this will influence water flow discharge. For safety reasons, we must execute strict adjustment measures and well-arranged ice prevention measures.

According to the results of the ice simulation during winter water transfer at the main channels, we propose the winter water flow rate as 100 m^3/s and 200 m^3/s starts from No. 163km river section, the flow rate along the channel is controlled under 0.6 m/s. Plus effective ice stopping measures, we can distribute flowing ice evenly at all river sections, and when the temperature conditions are sufficient, ice covers can be formed, and when the river channels have continuous ice covers, the comprehensive roughness coefficient at the river channels under the ice cover is 0.017, the calculated water transfer in the channel with ice covers has reduced 20% – 30% of that without ice covers. It is forecasted that at cold years, the position for easy ice jam at wide open channel sections of the channel and ice blocking thickness can be seen at table (2).

The measures to prevent ice jam and ice disasters

During winter water transfer period, by reducing flow rate, reducing flow velocity (the average is smaller than m/s) or building ice stopping chain on the river surface at main

Table 2. The ice jam thickness at bigger open channel sections

Distance /km	Model temperature year	Discharge (m^3/s)	Velocity (m/s)	Depth of flow /m	Froude numbers	Thickness of ice jam /m
215	Cold	415	1.1	6.0	0.143	1.80
282	Cold	415	1.0	6.0	0.143	2.10
327	Cold	250	1.0	5.5	0.136	1.50
347	Cold	200	1.0	5.5	0.136	1.50
460	Cold	200	1.0	5.5	0.136	1.60
497	Cold	130	0.9	4.5	0.135	1.30
592	Cold	130	0.9	4.5	0.135	1.35
682	Cold	90	0.8	4.3	0.123	1.40
710	Cold	50	0.9	3.5	0.154	1.20
741	Cold	40	0.8	3.5	0.136	1.00

water buildings, in order to promote the faster formation of even and continuous ice covers at the upper reaches of ice stopping chain. In this way, we can reduce ice forming volume to prevent ice jam at the buildings. After water surface ice cover is formed, if the channel flow rate is controlled within certain range, we can then have normal water transfer conditions.

The main measures to prevent ice jam are: (1) Build a ice stopping chain at the section 300~500 m away from the ice jam channel cross section or siphonage; (2) Install a submerge pump at the upper reaches of the gateway; (3) When water transfer is under ice cover, we must restrict flow velocity increase and water level sudden lowering; (4) At the both sides of the channels in north, we build flood distribution gate and floor adjusted reservoir for channel water filling up. We must build automatic monitoring system of ice and flood prevention, to carry out real time monitoring and forecast, and on this basis we can realize ice prevention measures.

CONCLUSION

According to the results of the preliminary research and the statistics from the collected materials, water transfer canal in south of the Yellow River can be operated normally; But at the north of the Yellow River, the ice flowing rate during water transmission in cold years are bigger than the max. Discharge of ice flowing in the channel, ice can pile up and be blocked at the narrow cross sections of the channel or at the buildings such as siphonage, and ice jam can be easily formed at the open channels near Beijing; In this case have to build ice stopping engineering project at the relevant position.

ACKNOWLEDGEMENTS

This paper is based on the works supported by Bureau of South-to-North Water Transfer Ministry Water Resourcts,the authors also thank to Prof. Li Guifen for her help with the investigation.

REFERENCES

Lennart Billfalk, Breakup of Solid ice Covers due to Water level Variations CRREL, Report 82-3.

Jin Guohou, Gao Peisheng. The preliminary analysis and research on the water transmission safety and strategy for the icy period mathematics model of Yellow River-Jiqing River channel winter ice analysis. *Academy of Water Resources and Hydro Power.* July 1987.

Beijing Miyun winter water transmission test team. *Summary of Beijing Miyun water transmission winter test observation*. March 1989.

17th International Symposium on Ice
Saint Petersburg, Russia, 21 - 25 June 2004
International Association of Hydraulic Engineering and Research

FISH HABITAT UNDER ICE COVER IN REGULATED RIVERS

Elena Dolgopolova[1]

ABSTRACT
River flow regulation impact on habitat conditions in ice-covered stream is investigated. The experimental results of velocity, turbulence and pressure fluctuations influence on fish behavior in open flume are presented. Critical magnitudes of velocity, pressure and turbulent intensity obtained in experiments with fish in laboratory flume are compared with those in ice-covered stream in regulated river.

INTRODUCTION
Most of the major rivers of the world are now impounded at some point in the basin, and restrictions for fish migration through hydro constructions were considered in many works, for example by Pavlov et al. (2002). Organisms in lotic waters below reservoirs must adapt to often-erratic discharges that embody the limnological characteristics of the impoundment, or be eliminated from tailwater areas. Although problems associated with impoundments have been considered in the variety of papers, effects on the biota of downstream lotic reaches are treated only cursorily, if at all. One of such problems is the impact of flow regulation on habitat conditions of downstream lotic reaches under ice cover. This problem is of great importance for the Siberian Rivers in Russia, where several species feed and even spawn under ice-cover (for example: Siberian sturgeon (*Acipenser baeri* Brandt), salmon (*Salmo trutta* L.), etc.). These species use for spawning and juvenile fattening ice-covered reach of the river. Ice cover considerably changes hydraulic characteristics of a stream (Tesaker 1998), that in turn influences the habitat conditions of regulated rivers, which are under consideration of this study.

ICE-COVERED STREAMS IN REGULATED RIVERS
River bed morphology
Freezing of a river and formation of water opening in the tail-water is often connected with production of frazil and bottom ice, which occupy considerable part of the river cross-section. Sometimes an ice-covered flow transforms into several small streams, the velocities of each of them being more than that of the initial flow at the same places in summer (Brown et al., 1998, Majewski, 1994). Due to velocity increase erosion of the areas stable in summer begins, that change living conditions of bottom-dwelling fauna.

[1] Water Problems Institute RAS, ul. Gubkina, 119991 Moscow, Russia. E-mail: endol@aqua.laser.ru

Sediment transport and turbidity

Periodic increase of velocity in ice-covered flow in regulated river resulted in increase of sediment transport. Transport of fine-grained sediment carrying metals and other pollutants is of paramount importance (Beltaos and Burrell, 1998). Milburn and Prowse (1998) show, that the change of ice-covered flow structure induce local decrease of transport capacity of the stream, which results in enhanced local deposition of the fine-grained sediments.

There is lack of data on turbidity of ice-covered flow below a dam; however the conclusions made by Lowe (1979) for open regulated river are valid for the water opening in winter. Suspended silt and other sestonic river particles are usually reduced to relatively low levels by settling in lentic waters of reservoirs. The decreased turbidity leads to increased light penetration, which favors submerged phytobenthos. The selective release of highly turbid waters from reservoirs including phytoplancton is often used to combat reservoir siltation. This would decrease light penetration, and silt would settle on the bed of the controlled stream, that would negatively affect submerged phytobenthos.

Mean velocity and turbulent fluctuations of velocity

River flow regulation results in decrease of mean summer discharge Q_s and in essential increase of winter discharge Q_w caused by human activity. Examples of ice-covered flow structure in regulated river (at a distance ~50 km down stream the tail water) considered by Dolgopolova and Tesaker (2000, 2002) show velocity of the stream under ice cover to be the same as for open stream in summer. Comparison of turbulence intensity of ice-covered and open flow in the River Moskva revealed that depth averaged magnitude of turbulence intensity $\overline{\sigma_u}$ is about 5 times larger for ice-covered flow than that for the open flow. These studies show considerable increase of the bottom shear stress in ice-covered stream as well (Dolgopolova, 2002).

Results of investigation of standard deviation of fluctuations of longitudinal velocity component σ_u in the lower pool give for 2D task: $\sigma_u \approx (0.20 \div 0.23)\, U$, and for 3D task: $\sigma_u \approx (0.30 \div 0.37)\, U$, ($U$ is depth averaged velocity at hydrograph peak near erosion pool). In the bulk of the stream the study gives $\sigma_u \approx (0.30 \div 0.37)\, U$ (Lyather, 1968).

Pressure

To study jet pressure effect inducing the failures of hydro constructions the investigations of standard deviation of pressure fluctuations σ_p in the lower pool of hydro plant were carried out, which show near the reach of compressed stream before alleviators $\sigma_p \approx 0.05U^2$, that is much less than that after the alleviators – $\sigma_p \approx 0.1U^2$ (amplitude of pressure fluctuations is normalized by fluid density) (Lyather, 1968). Pressure increase in the lower pool was confirmed by Fiorotto, Rinaldo (1992), who found pressure at hydrograph peak to be 2.5 times larger than the mean pressure.

Water temperature

Temperature regime of a stream in winter is considerably changed due to flow regulation. Mean summer temperature becomes 1 – 5° C lower and mean winter temperature becomes 1-3 ° C higher than that under natural conditions (Stanford, Ward

1979). During freeze-up the outlet water from a reservoir is warmer than that in the lower pool by 1.5 – 5°C. To cool it to 0º C it is necessary some time depending on exchange processes with atmosphere. That is why all northern regulated rivers create a water opening in the lower pool. For example, water openings at the Siberian Rivers extend from 4 – 10 to 220 km and more in cold winters (Kozlov, 2000). Water of the reaches covered with compact ice is very well mixed with temperature ~ 0º C near ice cover and t = 0.1 – 0.5º C near bottom. Due to flow regulation ice break at the Siberian Rivers occurs in some years 1 – 1.5 month earlier than that under natural conditions (Kozlov, 2000), that influence on the dates of spawning season and hatching of larvae.

Oxygen

The important characteristic of water quality of ice-covered flow is concentration of dissolved oxygen. White (1998) has mentioned, that the occurrence of oxygen depressions in rivers under winter conditions have been attributed to lack of reaeration due to the ice cover, oxidation of organic material and inputs of oxygen-depleted groundwater. Water opening in lower pool of hydro plant increases of oxygen concentration in water at this reach.

FISH RESPONSE ON VARIATION OF STREAM CHARACTERISTICS

Orientation of fish in space is realized by different mechanisms, one of which is moving against the stream. There are several quantitative characteristics of this movement among them are critical velocity of the flow (the velocity of the flow, to which fishes can not resist) and buoyancy of fish, which can be measured as time period during which fish can resist the stream of definite mean velocity.

Discharge, velocity and intensity of turbulence

The main results of investigations of fish behavior under varying flow conditions were obtained in laboratory flume (length=1.5 m, width=0.1 m), upper and lower ends being limited by nets (Pavlov et al., 1982). Influence of change of velocity and turbulence intensity on fish movement was studied with roach juvenile (*Ratilus ratilus* L.).

Fish behavior was studied under unstable flow conditions and nonuniform velocity distribution through the flume width, that evaluated by the ratio of maximum velocity V_l to the minimum one V_s ($V_l/V_s = 1.0;\ 1.5;\ 2.0$) (Pavlov et al., 1982). The change of ratio σ_l/σ_s in different areas of the flow reached 2.6. It has been established that when σ_l/σ_s changes in the range 1.2 – 2.2 juvenile prefer the areas of larger turbulence, and at σ_l/σ_s >2.2 fish choose more quiet reaches.

Experimental data show threshold sensitivity of juvenile to variation of velocity fluctuations σ_l/σ_s =30 – 40 % at a distance of 0.1 m, at which juvenile begin to choose a definite turbulent zone. At σ_l/σ_s < 30%, the favorable areas were chosen by fish only by mean velocity of the flow (Skorobogatov et al., 1996).

Investigation of buoyancy of four species of sturgeon fry (*Acipenseridae*) at various velocities (0.158 and 0.2 m/s) shows juvenile buoyancy fall as mean velocity increases (Khodorevskaya, 1979). The study of behavior of white sturgeon juvenile (*Acipenser transmontanus*) under flow regulation conditions carried out by Parkinson (2003) shows that stable low discharges *Q* allow fish to bring into habitat more areas than in case of

rapidly fluctuating (~3.5 times) or high discharge. Photos demonstrate juvenile gathering at high *Q* at a small area, where the deficiency of oxygen and food can arise. The role of mean velocity distribution in a river cross section for fish habitat was studied by Beebe (1996), who found importance of local velocity gradients and sediment transport for management of benthic and fish habitat.

Pressure

The study of fish response to changes of turbulence and pressure *p* of a flow shows that there is a criteria magnitude σ_u =6.49 cm/s, at which small variations of pressure stop fish moving against the stream (Skorobogatov et al., 2000). As σ_u and *p* considerably exceed critical magnitudes during a flush, fish expend more and more energy for orientation in the stream, and at the end are drifted down stream by flow.

Sediment

Influence of sediment transport in ice-covered flow in regulated river on biota remains an open question. However, Henricson and Müller (1979) noted that river flow regulation causes reduction of biomass of zoo benthos from June till September. The authors present several causes of the fact, one of which is the increase of sediment transport that proved fatal for passively feeding organisms. Apparently deterioration of nutritive base due to increase of sediment transport is characteristic for ice-covered flows in regulated rivers as well.

Dissolved oxygen

The decrease of dissolved oxygen in ice-covered flow is often followed by fish-kill. Fish-kills regularly occur in the Upper Ob, where concentration of O_2 ~ 1 mg/l because of inputs of oxygen-depleted groundwater and great amount of humic substances in water of tributaries of Ob (Berezina, 1973). Even tench (*Tinca tinca* L) during hibernation consumes– 6.05 cm^3 O_2 for 1 kg of its weight at 0º C (Yudkin, 1970).

Flow velocity ensures an adequate O_2 supply of the bottom layer, where invertebrates inhabit, and provide development of nutritive base of a river. It is well known that the optimum bottom velocity varies in the range 0.15 – 0.9 m/s (Dolgopolova and Tesaker, 2000). River flow regulation causing mean velocity increase in comparison with natural conditions benefits O_2 distribution to this layer and improve habitat conditions in case the concentration of oxygen in the stream is sufficient. Increase of turbulence intensity and creation of water opening in winter due to river flow regulation promote increase of O_2 in water, but the increase of temperature may reduce the effect.

Temperature

Water temperature considerably influences spawning dates and development of fish roe. For example, at *t* = 1.6º C larvae of salmon (*Salmo trutta* L.) hatch in 156 days, and at *t* = 10º C – in as short as 41 days (Yudkin, 1970). Acceleration of development of larvae with temperature increase due to river flow regulation may play positive and negative role as hatchlings appeared too quickly may get into unfavourable conditions.

There is lack of data on temperature distribution of ice-covered flow down stream the water opening. However one may suppose temperature at the ice edge is ~0.1º C at

which possible concentration of dissolved oxygen is maximum – at t ºC = 0 concentration of O_2, ($cm^3/1$) = 10.29.

CONCLUSIONS

Increase of mean velocity, pressure and turbulence intensity at hydrograph peak favours drift of fish down stream deteriorating habitat condition in regulated river.

Changes of sediment transport due to flow regulation negatively impact nutritive base of ice-covered flow down stream the water opening.

Increase of water temperature in the lower pool in winter and change of ice break dates may have both negative and positive influence on river biota habitat conditions.

Increase of oxygen concentration due to exchange with atmosphere at the lower pool does not radically improve oxygen deficit in ice-covered flows. Lack of experimental data prevents one to make a concrete conclusion about river flow regulation impact on temperature and concentration of oxygen of water of ice-covered reaches of regulated streams.

ACKNOWLEDGMENT

This work was partially supported by the RFBR, Grant No.03-05-64237

REFERENCES

Beebe, J.T. Fluid speed variability and the importance to managing fish habitat in rivers. *Regulated rivers*:*Research &Management,* 12 (1996) 63-79.

Beltaos, S., Burrell, B.C. Transport of metals on sediment during the spring breakup of river ice. In *Proceedings of the 14-th IAHR Symposium on Ice*. Rotterdam, Balkema 2 (1998) 793-800.

Berezina, N.A. Hydrobiology. Moscow, Food Industry Press (1973) 495 p.

Brown, R.S., Power, G., McKinley, R.S. Effects of hanging dams, surface ice break-up, and flooding on fish. In *Proceedings of the 14-th IAHR Symposium on Ice*. Rotterdam, Balkema 1 (1998) 175-181.

Dolgopolova, E.N., Tesaker, E. Turbulent structure of ice-covered flow and ice impact upon habitat in rivers. In *Proceedings of the 15-th Symposium on Ice*. Gdansk, Poland (2000) 381 - 390.

Dolgopolova, E.N. Estimate of turbulence energy in ice-covered flow and its influence on river habitat. In *Proceedings of the 16-th IAHR Symposium on Ice*. Danedin, New Zealand 1 (2002) 262-267.

Dolgopolova, E.N. Friction stress at the bed of under-ice flow and its infuence on the biota living conditions in rivers. *Water Resources:* 29(3) (2002) 282 - 288.

Fiorotto, V., Rinaldo, A. Turbulent pressure fluctuations under hydraulic jumps..*Journal of Hydraulic Research*: 30 (5) (1992) 499-520.

Henricson, J., Müller, K. Stream regulation in Sweden with some examples from central Europe. In *Proceedings of International Symposium on Regulated Streams*. Plenum Press, New York (1979) 183-199.

Lyather, V.M. Turbulence in hydraulic works. Energy, Moscow (1968) 408 p.

Khodorevskaya, R.P. Buoyancy ability of sturgeon youth. In *Development of fish industry in reservoirs of the USSR*. Science, Moscow (1979) 201 - 208.

Kozlov, D.V. Ice of fresh water reservoirs and streams. Moscow University of Engineering Environment Press, Moscow (2000) 262 p.

Lowe, R.L. Phytobenthic ecology and regulated streams. In *Proceedings of International Symposium on Regulated Streams*. Plenum Press, N. Y. (1979) 25-34.

Majewski, W. Flow characteristics in open channels with floating ice cover. In *Proceedings of the 12-th IAHR Symposium on Ice*. Trondheim, Norway, 1 (1994) 22-30.

Milburn *D.*, Prowse, T.D. Observations on the role of an ice cover in sediment deposition. In *Proceedings of the 14-th IAHR Symposium on Ice*. Rotterdam, Balkema 1 (1998) 189-196.

Parkinson, S.K. Response of white sturgeon to various hydropower operating regimes. In *Proceedings of XXX IAHR Congress, JFK SPC*, Thessaloniki, Greece (2003) 1-8.

Pavlov, D.S, Lupandin, A.I., Kostin, V.V. Downstream migration of fish through dams of hydroelectric power plants. Trans. T. Albert, trans. Ed. G.F. Cada. ORNL/TR-02/02 Oak Ridge National Laboratory, Oak Ridge Tennessee, USA (2002) 249 p.

Pavlov, D.S., Skorobogatov, M.A., Shtaf, L.G. Influence of turbulent intensity on the critical velocity of flow for fishes. *Reports of Academy of Sciences of USSR* 267(4) (1982) 1019 - 1021.

Skorobogatov, M.A., Lupandin, A.I., Pavlov, D.S. Fish response on variation of hydrostatic pressure in flows of different turbulence. *Reports of RAS* 374(5) (2000) 715-717.

Skorobogatov, M.A., Pavlov, D.S., Lupandin, A.I. Influence of velocity and intensity of turbulence distribution on movement of roach rutilus in water flow. *Problems of Ichthyology* 36(5) (1996) 687 - 692.

Stanford, J.A., Ward, J.V. Stream regulation in North America. In *Proceedings of International Symposium on Regulated Streams*. Plenum Press, N. Y. (1979) 215-236.

Tesaker, E. Mitigation of ice effects of the habitat in regulated and natural rivers. In *Proc. of the 14-th IAHR Symposium on Ice*. Rotterdam, Balkema 2 (1998) 161-168.

White, K.D. 1-D streamwise finite element model of dissolved oxygen under river ice. In *Proc. of the 14-th IAHR Symposium on Ice*. Rotterdam, Balkema 2 (1998) 801-807.

Yudkin, I.I. Ichthyology. Moscow, Food Industry Press (1970) 379 p.